

2018-07-03

The Effects of Nicotine on Stem Cell Derived Cardiomyocytes

Jordan M. Greenberg

University of Miami, jordan.greenberg729@gmail.com

Follow this and additional works at: https://scholarlyrepository.miami.edu/oa_dissertations

Recommended Citation

Greenberg, Jordan M., "The Effects of Nicotine on Stem Cell Derived Cardiomyocytes" (2018). *Open Access Dissertations*. 2123.
https://scholarlyrepository.miami.edu/oa_dissertations/2123

This Embargoed is brought to you for free and open access by the Electronic Theses and Dissertations at Scholarly Repository. It has been accepted for inclusion in Open Access Dissertations by an authorized administrator of Scholarly Repository. For more information, please contact repository.library@miami.edu.

UNIVERSITY OF MIAMI

THE EFFECTS OF NICOTINE ON STEM CELL DERIVED CARDIOMYOCYTES

By

Jordan Michael Greenberg

A DISSERTATION

Submitted to the Faculty
of the University of Miami
in partial fulfillment of the requirements for
the degree of Doctor of Philosophy

Coral Gables, Florida

August 2018

©2018
Jordan Michael Greenberg
All Rights Reserved

UNIVERSITY OF MIAMI

A dissertation submitted in partial fulfillment of
the requirements for the degree of
Doctor of Philosophy

THE EFFECTS OF NICOTINE ON STEM CELL DERIVED CARDIOMYOCYTES

Jordan Michael Greenberg

Approved:

Herman S. Cheung, Ph.D.
Professor of Biomedical Engineering

Daniel Pelaez, Ph.D.
Research Assistant Professor of
Ophthalmology

C.Y Charles Huang, Ph.D.
Associate Professor of
Biomedical Engineering

Edward Dauer, M.D.
Research Associate Professor of
Biomedical Engineering

Wayne Balkan, Ph.D.
Research Associate Professor of
Medicine

Guillermo J. Prado, Ph.D
Dean of the Graduate School

GREENBERG, JORDAN MICHAEL

(Ph.D., Biomedical Engineering)

The Effects of Nicotine on
Stem Cell Derived Cardiomyocytes

(August 2018)

Dissertation supervised by Professor Herman S. Cheung.

No. of pages in text. (101)

Accurate models of healthy and diseased states are crucial to development of future therapeutics. Up until recently any studies of the molecular mechanism of diseases affecting cardiomyocytes required the use of animal models which do not accurately model the human condition, or use hard to obtain primary patient derived cells that can vary widely from patient to patient. The recent rise of stem cells has allowed for the generation of models of cardiomyocytes that can be used for studies of development, disease modeling, or drug screening. Although great insight has been gained using stem cell derived cardiomyocytes, issues of starting cell lines and relative maturity of differentiated cells has made the landscape murky. This thesis will detail the development of a cardiomyogenic lineage from two independent cell sources: an adult stem cell source derived from patient dental tissue, and commercially available pluripotent stem cells.

Following development of a model of intracellular calcium cycling of stem cell derived cardiomyocytes, I use this model to determine the effects of nicotine on cardiomyocyte development. 1 in 10 cardiovascular disease deaths is related to smoking, however the molecular mechanism that underlie the development of smoking induced cardiovascular disease remain unclear. In addition to tobacco usage many users attempt to curb nicotine withdrawal symptoms while quitting tobacco through the use of nicotine replacement therapies such as gums, transdermal passages and as of recently, electronic cigarettes. Therefore, the effect of nicotine on cardiomyocytes is of great interest to the scientific community. Using a model of cardiomyocytes, I investigate changes in calcium cycling

of induced pluripotent stem cell derived cardiomyocytes subject to nicotine addiction at every media change. In these studies, I show that nicotine induces increased intracellular Ca^{2+} loads through activation of $\alpha 7$ nicotinic acetylcholine receptors. I show that nicotine induced increased Ca^{2+} load leads to increased levels of kinase activity. Finally, I show that cardiomyocytes subject to nicotine treatment display a fetal like gene program that is indicative of hypertrophic growth, commonly associated with cardiovascular disease.

Given the results presented here further studies on the development of nicotine induced cardiovascular disease can be carried out. Further, new therapies aimed at slowing the progression of disease may be developed with more accuracy, targeting involved proteins and pathways.

TABLE OF CONTENTS

Page

LIST OF FIGURES	iv
LIST OF TABLES.....	vii
LIST OF ABBREVIATIONS.....	viii
LIST OF PUBLICATIONS.....	ix

Chapter

1 INTRODUCTION	1
Rates and Risks of Nicotine Usage.....	2
Cardiomyocytes and Nicotine.....	4
2 BACKGROUND	7
Cardiomyocyte Physiology and Development.....	7
Current Models of Human Adult Cardiomyocytes.....	15
Nicotine and Stem Cells.....	21
3 ADULT STEM CELL DERIVED MODEL.....	31
Motivation.....	31
Materials and Methods.....	34
Results.....	40
Discussion.....	47
4 PLURIPOTENT STEM CELL DERIVED MODEL	51
Motivation.....	51
Materials and Methods.....	54
Results.....	61
Discussion.....	80
5 CONCLUSIONS AND FUTURE WORK.....	84
REFERENCES.....	88

LIST OF FIGURES

Figure 1.1 - Hypothesized mechanism of action of the effects of nicotine in iPS derived cardiomyocytes. Page 6

Figure 2.1 - Flow of calcium ions that controls the contraction of cardiomyocytes. Page 8

Figure 2.2 - CaMKII regulation in cardiomyocytes. Page 13

Figure 2.3 - Prototypical structure of nicotinic acetylcholine receptors. Page 26

Figure. 3.1 - Gene expression changes following directed differentiation of neural crest stem cell derived cardiomyogenic cells. Page 41

Figure. 3.2 - Immunohistochemical analysis of two important proteins: the sarcomeric proteins, cardiac troponin I (cTnI) and skeletal muscle actin (α -SMA), in NCSC-CMs after completion of the 2-week growth factor cocktail regime. Page 42

Figure. 3.3 - NCSC-CM response in Ca 520 AM fluorescence to ionomycin. Page 43

Figure 3.4 - PIV of NCSC-CM cardiosphere. Within NCSC-CM cardiospheres, visible contraction could be observed. Page 44

Figure 3.5 - Analysis of spatial effects: average velocity of contraction was measured along the beam path of the IR source. Page 44

Figure 3.6 - JC-1 staining of NCSC-CMs after long-term IR stimulation to test whether applied radiation causes permanent mitochondrial membrane depolarization. Page 46

Figure 4.1 - Schematic of iPS cell differentiation. Page 56

Figure 4.2 - Immunohistochemical staining of $\alpha 7$ nicotinic acetylcholine receptor on naive human induced pluripotent stem cell. Page 62

Figure 4.3 - iPS-CM respond to electrical field stimulation. Page 63

Figure 4.4 - 20mM Caffeine elicits a rapid release of calcium from intracellular SR stores. Page 63

Figure 4.5 - Ryanodine diminishes iPS-CM contraction by inhibiting intracellular SR calcium release by blocking RyR2 channels in the SR. Page 64

Figure 4.6 - Thapsigargin slows iPS-CM contraction by inhibiting intracellular SR calcium cycling by blocking reuptake of Ca^{2+} into the SR via SERCA channels. Page 64

Figure 4.7 - 1 μM Nicotine induces increased calcium load in iPS-CM. Page 65

Figure 4.8 - While undergoing spontaneous contraction iPS-CM reach peak calcium levels quicker and are also faster to reuptake Ca^{2+} post contraction. Page 66

Figure 4.9 - While being electrically paced, groups treated with nicotine reach peak calcium levels faster than control, but reuptake does not appear to be effected by 1 μM nicotine. Page 66

Figure 4.10 - 1 μM Nicotine induces an increase in protein expression of CaMKII. Page 68

Figure 4.11 - 1 μM Nicotine induces an increase in protein expression of Thr²⁸⁶CaMKII. Page 69

Figure 4.12 - 1 μM Nicotine increases in the ratio of Thr¹⁷Phospholamban relative to total phospholamban. Page 70

Figure 4.13 - Genetic expression analysis for NK Homeobox 2 locus 5 (NKX2.5) following treatment with 1 μM nicotine with and without pretreatment of pharmacological agents. Page 72

Figure 4.14 - Genetic expression analysis for myosin heavy chain β (MYH7) following treatment with 1 μM nicotine with and without pretreatment of pharmacological agents. Page 73

Figure 4.15 - Genetic expression analysis for cardiac muscle troponin T (TNNT2) following treatment with 1 μM nicotine with and without pretreatment of pharmacological agents. Page 74

Figure 4.16 - Genetic expression analysis for natriuretic peptide A (NPPA) following treatment with 1 μM nicotine with and without pretreatment of pharmacological agents Page 75

Figure 4.17 - Genetic expression analysis for natriuretic peptide B (NPPB) following treatment with 1 μM nicotine with and without pretreatment of pharmacological agents Page 76

Figure 4.18 - Genetic expression analysis for ryanodine receptor 2 (RYR2) following treatment with 1 μM nicotine with and without pretreatment of pharmacological agents Page 77

Figure 4.19 - Genetic expression analysis for calsequestrin (CASQ2) following treatment with 1 μM nicotine with and without pretreatment of pharmacological agents Page 78

Figure 4.20 - Genetic expression analysis for phospholamban (PLN) following treatment with 1 μ M nicotine with and without pretreatment of pharmacological agents
Page 79

Figure 4.21 - Genetic expression analysis for Sarcoplasmic/Endoplasmic Reticulum Calcium ATPase 1 (ATP2A1) following treatment with 1 μ M nicotine with and without pretreatment of pharmacological agents
Page 80

LIST OF TABLES

Table 2.1 - Review of expression of nAChR in stem cells. Page 28

Table 3.1 - Forward and Reverse Primers used for gene expression analysis in adult stem cell model. Page 37

Table 4.1 - Forward and Reverse primers used for gene expression analysis in pluripotent stem cell model. Page 58

Table 4.2 - Concentration and part numbers of antibodies used for pluripotent stem cell model. Page 59

LIST OF ABBREVIATIONS

CaMKII- Calcium Calmodulin Dependent Protein Kinase II

CICR- Calcium Induced Calcium Release

CSC- Cardiac Stem Cell

ECC- Excitation Contraction Coupling

iPS- Induced Pluripotent Stem Cell

MSC- Mesenchymal Stem Cells

nAChR- Nicotinic Acetylcholine Receptor

NCSC- Neural Crest Stem Cell

NCX- Sodium Calcium Exchanger

NRT- Nicotine Replacement Therapy

PLN- Phospholamban

PS-Primitive Streak

RyR2- Ryanodine Receptor Type 2

SACO- Asynchronous Ca^{2+} oscillations

SR- Sarcoplasmic Reticulum

SERCA- Sarco(Endo)Plasmic Reticulum Calcium ATPase

TPRC- Transient receptor potential channels

VDCC- Voltage Dependent Calcium Channels

LIST OF PUBLICATIONS

Portions of this thesis have been previously published in peer reviewed academic journals.

Chapter 2:

The routes of exposure section has been taken from:

The deleterious effects of cigarette smoking and nicotine usage and mesenchymal stem cell function and implications for cell based therapies. **Jordan M. Greenberg**, Carlos M. Carballosa, Herman S. Cheung. Feb 2017. Stem Cells and Translational Medicine, AlphaMed Press. September 2017. (6)9:1815-1821

The nicotine and nicotinic acetylcholine receptor subsection, including Table 2.1 has been taken from:

Expression and function of nicotinic acetylcholine receptors in stem cells. Carlos M. Carballosa, **Jordan M. Greenberg**, Herman S. Cheung. AIMS Bioengineering, AIMS press. July 2016. (3)3: 245-263

Both of these articles are collaborative efforts between myself, my peer Carlos Carballosa and my mentor Dr. Herman Cheung. All text and figures were prepared by myself and Mr. Carballosa. Conceptual design, editing, and final review were done by all authors.

Chapter 3:

This chapter has been published in its entirety in:

Neural crest stem cells can differentiate to a cardiomyogenic lineage and contract in response to IR stimulation. **Jordan M. Greenberg**, Vicente Lumbreras, Daniel Pelaez, Suhrud Rajguru, Herman S. Cheung. *Tissue Engineering*, Mary Ann Liebert Publishing, October 2016; (22)10: 982-990

This work was conceptualized by my mentor Dr. Herman Cheung, and a collaborator from the department of Biomedical Engineering and Otolaryngology, Dr. Suhrud Rajguru. All experiments were performed by myself and Dr. Daniel Pelaez. The text and figures

were prepared by myself with the assistance of my peer Dr. Vicenete Lumbreras. Final draft approval was done by all authors.

Chapter 4:

This chapter is being prepared for submission.

Conceptualization and design of experiment was performed by myself, and my mentor Dr. Herman Cheung. All experiments were performed by myself, with the assistance of Dr. Raul Dulce for the IonOptix experiments. I prepared and wrote the manuscript.

CHAPTER 1. INTRODUCTION

According to the Tufts Center for Drug Development, the cost to bring a prescription drug to market increased 145% from 2003-2013 and is estimated to be \$2.6 billion per drug that receives market approval (1). Cardiovascular toxicity is the most frequent adverse drug reaction and the cause of 45% of post-approval drug withdrawals (2). To reduce cost and adverse events, accurate, cheaper models of cardiomyocytes and diseased state cardiomyocytes need to be developed. Until recently data on human myocytes was limited to clinically available measurements such as blood pressure and EKG measurements, or patient derived primary cells which can be difficult to obtain, and vary widely from patient to patient (3). As an alternative, animal models have provided some insight into cardiomyocyte function and physiology but inter-species variations have limited the use of these cells (3, 4).

Within the last 20 years, the discovery of stem cells has allowed for faster, cheaper and more consistent models of cardiomyocytes. The concept of stem cells dates back to the 1970s when the discovery of blood formation was refined (5), but the seminal work that started the idea of stem cell technology was published in 1998 by James Thomson and colleagues at the University of Wisconsin. Thomson was the first to report the derivation of a pluripotent stem cell line derived from the inner cell mass of human blastocysts (6). Since this report, the field of stem cells and regenerative medicine has exploded leading to characterization and isolation of several classes of stem cells, each with a unique set of advantages and disadvantages. Stem cells are now being used as a model to gain insight into cardiomyocyte physiology and allowing for *in vitro* modeling of cardiomyocytes for

faster, higher throughput screening of drugs, as well as studies of development and disease modeling.

While stem cells have allowed for tremendous growth in knowledge of cardiomyocytes, the most appropriate stem cell source for cardiomyocyte research is still under debate. The projects presented herein detail the development of a model of human cardiomyocytes from two unique stem cell populations including human adult stem cells derived from the neural crest and commercially available human induced pluripotent stem cells. Using the induced pluripotent stem cell model of cardiomyocytes, the effects of nicotine on cardiomyocyte development are characterized.

Rates and Risks of Nicotine Usage

Cigarette smoking is the leading cause of preventable death both in the United States and worldwide, and is responsible for 1 in 5 deaths in the United States. Diseases associated with smoking include a wide array of cancers, strokes and cardiovascular disease (7). According to the surgeon general, 140,000 individuals die premature deaths from cigarette smoking induced cardiovascular disease, 1 in 10 deaths from cardiovascular disease worldwide were attributed to smoking, and in the US, smoking accounts for 33% of all deaths from cardiovascular disease and 20% of ischemic heart disease in persons older than 35 (8). Nicotine usage among pregnant women also presents a serious health concern. Nicotine rapidly crosses the placental barrier and nicotine concentrations in the fetus can be 15% higher than maternal levels (9). According to data from the CDC, 8.4% of pregnant women report smoking cigarettes at some point during pregnancy. Tobacco exposure during the first trimester lead has been linked to increased spontaneous abortions and use during the third trimester linked to premature delivery rates, and decreased birth weights

(10). Of pregnant women who reported smoking during the first and second trimester, 20.6% reported quitting by the third (11). This provides little solace in regards to heart development however as the heart is the first organ in the fetus to fully develop and function (12). In regards to heart development numerous studies have shown that tobacco usage among pregnant women is linked to increased blood pressure in infants (13, 14). Additionally, nicotine usage during pregnancy may also increase the risk of individuals to many diseases later in life, including cardiovascular disease (15).

Despite knowing the risks, the addictive properties of tobacco usage make cessation difficult for most. Each year 70% of smokers report they would like to quit, but only 3% successfully do (16). Many of those attempting to quit will turn to nicotine replacement therapies (NRT) to counter withdrawal symptoms associated with nicotine cessation. NRTs are effective in increasing the likelihood of successfully quitting but the long term effect of sustained nicotine delivery still presents a severe risk factor for cardiovascular disease (17). In addition to tobacco consumption and NRTs, the recent advent of the electronic cigarette has drastically changed the landscape of nicotine usage. Billed as a safer alternative to smoking cigarettes, e-cigarettes heat a liquid into an aerosol which is inhaled by the user. This liquid may contain various concentrations of nicotine and/or flavoring agents. Since being introduced to the market, teenage populations have seen a rapid rise in the use of e-cigarettes. From 2011-2015 e-cigarette use among high school students rose from 1.5% to 16% and 0.6 to 5.3% among middle schoolers (18). Continued population dependence on nicotine underscores the need for understanding of the mechanism of action of nicotine in cardiomyocytes.

Cardiomyocytes and Nicotine

Cardiomyocytes are the cell that is responsible for the generation of the contractile force needed to pump oxygenated blood from the heart to the rest of the body. Within the myocardium contraction of cardiomyocytes is mediated through the flow of calcium ions. Briefly, membrane depolarization from an action potential induces the opening of L-type voltage gated calcium channels (VDCC). Following calcium influx through VDCCs, stores of calcium in the sarcoplasmic reticulum (SR) are released and Ca^{2+} ions bind to muscle fibers to allow for contraction. Following contraction calcium is reuptaken into the SR to prime it for the next cycle (19).

In addition to its role as a mediator of contraction, calcium has shown increasingly important roles as a secondary messenger in regulatory processes, including inducing changes in Ca^{2+} cycling and regulation of gene expression (20). Dysfunction in calcium cycling is also becoming increasingly known to be associated with cardiovascular disease (21). Hoshijimi *et. al* have shown that targeting defects in SR Ca^{2+} cycling is sufficient to reverse advanced heart failure in mice, and suggest that SR Ca^{2+} cycling is the final common pathway for the progression of many forms of heart failure (22). To highlight the regulatory role that Ca^{2+} can play in cardiomyocytes consider calcium/calmodulin dependent protein kinase II (CaMKII) which is activated by increased intracellular Ca^{2+} . In response to activation, CaMKII signaling has the potential to directly alter gene expression and can induce gain or loss of function of several key Ca^{2+} regulator proteins in cardiac contractility (19). (See Figure 2.2 for detail)

As previously mentioned, nicotine usage has long been known to be detrimental to cardiovascular health, including increased risk of atherosclerosis, hypertension, and

myocardial infarction (23). With respect to cardiomyocytes specifically, nicotine is known to induce cardiomyocyte hypertrophy (increased size) and apoptosis, however the molecular mechanism underlying nicotine induced changes remains mostly unknown (24, 25). Nicotinic acetylcholine receptors (nAChR) are pentameric ligand gated ion channels which are the primary receptor of nicotine. Activation of these channels in response to nicotine opens the channel and allows for the influx of ions into the cell. Depending on the various monomers that compose the pentameric receptor, the permeability of these channels to various ions can differ (26). The $\alpha 7$ homopentameric channel is known to be expressed in mice pluripotent stem cells and at all embryological stages of cardiomyocyte development of the rat myocyte (this has not been studied in humans as of yet), and is the most permeable nAChR for Ca^{2+} ions (26-28). It is hypothesized in chapter 4 of this report that entry of Ca^{2+} through $\alpha 7$ nAChRs of stem cell derived cardiomyocytes will lead to increased calcium loads inducing activation of CaMKII signaling pathways and alter gene expression to patterns indicative of cardiomyocyte hypertrophy (Figure 1.1).

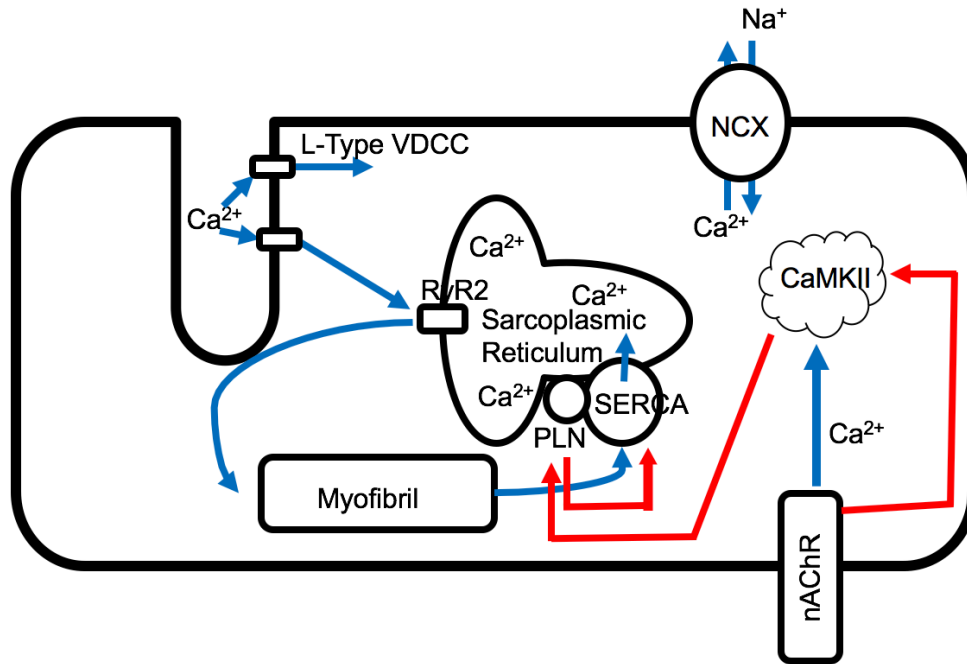


Figure 1.1 - Hypothesized mechanism of action of the effects of nicotine in stem cell derived cardiomyocytes. Blue arrows indicate the flow of Ca²⁺ ions, red arrows indicate regulatory control.

CHAPTER 2. BACKGROUND

Cardiomyocyte Physiology and Development

In order to develop accurate models of cardiomyocytes, an understanding of the development and physiology of cardiomyocytes is necessary. The following sections detail the mechanism of contraction of cardiomyocytes and the cycling of calcium ions in this process. The role of calcium cycling in differentiation and development is then highlighted and finally, this section concludes with a discussion of regulation of intracellular Ca^{2+} cycling in cardiomyocytes and how defects in calcium cycling are associated with cardiovascular disease.

Cardiomyocyte Physiology

Cardiomyocytes are the force generating unit of the heart and are responsible for generating contraction. Contraction of cardiomyocytes occurs via excitation contraction coupling (ECC) mechanism, in which an electrical signal (action potential) leads to a mechanical response (contraction). In the specific case of cardiomyocytes, contraction is controlled through the process known as calcium induced calcium release (CICR). As a result of the depolarization from the action potential, voltage gated calcium channels (VDCC) in T-Tubules of myocytes open and allow the inward flux of calcium ions into the cytosol. Within the cytosol calcium ions stimulate ryanodine receptor (RyR) channels located on the sarcoplasmic reticulum (SR) to open. As the sarcoplasmic reticulum is the primary site of calcium storage, opening of RyR channels leads to increased cytosolic concentration of Ca^{2+} ions. In the cytosol, Ca^{2+} ions bind to troponin which in turn causes cardiac troponin to bind to troponin I. After Ca^{2+} binding, troponin I is pulled off its active site on the actin filament and tropomyosin, the third component of the troponin complex,

rolls further into the groove of the actin filament. Myosin is then able to bind to actin, causing the contraction of the cardiomyocyte (19).

Post contraction it is necessary for calcium to be sequestered to allow for relaxation and refilling of stores for the next contractile event. Sequestration of calcium post contraction is accomplished via two major ion channels. The largest amount of Ca^{2+} reuptake is accomplished via the sarco(endo)plasmic reticulum Ca^{2+} ATPase (SERCA). This channel is responsible for reloading the calcium stores in the sarcoplasmic reticulum and accounts for approximately 70% of calcium reuptake in humans. Most of the remainder of the intracellular calcium is transported out of the cell through the Sodium-Calcium exchanger (NCX). A small portion of calcium is also uptaken by the mitochondria via the mitochondrial calcium uniport (mCU); however, this is a very slow process under physiological conditions (19) (Figure 2.1).

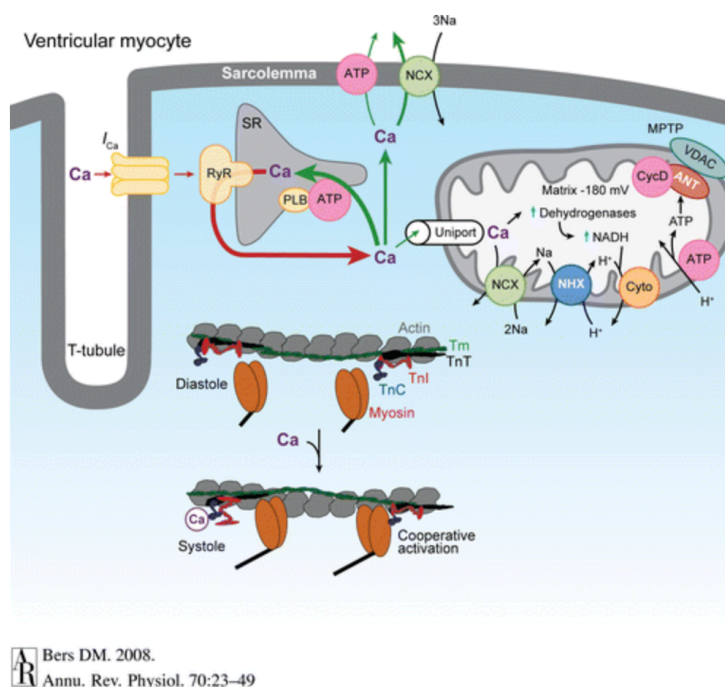


Figure 2.1 - Flow of calcium ions that controls the contraction of cardiomyocytes. Figure taken from (19)

Cardiomyocyte Development

In addition to its role in mediating contraction, Ca^{2+} cycling is known to be crucial to the development of the heart. The heart is the first of the major organs to develop during human gestation. At embryological stage 6 (E6), corresponding to day 14 in human gestation, prior to gastrulation, the epiblast forms the primitive streak (PS) in which mesenchymal cells arrange into a midline structure that forms in the posterior and runs anteriorly until it covers approximately 80% of the epiblast (29). This PS marks the site of eventual gastrulation and functions to topographically position mesoendodermal cells for germ layer formation. Cardiac precursor cells are among the first of the mesoendoermal cells to ingress during gastrulation at E7, week 3 in human gestation. Following gastrulation, cardiac progenitor cells migrate away from the primitive streak to the anterior lateral section of the blastocyst and form the cardiac crescent at E7.5. At E8, the cardiac crescent fuses at the midline and forms the first heart field derived linear tube. The first heart field derived linear tube begins to contract and undergoes rightward looping and rapid growth during embryological stage 8.5 (E8.5), corresponding to week 4 of human gestation. Through cell proliferation and recruitment of cells, the heart tube expands and formation of the second heart field occurs. At E10.5 (day 32 in humans) the heart shows well developed chambers and by E14.5 (~7 weeks in humans) has fully separated chambers and is connected to the pulmonary trunk and aorta (30).

In addition to proliferation and recruitment of cells, myocytes already present undergo physiological hypertrophy, or increases in cellular size (31) to populate the expanding heart. Estimates have placed the increase in cardiomyocyte size due to hypertrophy to be 30-40 fold (32). The molecular cues underlying physiological hypertrophy associated with

myocardial development are only recently beginning to be elucidated. Classical theory of myocardial development suggested that blood flow and contraction from the linear heart tube onward are necessary stimuli for hypertrophic growth and population of chambers; however, Andersen et. al. have since shown that neither is a requirement for the onset of physiological hypertrophy and that hypertrophy is a result of the calcium conduction pathway (33, 34). Through the use of zebrafish embryos as a model organism of cardiomyocyte development it has now been shown that that voltage gated calcium entry through VDCC channels and subsequent calcineurin activation via downstream signaling mechanism are the stimulus that initiate the onset of physiological hypertrophy (33, 35).

In addition to its role in activating hypertrophic growth, Ca^{2+} cycling also precedes the first contraction of nascent cardiomyocytes. Before the onset of contraction of myocytes, asynchronous calcium oscillations (SACO) can be observed in the developing cardiac crescent. These transients vary in duration and frequency and are much slower to reach peak amplitude than the Ca^{2+} oscillations observed in later stage cardiomyocytes. The first observed oscillations are believed to be exclusively regulated through the sodium calcium exchanger 1 channel (NCX1). As the myocardium continues to develop, VDCC channels begin to transport calcium ions in addition to NCX1, and transients begin to propagate through the entire cardiac crescent. Eventually, NCX1 activity ceases leaving VDCC responsible for flow of ions. At this stage, the predominant calcium storage organelle, the sarcoplasmic reticulum, is still non-functional, however as looping occurs at E8.5, there is a rapid transition in which the SR becomes functional and the primary mechanism for controlling intracellular calcium levels in the myocyte (36). The authors of the study first describing this process hypothesize that one of the purposes of SACO is to activate calcium

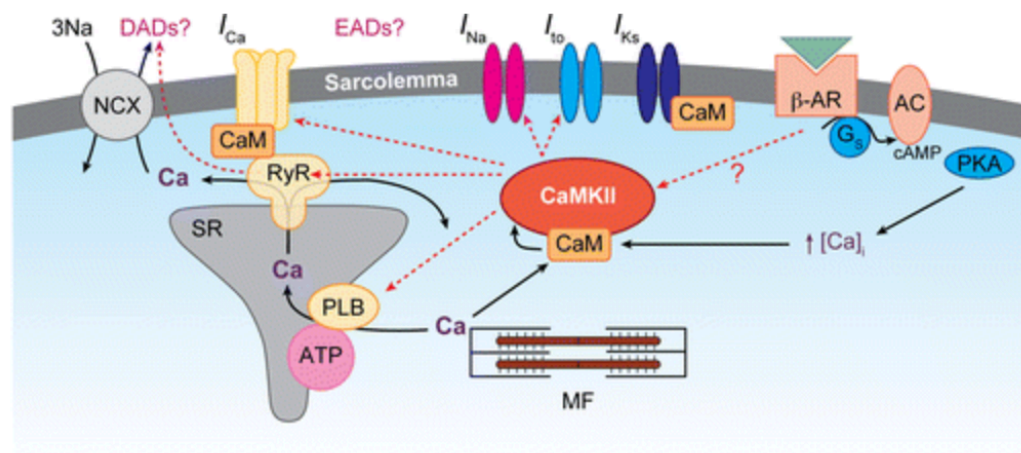
calmodulin dependent protein kinase II (CaMKII) signaling pathways that are necessary for upregulation of genes for further differentiation and development (36). These results are relatively recent and the role of Ca^{2+} cycling in differentiation is just beginning to be elucidated, but it appears to be critical to the development of cardiomyocytes.

Regulation of Ca^{2+} Cycling and CaMKII

As can be seen from the previous discussion, proper handling of Ca^{2+} is paramount to the differentiation and functionality of the cardiomyocyte. Dysfunction in Ca^{2+} cycling pathways are rapidly gaining interest and are believed to be key mediators of cardiac disease (37). Within the cardiomyocyte CaMKII is an important sensor of altered Ca^{2+} handling and an effector of changes associated with altered Ca^{2+} handling (38). CaMKII is a multimeric protein that is comprised of 12 subunits arranged as two hexameric rings in parallel with one another. Monomers assemble around a C-terminal hub, leaving the catalytic N-terminal available for binding of substrates. Within the linker region connecting the N and C-terminus is a regulatory domain which can block catalytic activity of the protein, and under basal conditions result in auto inhibition. Binding of calmodulin (CaM), an intermediate Ca^{2+} binding protein, during periods of elevated $[\text{Ca}^{2+}]_i$ induces conformational change and releases the autoinhibition allowing CaMKII to phosphorylate substrates. During lengthy or high frequency calcium transients CaMKII can autophosphorylate at T287 which increases the affinity of CaMKII for CaM, as well as prevents the regulatory site from reassociating preventing autoinhibition (39). CaMKII has several targets that directly affect intracellular calcium cycling in cardiomyocytes, and evidence is mounting that the CaMKII pathway is a core mechanism for promoting heart failure (40).

One of the most controlled processes in cardiomyocytes is the reuptake of Ca^{2+} into the SR post contraction via SERCA channels. SERCA reuptake is controlled through the regulator protein phospholamban (PLN), a 52-amino acid protein which is highly conserved among many species, highlighting its critical role. The action of PLN is regulated via phosphorylation of serine 16 and threonine 17 residues. In its unphosphorylated state PLN is found closely associated with the SERCA channels and inhibits the reuptake of calcium by altering the affinity of SERCA channels to Ca^{2+} . Phosphorylation of PLN is controlled via the action of cAMP-dependent protein kinase (PKA) and CaMKII with PKA phosphorylating Ser16 and CaMKII, Thr17. Following phosphorylation, PLN disassociates from SERCA and allows for greater uptake of Ca^{2+} into the SR. Phosphorylation at either site is sufficient to release the inhibition of SERCA (41). Large amounts of evidence now suggest that defects in the reuptake of Ca^{2+} into the SR, under the control of PLN, is a key factor in the development of cardiovascular disease (42).

In addition to PLN, RyR and VDCCs are other key substrates for CaMKII and its effector role in Ca^{2+} homeostasis (Figure 2.2) (43). Under non-diseased states the synergistic effects CaMKII can bring about can be observed in its role in the “fight-or-flight” response. In this mechanism, as a response to stimulus, Ca^{2+} is released from the SR into the cytoplasm where it activates CaMKII. CaMKII then phosphorylates VDCC which allow for more frequent longer opening of this channel, phosphorylates RyR2 which increases the force of contraction, and lastly phosphorylation of PLN increases the rate of reuptake and sequestration of Ca^{2+} into the SR (43).




 Bers DM. 2008.
Annu. Rev. Physiol. 70:23–49

Figure 2.2 - CaMKII regulation in cardiomyocytes. Figure taken from (19)

Hypertrophy and Dysfunction in Calcium Cycling

During development hypertrophy is necessary to populate the rapidly expanding myocardium however, as a response to increased demand the same pathways that occur during physiological hypertrophy can get activated and can induce pathological hypertrophy. Increased demand can be brought about through a variety of mechanisms including pressure overload, mutations in sarcomeric proteins, or loss of cardiomyocyte mass due to a previous infarction. In pathological hypertrophy as the myocardium is put under increased load, myocytes attempt to compensate by increasing their size, increasing protein synthesis, and heightening organization of the sarcomere. Hypertrophic growth is commonly presented with many forms of heart disease including ischemic disease, hypertension, and congestive heart failure (44).

The onset of pathological hypertrophy has been well documented however the molecular mechanism that underlie this process are still being discovered. Unsurprisingly,

as with developmental hypertrophy it is becoming more evident that calcium cycling is a key mediator in the process of pathological hypertrophy. In 1986 Pearce et. al. was one of the first to show that increased intracellular calcium loads are associated with initiation of cardiomyocyte hypertrophy (45). In 1999, pharmacological studies began to show a link between CaMKII and hypertrophic responses in cardiomyocytes as measured by increased expression of atrial natriuretic factor (ANF), a marker of hypertrophy (46). Since this study numerous groups have studied the role of CaMKII in hypertrophy and heart failure and have shown that CaMKII activity is increased in animal and human models of heart failure, that overexpression of CaMKII causes hypertrophy and heart failure, and that inhibition of CaMKII improves hypertrophy and heart failure (40).

Calcium cycling changes that accompany pathological hypertrophy may also help to provide a greater understanding of the role of calcium in developmental pathways. One of the key indicators of hypertrophy is a reversion to the fetal like gene expression pattern that is observed during development (47). Stress signaling pathways that are activated during pathological hypertrophy largely locate to the nucleus where they activate transcription factors, and other epigenetic regulatory mechanisms such as microRNA production ultimately effecting gene expression (47). Fetal gene expression is characterized by increases in myosin heavy chain β (MYH7), increases in the early forming transcription factors such as GATA4 and NKX2.5 and downregulation of adult cardiac genes such as SERCA (48). It can be hypothesized that pathological hypertrophy is a resetting of myocytes to their early fetal like state and that by understanding the molecular mechanisms associated with pathological hypertrophy, the understanding of the role Ca^{2+} cycling in development and disease can progress.

Current Models of Cardiomyocytes

With an understanding of cardiomyocyte development and physiology this section aims to summarize the currently used models of cardiomyocytes including the advantages and disadvantages of each.

Animal Models

Many different species have been used as a model organism for cardiomyocyte studies including: zebrafish, small mammals such as mice and rats, and larger mammals such as swine. Basic principles such as ECC and CICR are conserved among these species but large differences from human cells do exist. While small mammals are cheap, easier to handle and have a shorter life span than other animals, they have a rapid heart rate that can reach 800 beats per minute (bpm) compared with 72 for humans, which necessitates adaptations in how the heart functions. For example, in humans, SERCA reuptake in the sarcoplasmic reticulum accounts for approximately 76% of calcium released during contraction, whereas in small mammal models it is responsible for 90-92% of calcium release (4).

Larger animal models such as swine and sheep, while more accurate models of human cardiomyocyte physiology than small mammals, are expensive to house and maintain, and still do not model the human myocyte completely. Swine models express a higher ratio of N2BA:N2B tintin isoforms (4). In humans, studies have shown that while total tintin amount remains unchanged in end stage failing hearts, N2BA comprised a greater fraction of tintin amount in these individuals, a key consideration when deciding on an appropriate model (49).

In vitro models Derived from Animals.

To study the molecular mechanism and development of cardiovascular diseases, *in vitro* models of cardiomyocytes are highly sought after. The most commonly used model of cardiomyocytes *in vitro* is neonatal cells isolated from rat or mice pups. Neonatal cardiomyocytes have several advantages over adult myocytes, especially in studies of myofibrillogenesis and myofibrillar function. First, neonatal cells are easier and cheaper to isolate than their adult counterparts. Further, neonatal cells continue to proliferate in culture allowing for larger yields from each animal, and lastly neonatal cells will spontaneously contract in culture after 2-3 days whereas adult cells usually require electrical pacing to achieve contractile activity (50). Neonatal cells however are also somewhat immature in phenotype, an especially important consideration when investigating intracellular Ca^{2+} signaling as this mechanism is typically later to develop (51).

In order to reduce costs associated with animal husbandry immortal cell lines derived from animals are commercially available and purport to be accurate models of cardiomyocytes. One such cell line is the H9c2 myoblast line established in 1976 by Kimes & Brandt that derives from ventricular tissue from a 13 day embryonic rat heart (52). H9c2 cells have been used in numerous study to study myocyte physiology *in vitro* (53-55). H9c2 cells represent a valuable tool for studying myocyte physiology as under normal culture conditions they continue to divide and remain de-differentiated; however, under low serum conditions in the presence of retinoic acid, H9c2 myoblasts will fuse to form multinucleated cells with a low proliferative capacity, more reminiscent of cardiomyocytes. Further, stimulation with electrical stimulation or acetylcholine is capable of firing action potentials and inducing contraction in culture (52, 56). H9c2 cells have

been successfully shown to be animal-free alternative to rat neonatal cells in their ability to model hypertrophy (55). However, analysis and conclusions derived from studies using H9c2 need to be aware that as passage number of these cells increases there are morphological changes to cultured cells, increased oxidative stress, and increased response to cardiotoxic drugs (57).

HL-1 cells were first described in 1991 by Claycomb et. al. and are another popular choice for *in vitro* studies of cardiomyocytes (58). HL-1 cells derive from a mouse atrial cardiomyocyte tumor line and are reported to be the only model of cardiomyocytes that “continuously divide, spontaneously contract, and maintain a differentiated adult cardiac phenotype through indefinite passages” (59). These cells require a specialized media however, that is costly or difficult to manufacture, and many groups report mixed results with use of these cells and their ability to maintain their contractile characteristics (51).

Stem Cells

In order to accurately model the human cardiomyocyte, investigators have been turning to stem cells as a model of cardiomyocytes. Stem cells are defined by their ability to self-renew, and differentiate into specialized cell types (60). The use of stem cells as a model of cardiomyocytes provides many advantages over the previously discussed animal lines. First is their obvious ability to mimic the human phenotype more accurately than any animal model. Second, culture of stem cells is relatively cheap compared with animal husbandry, and self-renewal allows for long term culture and continuity of cell lines through multiple studies.

Stem cells can be broken down into two classes based on their potency, or ability to differentiate to different cell types. The first class of stem cells discussed in this section are

adult stem cells. Adult stem cells are stem cells which exist in the post-natal body and function to replace dying cells or regenerate damaged tissues. Adult stem cells have been isolated from fetal structures such as umbilical cord blood and matrix (61), Wharton's jelly (61), and amniotic fluid (62). Post-natal, adult stem cells are found in high number in bone marrow, but have been identified in other structures such as dental tissue (63, 64). Perhaps the most widely studied adult stem cells are mesenchymal stem cells which are multipotent stem cells that have been shown to differentiate into many cell types including mesenchymal tissues such adipocytes, chondrocytes, osteocytes, as well as endodermal tissues such as hepatocytes and ectodermal tissues such as neurons (65). Less potent tissue specific adult stem cells have also been identified including neural stem cells which can only differentiate to neural or glia (66), and cardiac stem cells which differentiate primarily to myocytes but can also differentiate to smooth muscle and endothelial cells (67). The other class of stem cells are pluripotent stem cells. Pluripotent stem cells can be isolated from the inner cell mass of blastocyst stage embryos in which case they are termed embryonic stem cells (ESCs) (65) or can arise from reprogramming of somatic cells using various techniques which are termed induced pluripotent stem cells (iPS) (68). Pluripotent stem cells are capable of differentiating to any cell type of the adult body (65).

Adult Stem Cell Derived Cardiomyocytes

Adult stem cells derived cardiomyocytes would be represent a great tool for both clinical use due to the ability for use in autologous (the use of a patients own stem cells) transplantation and associated immune compatibility, as well as *in vitro* experimentation due to their easy, ethically uncontentious isolation. Adult stem cell therapies were some of first to be investigated clinically with studies transplanting these cells following myocardial

infarctions in an effort to reverse remodeling processes. Clinical transplantation of adult stem cells such as mesenchymal stem cells has shown improvement when transplanted post myocardial infarction, including improved ejection fraction and decreased scar size post infarction. However, these studies have failed to show engraftment of transplanted cells leading to the prevailing hypothesis that transplanted adult stem cells provide paracrine signaling rather than directly engrafting and repopulating the myocardium (69). Many groups hypothesize that increased engraftment will lead to greater clinical outcomes in cellular cardiomyoplasty procedures. In order to improve engraftment, it has been suggested that adult stem cells could be precommitted to a cardiac lineage prior to transplantation (70, 71). While hypothesized, the ability to precommit adult stem cells to a cardiomyogenic lineage has proved to be elusive. Studies of mesenchymal stem cells *in vitro* have generated cells that appear to express cardiomyocyte-like proteins but fail to functionally differentiate including lack of contraction (72).

In addition to using mesenchymal stem cells as a potential source for cardiomyocytes, the last two decades have brought about a paradigm shift from the understanding that the myocardium is a terminally differentiated structure that does not undergo myocyte replacement to one which does have some natural turnover, albeit at very low numbers by cardiac stem cells (CSC). The first report of the presence of CSCs was in 2003 by Beltrami *et al.* who report a population of cardiac stem cells in rats that are defined by the expression pattern $\text{Lin}^- \text{C-kit}^+$ that are self-renewing, and give rise to cardiomyocytes, endothelial cells and smooth muscle cells (73). Since the first reported publication there has been much debate about the existence and nature of CSCs, and many different populations of CSCs have been identified. *In vivo* these cells are very rare and a recent publication has estimated

that these cells make up just 0.005-2% of all adult cardiac cells (74). Whether or not c-kit^+ cells are actually CSCs is also still being debated in the literature. Co-localization studies have shown that c-kit^+ cells do not colocalize with NKX2.5 or cTnT both markers of cardiac differentiation, but do localize with endothelial cells. Following left anterior descending artery ligation, fate mapping studies showed that these c-kit^+ cells showed no differentiation to myocytes, suggesting the phenotype of these cells is that of an endothelial cell and not a resident cardiac stem cell (75).

A new potential source for adult stem cell derived cardiomyocytes is hypothesized in chapter three of this report. In these studies we characterize the differentiation potential of neural crest stem cells isolated from dental tissue, and subject them to infrared stimulation in an attempt to generate a contractile cardiomyocyte model from adult stem cells.

Pluripotent Stem Cells

Pluripotent stem cell derived cardiomyocytes have shown the most promise *in vitro* as a model of human cardiomyocytes. Under proper culture conditions these cells have been shown to successfully differentiate into cardiomyocytes which beat spontaneously, express appropriate sarcomeric proteins and ion channels, and display cardiac type action potentials and calcium cycling; however, these characteristics are more representative of developing fetal hearts and not that of adult myocytes (76). The first studies of embryonic stem cell derived cardiomyocytes demonstrated that the cells, while contractile and displaying Ca^{2+} transients, were insensitive to drugs that interfere with sarcoplasmic calcium release such as ryanodine (inhibitor of RYR2 channels), thapsigargin (inhibitor of SERCA channels), or caffeine (elicits rapid release of Ca^{2+} from the SR). Further, these studies have shown that verapamil, an inhibitor of VDCC channels was successful in inhibiting contraction

indicating that observed calcium transients in pluripotent stem cell derived CMs are transsarcolemma calcium influx rather than SR calcium release. Lastly, these studies showed that there was no protein expression of the SR regulatory proteins calsequestrin or phospholamban. Taken collectively, early studies of pluripotent stem cell derived cardiomyocytes suggested that Ca^{2+} handling of these cells is not an accurate model of the adult phenotype likely due to SR immaturity (77).

Since these first reports new protocols to differentiate pluripotent stem cells to cardiomyocytes have emerged which have helped to develop a model of cardiomyocytes that cycle Ca^{2+} through the SR as would more indicative of the adult phenotype. In a recent study undertaken by Hwang et al. the authors studied three independently generated induced pluripotent stem cell derived cardiomyocytes (iPS-CM) to compare the relative maturity of calcium cycling. Cell lines derived from Stanford University, Vanderbilt University, and the University of Wisconsin were developed and differentiated using different protocols and showed that between day 15 and 21 post induction of differentiation, calcium cycling switches from a transsarcolemma to a SR mediated cycling pattern. After 21 days all three cell lines were responsive to caffeine, indicating functional SR stores, and the authors therefore conclude that iPS-CM are capable of displaying “relatively mature” calcium cycling (78). It is important for any study to fully characterize the calcium cycling parameters of pluripotent stem cell derived cardiomyocytes before further experiments into these pathways, as done in chapter 4 of this report.

Nicotine and Stem Cells

Stem cells have helped the scientific community to gain greater insight into the molecular mechanism underlying diseased state than ever before. For the first time,

researchers are able to induce diseased state and characterize the changes in cell processes associated with this transition. In addition, manipulation and innervation at various stages can be achieved and studied to allow for the development of future therapeutics. Chapter 4 of this report aims to use a pluripotent stem cell model to model the effects of nicotine on cardiomyocyte development. The following sections summarize effects of nicotine on cardiovascular health, routes of exposure of nicotine, detail the nicotinic acetylcholine receptor and summarize the known effects of nicotine on stem cells.

Health Effects

Nicotine usage has long been known to be a risk factor for the development of cardiovascular disease. It is thought that initiation of cardiovascular disease from smoking is largely the result of atherosclerosis. As a result of several mechanisms including reduced nitric oxide availability, increased expression of adhesion molecules, and endothelial dysfunction, platelets begin to adhere to vessel walls along with macrophages, creating a procoagulant and inflammatory environment (79). As this process continues, the artery becomes more occluded and in a large number of patients eventually becomes completely occluded leading to a myocardial infarction. It has been estimated by the World Health Organization that women who actively smoke cigarettes have a six-fold higher increase of undergoing an MI and three times higher in males. Additionally, of active smokers who undergo an MI, 56% will continue to actively smoke 1 year after the infarction (80).

Following an MI the heart undergoes many changes that negatively impact performance of the myocardium including remodeling of the ischemic site by infiltrating fibroblasts and the creation of scar tissue. Studies have shown that single MI can wipe out up to 25% of the myocyte population in a few hours (32). To compensate the non-ischemic

myocytes in the myocardium begin to undergo pathological cardiomyocyte hypertrophy. Sustained hypertrophic responses may ultimately lead to heart failure and the pathophysiology of hypertrophy is commonly associated with various adverse outcomes including ischemic disease, hypertension, and heart failure (44, 81). In a recent 2016 study of 422 clinical patients, Li et. al. showed that cigarette smoking was statically correlated with higher incidence of cardiomyocyte hypertrophy (25).

Route of Exposure

Exposure to cigarette smoke, which contains over 7,000 chemicals and 250 known toxins (82), can occur through several different methods. Mainstream or “first-hand” smoke is the predominant form of toxic exposure for active smokers and is generated from the filtered end of the cigarette. Smoke produced from the lit end of the cigarette is considered sidestream or “second-hand” smoke and affects both active smokers and innocent bystanders. “Third-hand” smoke is also a possible route of exposure occurring through direct contact with surfaces containing main- or sidestream smoke deposits. Exposure to ecig vapor can occur in similar fashions, except ecigs do not produce any “sidestream” smoke.

Internalization of cigarette smoke or ecig vapor occurs primarily through the respiratory system. The absorption of nicotine into specific tissues is largely dependent on the pH of tissue (83). Nicotine is a weak base (pKa of 8.0) and is therefore more readily absorbed in slightly basic conditions where nicotine is less “ionized” (83). Flue-cured cigarette smoke is slightly acidic (pH 5.5-6.0); therefore, the nicotine delivered from cigarette smoke is not rapidly absorbed in the naturally acidic oral cavity (83). However, recent reports suggest that cigarette smoke may be more alkaline than originally thought

(83), thereby increasing nicotine absorption in the oral cavity. Ecig liquids, on the other hand, is characterized by a slightly more basic pH (84). Therefore, it is believed that nicotine delivered from these devices is more readily absorbed in the mouth than nicotine delivered from traditional cigarette smoke. Nicotine has also been measured in smoker saliva, which traps ionized nicotine and maintains elevated levels of exposure in the mouth. In fact, salivary nicotine has been measured to be almost 10.5 times higher than in the blood plasma (85). After the oral cavity, the smoke/vapor passes into the lungs, where the physiological pH (7.4) and large surface area of the alveoli facilitate rapid absorption of nicotine into the bloodstream for subsequent total body distribution via the circulatory system (83). In pregnant individuals nicotine is known to rapidly cross the placental barrier and fetal concentrations of nicotine are generally 15% higher in fetal blood versus maternal blood (10).

Nicotine and Nicotinic Acetylcholine Receptors

Nicotinic acetylcholine receptors (nAChRs) belong to the cholinergic family of receptors and are a class of ligand-gated ion channels that respond to the neurotransmitter acetylcholine as well as other ligands such as choline and nicotine. Functional nAChRs are composed of 5 transmembrane subunits that are arranged together to form a transmembrane pore. These pentameric receptors are created from various combinations of the 16 different nAChR subunit types. All subunits share the same molecular structure: an extracellular domain, four transmembrane subunits (TM1-TM4), and a cytoplasmic domain; however, each subunit has differences in its amino acid sequence (26) (Figure 2.3). Accordingly, subunits are classified as either α or non- α type based on the presence of a cysteine-cysteine residue within the N-terminal domain near the entrance to TM1 (26). The Cys-

Cys pair is only found on α subunits and is required for agonist binding. In total, there are 9 α subunits: $\alpha 1-7$, $\alpha 9$, $\alpha 10$, ($\alpha 8$ is identified in avian libraries but has not been observed in mammalian species) and 7 non- α subunits: $\beta 1-4$, γ , δ , and ϵ (26, 86).

The affinity for ligands and the ion gating properties of the nAChR depends on the specific subunit composition of each receptor (26). For instance, the binding affinity for nicotine, a typical nAChR agonist, is higher in nAChRs that contain the $\alpha 4$ subunit versus those that contain the $\alpha 7$ (87). This specificity is also observed for binding of receptor antagonists, which can competitively bind to nAChRs causing desensitization and inhibit activation. α -bungarotoxin (α -BTX), for example, binds specifically to $\alpha 7$ nAChR (88), whereas dihydro- β -erythroidine (DH β E) binds specifically to $\alpha 4$ containing nAChRs (28). On the other hand, mecamylamine (MECA) is a non-specific antagonist and therefore it binds to all nAChRs, regardless of subunit composition (89). In addition to ligand affinity these receptors also vary in their ion gating properties. For example, nAChRs composed of $\alpha 4$ subunits are much less permeable to Ca^{2+} ions than the $\alpha 7$ homopentameric nAChRs, which are considered to be the most permeable nAChR to Ca^{2+} (87).

nAChRs are highly conserved among all species and are widely expressed throughout the body; however, they are predominantly found in muscle (muscular nAChRs) and neuronal (neuronal nAChRs) tissues. Muscular nAChRs are found in skeletal muscles where they mediate neuromuscular transmission at the neuromuscular junction. Neuronal types, on the other hand, are mainly found in the peripheral and central nervous systems, but have been located in non-neuronal tissues including stem cells (90, 91). Muscle nAChRs are heteropentameric (i.e. 5-different subunits) and consist of $\alpha 1$, $\beta 1$, γ , and either δ or ϵ subunits in the 2:1:1:1 stoichiometric ratio (26). Neuronal nAChRs, however, can

exist as either hetero- or homopentamers (i.e. 5-identical subunits). Heteropentameric nAChRs are the more predominately found form of neuronal nAChR as they can exist in several different combinations. For example, studies show that $\alpha 2-4$ and/or $\alpha 6$ nAChR subunits typically assemble with $\beta 2$ and/or $\beta 4$ subunits, but they can also assemble with $\alpha 5$ or $\beta 3$ subunits to make functional nAChRs (86). Homopentameric nAChRs, on the other hand, are less diverse and can only be formed from $\alpha 7$, $\alpha 9$, and $\alpha 10$ subunits (Figure 2.3).

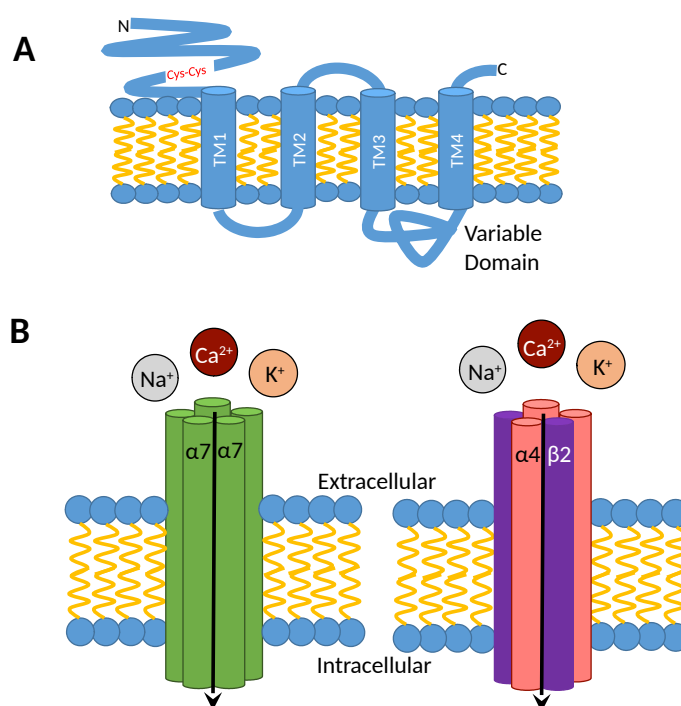


Figure 2.3 - A: Subunit structure of nAChR showing the cys-cys pair that defines α -subtype nAChRs. B: A prototypical $\alpha 7$ homopentameric nAChR (left) and heteropentameric $\alpha 4 \beta 2$ nAChR (right).

Multiple groups have reported the presence of nAChRs in both adult and pluripotent stem cells (Table 2.1). In regards to human ESC's all subunits have been identified at the gene level, whereas only $\alpha 3$ and $\alpha 7$ have been identified on the protein level (92). Confirmation of RT-PCR results were carried out for $\alpha 3$, $\alpha 4$, $\alpha 7$, $\beta 2$ and $\beta 4$ using immunohistochemistry which showed that of those studied only $\alpha 3$ and $\alpha 7$ were present

(92). Meanwhile, non-human primate ESC's (nhpESC) show expression of $\alpha 1$, $\alpha 5$, $\alpha 7$, $\beta 1$, and $\beta 2$ subunits at the genetic level (93). This data however is incomplete as these were the only subunits that were investigated in these studies. These subunits were selected as they represent the most likely subunits found in the downstream application investigated, nhpESC derived lung epithelial cells (93). Murine ESC's show genetic expression of $\alpha 3$, $\alpha 4$, $\alpha 7$ and $\beta 2$ subunits (93), but, similar to the previous studies this study only investigated these specific subunits. Murine iPSCs have been shown, via western blot, to express $\alpha 4$ and $\alpha 7$ and lower expression of $\alpha 1$ and $\alpha 3$ relative to $\alpha 4$ (28). Once again, however, only a limited number of subunits were investigated: $\alpha 1$, $\alpha 3$, $\alpha 4$, $\alpha 7$ and $\alpha 9$ (28). In another study, the same group verified detection of the $\alpha 4$ and $\alpha 7$ subunits through immunofluorescence and western blot (94). All of these results have been compiled by investigating small subsets of possible subunits, and a complete study of all genes and proteins of possible subunits has yet to be completed. In addition to this, none of these studies performed immunostaining or western blot using knock out controls. It has been previously shown that the antibodies for $\alpha 3$, $\alpha 4$, $\alpha 7$, $\beta 2$, and $\beta 4$ subunits are not highly specific and that data utilizing either immunoblotting or immunostaining for these subunits should be coupled with additional technical data to support these findings (95).

Table 2.1- Review of expression of nAChR in stem cells Summary of stem cell nAChR expression from studies reviewed in text. Brackets denote which subunits were investigated in each respective study. N/A corresponds to a lack of any subunit investigation.

Pluripotent Stem Cells						
Cell Source	Species	Subunit Expression	mRNA	Subunit Protein Expression	Functional nAChRs	Ref
iPSC	Murine (20D17)	N/A		α : $\alpha 4, \alpha 7$ β : N/A [$\alpha 1, \alpha 3, \alpha 4, \alpha 7, \alpha 9$]	$\alpha 4, \alpha 7$	(28)
iPSC	Murine (20D17)	N/A		α : $\alpha 4, \alpha 7$ β : N/A [$\alpha 4, \alpha 7$]	$\alpha 4, \alpha 7$	(94)
ESC	Monkey (nhpESC 4706)	α : $\alpha 1, \alpha 5, \alpha 7$ β : $\beta 1, \beta 2$ [$\alpha 1, \alpha 5, \alpha 7, \alpha 9, \beta 1, \beta 2$]	$\alpha 1, \alpha 5, \alpha 7$	N/A	N/A	(93)
ESC	Murine (CGR8)	α : $\alpha 3, \alpha 4, \alpha 7$ β : $\beta 2$ [$\alpha 3, \alpha 4, \alpha 7, \beta 2$]	$\alpha 3, \alpha 4, \alpha 7$	N/A	N/A	(96)
ESC	Human (WH09)	α : $\alpha 1 - \alpha 7, \alpha 9, \alpha 10$ β : $\beta 1 - \beta 4$ [$\alpha 1 - \alpha 7, \alpha 9, \beta 1 - \beta 4$]	$\alpha 1 - \alpha 7, \alpha 9, \alpha 10$	α : $\alpha 3, \alpha 7$ β : N/A [$\alpha 3, \alpha 4, \alpha 7, \beta 2, \beta 4$]	N/A	(92)
Adult Stem Cells						
Cell Source	Species	Subunit Expression	mRNA	Subunit Protein Expression	Functional nAChRs	Ref
BM-MSCs	Human	α : $\alpha 3, \alpha 5, \alpha 7$ β : N/A [$\alpha 3, \alpha 5, \alpha 7, \alpha 9, \beta 2 - \beta 4$]	$\alpha 3, \alpha 5, \alpha 7$	N/A	$\alpha 7$	(97)

MSCs	Human	α : $\alpha 1 - \alpha 5, \alpha 7, \alpha 9$ β : $\beta 2 - \beta 4$ [$\alpha 1 - \alpha 10, \beta 1 - \beta 4$]	α : $\alpha 7$ β : $\beta 2, \beta 4$ [$\alpha 3, \alpha 4, \alpha 7, \beta 2, \beta 4$]	$\alpha 7$	(98)
BM-MSCs	Human (M)	α : $\alpha 3, \alpha 5, \alpha 7, \alpha 9$ β : N/A [$\alpha 2 - \alpha 7, \alpha 9, \alpha 10$]	N/A	N/A	(99)
	Human (F)	α : $\alpha 2, \alpha 5 - \alpha 7, \alpha 9, \alpha 10$ β : N/A [$\alpha 2 - \alpha 7, \alpha 9, \alpha 10$]	N/A	N/A	
PDLSC	Human	α : $\alpha 7$ β : $\beta 4$ [$\alpha 1 - \alpha 7, \beta 1 - \beta 4$]	N/A	$\alpha 7$	(89)

Nicotine Exposure Effect on Development and Stem Cells

Studies looking at the role of nicotine and nAChR's in development are few and far between. There is a need for these studies however as nicotine is known to cross the placental barrier nicotine concentrations in the fetus can be 15% higher than maternal levels (10). In one of the few studies published, Ishizuka *et. al.* exposed murine iPS cells to 300 nM nicotine and showed that exposure induced significantly increased DNA synthesis in both naïve iPS cells and iPS derived mesodermal progenitor cells. This result could be inhibited by pretreatment with dihydro- β -erythrodine (DH β E), a specific $\alpha 4$ nAChR antagonist, α -bungarotoxin, a specific $\alpha 7$ nAChR antagonist, or KN-93 a CaMKII inhibitor (28).

Regarding cardiac development, a recent study looked at the exposure of zebrafish to tobacco smoke and e-cigarette extract and the associated effects on cardiac development. In zebrafish, following 72 hour exposure of 6.8, 13.7, and 34 μ M nicotine, the 34 μ M showed 0% survival and therefore the effect on cardiac development was not assayed. Of

those that were assayed cardiac development displayed increased defects in a dose dependent manner for the groups receiving cigarette smoke extract and e-cigarette extract, but interestingly not for those that received nicotine alone. Following 24 hour exposure, both the tobacco group and e-cigarette group showed decreases in the contractile genes CMLC2, and TNNT2, the transcription factor MEF2CA and the major gap junction in the myocardium GJA1. Additionally, observed was increase in the cardiac homeobox gene NKX2.5, but only in the tobacco cigarette group (100).

Ishizuka *et. al.*'s data suggests CaMKII activation is a mediator of the effects of nicotine, however studies looking at CaMKII activity and nicotine usage in the heart have not been carried out. In neurological studies, however, it has been observed that activation of CaMKII is related to nicotine's addictive properties and associated withdrawal symptoms. Evidence has shown that $\beta 2$ containing nAChR's mediate nicotine induced increases in CaMKII activation, and phosphorylation levels in several regions of the brain. Following cessation these phosphorylated levels reduce back down. Recently, Jackson *et. al.* studied showed the role CaMKII signaling plays *in vivo* using nicotine conditioned place preference (CPP) in C57Bl/6 mice. After administration of CaMKII antagonists, KN-62 and KN-93 nicotine induced CPP diminished indicating a role of CaMKII in the nicotine reward pathway in mice. (101). Chapter 4 of this report uses induced pluripotent stem cells to examine the effects of nicotine on cardiomyocyte development, including the role of nicotine induced CaMKII activity, and alterations in calcium cycling in iPS-CM treated with nicotine.

CHAPTER 3. ADULT STEM CELL DERIVED MODEL

Motivation

Myocardial infarction (MI) remains a leading cause of death worldwide (102). Following MI, there is a significant decrease in the number of functional cardiomyocytes, and extracellular matrix deposition by infiltrating fibroblasts leads to adverse myocardial remodeling (103). Current treatments post-MI aim to slow the decline in cardiac function caused by this deposition, but are unable to reverse the remodeling process (104). Within the last 20 years, however, cellular cardiomyoplasty has emerged as a potential therapy to help reverse myocardial damage that occurs as a result of an infarction (105). These therapies apply the perfusion of stem or progenitor cells following an MI in an effort to repopulate the myocardium with functional myocytes. Clinically, patients receiving perfusions of these cells showed modest improvement in cardiac functional parameters, such as increased ejection fraction and decreased end-systolic volume (106).

Mesenchymal stem cells (MSCs) were the first cell source to be investigated for cellular cardiomyoplasty (105). MSCs rapidly progressed through small and large animal preclinical models, and transplantation of MSCs showed gains in cardiac function following an MI; however, these results have been largely attributed to paracrine mechanisms as transplanted cells show low survival, engraftment, and differentiation in the host myocardium (107). The plasticity of MSCs toward a cardiomyogenic lineage has been debated in the literature, with several groups reporting the ability of MSCs to transdifferentiate into cardiomyocyte-like cells that exhibit a phenotype of cardiomyocytes, but fail to contract as functional cardiomyocytes (108-110).

It has been proposed that to increase the clinical efficacy of cellular cardiomyoplasty applications, transplantation of cardiomyogenic precommitted stem cells may be utilized in future studies (111). This has been clinically verified with the use of cardiopoietic cells in the C-Cure trial. In this trial, MSCs treated with a growth factor cocktail became primed to cardiomyocyte lineage specification and exhibited the cardiomyocyte transcription factors, NKX2.5, MEF2C, and GATA4. These lineage-specific stem cells were found to be safe and effective and are now in later stage clinical trials (112).

Ideally, an easily isolated cell source with high plasticity toward cardiomyogenic lineages would be used for cardiomyoplasty application. One such potential source of cells, which has been proposed, is stem cells derived from dental tissue (113). Dental tissue is known to harbor a population of stem cells, which are reportedly mainly mesenchymal in nature (114). Additionally, *in vitro* differentiation to cardiomyogenic lineages (115), and perfusion studies on small animal models following MI using stem cells derived from dental tissue have been carried out (116). One tissue in which potential stem cells may be found is from periodontal ligament (PDL). For some time, the PDL has been known to have a population of resident stem cells, and the cardiomyogenic potential of these stem cells has been established (117).

Recently, a stem cell subpopulation consisting of neural crest stem cells (NCSCs) residing in the PDL of excised impacted wisdom teeth has been identified. These cells are selected based on expression of migrating neural crest marker, connexin 43 (Cx43). These cells express the pluripotency markers, Oct4, Sox2, and Nanog, and will form teratomas *in vivo* (63, 117). During development, cells from the neural crest undergo an epithelial-to-mesenchymal transformation and migrate to various postnatal tissues (118). These cells

migrate as sheets and streams functionally coupled through gap junctions such as N-Cadherin and Cx43 (119, 120). The myocardium receives a postnatal contribution from the cardiac neural crest (CNC), which gives rise to the cardiac outflow tract, the heart valves, and the great arches (121). The cardiomyogenic potential of CNCs has been widely debated in the literature (122, 123); a recent report, however, shows that CNC cells possess full cardiomyocyte potential, but are undermined by changes in bone morphogenetic protein (BMP) and wnt signaling pathways (124). In addition to their contributions to the aforementioned structures, dormant NCSCs have also been identified in the postnatal myocardium. These cells have also been shown to migrate and differentiate into cardiomyocytes following injury such as MI (123-125). In addition to its role in neural crest migration, Cx43 is also the major gap junction protein in ventricular myocardium and is necessary for the electrical coupling and contractile wave propagation throughout the heart wall (126).

The present study examined the potential of NCSCs for future applications in cellular cardiomyoplasty. We successfully differentiated NCSCs to a cardiomyogenic lineage using chemically defined media. Following differentiation, cells were analyzed using immunostaining for expression of sarcomeric proteins, α -skeletal muscle actin and cardiac troponin I. Additionally, genetic expression for GATA4, MEF2C, TPM1, and GJA1/Cx43 was analyzed. To test the functionality of the stem cell-derived cardiomyogenic cells, pulsed infrared radiation (IR) was used to stimulate NCSC-derived cardiomyogenic cells (NCSC-CMs). Recent research in photonics has highlighted the ability of IR stimulation to stimulate a wide variety of cells, including neurons (127), hair cells (128), cardiomyocytes (129), and other stem cell-derived cells (130). Multiple groups have reported that pulsed

IR evokes intracellular Ca^{2+} responses and contraction in cardiomyocytes, which match the time course of the IR stimuli delivered (128, 129, 131, 132). In the present study, the IR-evoked contraction of NCSC-CM cardiospheres was monitored. Furthermore, we studied whether the derived cells continue to respond to long periods of IR stimulation and whether such stimulation may cause any irreversible damage to the NCSC-CMs.

Materials and Methods

Stem cell isolation and cardiomyocyte differentiation

Human Cx43^+ NCSCs were obtained and cultured as previously described (63). All protocols received University of Miami IRB approval. NCSCs were seeded onto collagen-coated silicone membranes (FlexCell, Hillsborough, NC) at a density of 2000 cells/cm². Membranes measured 5.58 cm² and were placed in polystyrene six-well culture dishes (Falcon, Tewksbury, MA). Culture media consisted of Dulbecco's modification of Eagle's medium (DMEM, Life Technologies, Grand Island, NY) supplemented with 10% heat-inactivated fetal bovine serum (HI-FBS; Atlanta Biologics, Flower Branch, GA), 1% penicillin/streptomycin (Life Technologies), and 0.1% amphotericin B (Thermo Scientific, Waltham, MA). Cells were cultured in these media overnight to promote adherence onto the silicone membranes. Once cells had adhered, cardiomyogenic differentiation was induced by replacing the previously defined medium with DMEM supplemented with 2% HI-FBS, 1% penicillin/streptomycin, 0.1% amphotericin B, 50 ng/mL Dickkopf-related protein 1 (DKK-1; Pepperotech, Rocky Hills, NJ), 25 ng/mL fibroblast growth factor 4 (FGF-4; Pepperotech), 2 ng/mL transforming growth factor β 3 (TGF- β 3; Pepperotech), 10 ng/mL vascular endothelial growth factor (VEGF; Pepperotech), 5 ng/mL Activin A (Pepperotech), 10 ng/mL insulin-like growth factor-1 (IGF-1; Pepperotech), 10 ng/mL

bone morphogenic protein 4 (BMP-4; Pepperotech), 250 nM cardiogenol C (Sigma-Aldrich, St. Louis, MO), and 10 nM oxytocin (Sigma-Aldrich). Differentiation media were replaced every 2 days for 2 weeks. To form aggregates, the cells were lifted using 0.05% Trypsin/EDTA (Life Technologies) and resuspended in DMEM supplemented with 10% FBS, 1% antibiotic–antimycotic, and 0.1% amphotericin B, at a concentration of 500,000 cells/mL. Ten-microliter droplets were placed on 9-mm polystyrene Petri dishes (VWR, Randor, PA). Petri dishes were inverted and cells were cultured according to the hanging drop aggregation assay for 2 days to promote three-dimensional aggregate formation. Aggregates were transferred to a 0.1% gelatin-coated six-well polystyrene dish for stimulation studies.

Immunohistochemical staining

NCSC-CMs were fixed in 10% neutral buffered formalin (VWR) at room temperature for 10 min. Following fixation, cells were washed three times in phosphate-buffered saline (PBS; Life Technologies). Cell membranes were permeabilized in either 0.2% Triton X-100 (Sigma-Aldrich) or with 0.25% Tween-20 (Sigma-Aldrich) in PBS at room temperature for 10 min. Cells were then washed three times and left in blocking buffer solution consisting of 0.05% Tween-20, 1% FBS, and 20 mg/mL bovine serum albumin (BSA; Life Technologies) in PBS for 1 h. After blocking, cells were incubated overnight at 4°C in 5 mg/mL BSA in PBS containing primary antibodies for cardiac troponin I (1:100; Abcam, Cambridge, MA), α -skeletal muscle actin (1:200; Abcam), and MEF2C (Abcam; 5 μ g/mL). Cells were then washed three times in PBS, and incubated in 5 mg/mL BSA in PBS containing secondary antibodies at 1:500 for 2 h at room temperature. Secondary antibodies used were goat anti-mouse Alexa Fluor 488 (Life Technologies) and goat anti-

rabbit Alexa Fluor 546 (Life Technologies). Cells were again washed three times in PBS, and one drop of VectaShield Mounting Media containing 1.5 $\mu\text{g}/\text{mL}$ 4',6-diamidino-2-phenylindole (DAPI; Vector Labs, Burlingame, CA) was added to each well. Cells were mounted with a clean glass coverslip and imaged on a Nikon T2i inverted fluorescence microscope (Nikon, Melville, NY). Background was removed and brightness and contrast adjusted using ImageJ (NIH, Bethesda, MD) software. Care was taken to ensure that equivalent processing occurred for all images.

Gene expression

RNA isolation

Total RNA was isolated by means of TRIzol reagents following the manufacturers' recommended protocol and resuspended in RNase- and DNase-free water. The RNA suspension was then frozen at -80°C overnight and quantified using a NanoDrop[®] spectrophotometer (Nanodrop Products, Wilmington, DE).

Reverse transcription

Reverse transcription of RNA to cDNA was performed by means of the High-Capacity cDNA Reverse Transcription Kit (Applied Biosystems, Grand Island, NY) as per the manufacturer's recommended protocol. Briefly, 1 μg of RNA for each sample was converted to cDNA and then diluted to a final concentration of 10 $\text{ng}/\mu\text{L}$ of PCR-grade water and used for gene expression analysis.

For MEF2C, GATA4, and TPM1, real-time PCR was carried out using the TaqMan[®] Fast universal PCR Master Mix (Applied Biosystems) and TaqMan probe

predesigned primers (Applied Biosystems). For NKX2.5, TNNT2, and GJA1/Cx43, real-time PCR was carried out using SYBR Green PCR Master Mix (Applied Biosystems) and custom-designed primers (Table 1) (Eurofins MWG Operon, Louisville, KY). For all the genes, 20 ng of cDNA was used for each reaction. The reactions were performed using an Agilent Technologies Stratagene Mx3000p real-time PCR system. Each reaction was run in triplicate for each assay and gene expression quantification was carried out by means of the comparative Ct method with GAPDH used as an endogenous control.

Table 3.1 - Custom Primers used for gene expression analysis in adult stem cell derived model

Gene	Forward Primer (5'-3')	Reverse Primer (5'-3')	Accession Number
Cx43/ GJA1	TATTGAAGAGCATGG TAAGG	TAGACTTGAAGAGA GATACTGA	NM_000165.4
TNNT2	GGTTACATCCAGAAG ACAGA	TCCTCTCAGCCAGAA TCT	NM_000364.3
NKX2.5	CTAGAGCCCGAAAAG AAAG	AGCATTTGTAGAAAG TCA	NM_00116617 6.1

Ionomycin assessment of Ca²⁺ stores

Ca520 (UPharm Laboratories, Parsippany, NJ) was stored in 10- μ M aliquots. Ca520 was diluted to 5 μ M in PBS and cells were incubated at 37°C for 90 min. Following dye loading, cells were washed with fresh Ca²⁺-free PBS and further incubated for 20 min at room temperature to allow for full acetoxymethyl (AM) ester cleavage. Imaging was performed at room temperature on a Leica SP5 confocal microscope with resonant scanner (Leica)

with 20 × water immersion objective (14–28 fps). In a subset of the cultures, ionomycin (1 μM), a positive control of Ca 520 AM, was delivered through pipettes positioned over the cells and changes in intracellular Ca²⁺ were measured.

IR stimulation

In this study, pulsed IR was used to assess the functionality of NCSC-CMs and study the elicited aggregate contraction. A Capella pulsed IR laser (Lockheed Martin Aculight, Bothell, WA) coupled to a low-OH 400-μm diameter optical fiber (Ocean Optics, Dunedin, FL) was used to deliver the IR pulses (0.25–2 pps) to the cardiomyocytes. The output fiber was mounted onto a micromanipulator (Narishige, East Meadow, NY) and was positioned roughly 200–400 μm from the cells using a pilot light. The output wavelength was 1862 nm, the pulse width was 2 ms, and the energy output at the fiber tip was ~668 mJ/cm², as measured in air using a digital optical power/energy meter (FieldMax_{II}; Coherent, Santa Clara, CA). This wavelength was selected based on results of previous studies in cardiomyocytes and neurons (127-129, 131).

Contraction analysis

Analysis of contraction of NCSC cardiospheres was accomplished using PIVlab—Time-Resolved Digital Particle Image Velocimetry (PIV) Tool for MATLAB version: 1.4 on a computer running Mac OS X. Videos were captured in AVI format using a Nikon T2i microscope and Nikon NIS-Elements Advanced Research software on a computer running Microsoft Windows 7. Captured AVIs were converted to a stack of TIFF images using ImageJ on a computer running Mac OSX. TIFF stacks were then imported into MATLAB (Mathworks, Natick, MA) for analysis using PIVLab. Analysis was carried out over a

region of interest surrounding the cardiosphere, which was drawn in the PIVLab graphical user interface. PIVlab results were calibrated using a scale bar obtained through still images from a Nikon T2i microscope and processed using Nikon NIS-Elements Advanced Research software on a computer running Microsoft Windows 7. Results from PIVLab were exported to a text file and imported into Microsoft Office Excel 2016 for Mac OSX to generate plots of velocity during stimulation. For spatial analysis, representative frames of contraction were chosen for each frequency investigated. A line vector was drawn using the PIVLab graphical user interface and displacement along the line was output as a text file. This text file was then imported into Microsoft Excel 2016 for plotting of data.

Long-duration stimulation and assessment of mitochondrial potential

Long-term stimulation was applied to NCSC-derived cardiomyocytes for 10 min (1 ms, 3 Hz, 661 mJ/cm²) on a cold pad in a laminar flow hood. Mitochondrial transmembrane potential was assessed at 24 h after stimulation by using 5,5',6,6'-tetrachloro-1,1',3,3'-tetraethyl-benzamidazolylcarbocyanine iodide (JC-1; Life Technologies). JC-1 (1.5 μM) in PBS was loaded for 30 min, following which JC-1-containing loading medium was replaced with fresh PBS, and membranes were mounted onto glass microscope slides and kept on ice until imaging. Carbonyl cyanide 4-(trifluoromethoxy)phenylhydrazone (FCCP; Sigma-Aldrich), a mitochondrial oxidative phosphorylation inhibitor, was used as a positive control for JC-1. FCCP was added to cells at 10 μM in PBS for 1 h and 30 min before JC-1 loading. After 1 h and 30 min, cells were washed in PBS and loaded for 30 min with 1.5 μM JC-1 in PBS. After 30 min, JC-1-containing loading medium was replaced with fresh PBS, and membranes were mounted onto glass microscope slides and kept on

ice until imaging. Imaging of JC-1 fluorescence was performed on a Zeiss LSM700 with a 20 × objective or a 63 × oil immersion objective (Zeiss, Thornwood, NY).

Statistics

The data are expressed as mean ± SEM unless otherwise indicated. qPCR was analyzed using the $\Delta\Delta C_T$ method (133) One-way analysis of variance (ANOVA) test, followed by a Dunnett *post hoc* test for multiple comparisons, was used for JC-1 analyses; *p* value of <0.05 was considered significant. All calculations were performed on a computer equipped with GraphPad Prism v 5.00c software for Mac OS X[®] (Graphad, La Jolla, CA), and graphs were generated using Microsoft Office Excel 2016 for Mac OS X.

Results

Growth factor treatment upregulates genetic expression and protein levels of cardiomyocyte-specific genes and proteins

Initially, NCSCs exhibited a spindle fibroblast-like phenotype. During differentiation, the group receiving the growth factor cocktail cells appears to become more opaque and flattened, both of which are typical of cardiomyocytes. Furthermore, spatial arrangement of cells receiving the treatment appears to be more aligned and organized. After 2-week exposure to the growth factor cocktail, NCSCs showed upregulation of select cardiomyocyte-specific genes and proteins compared with those not receiving the cocktail. At the genetic level, a significant increase was observed in the cardiomyocyte markers, NK2 homeobox 5 (NKX2.5) gene and troponin T type 2 (TNNT2). Although not significant, we also see positive increases in tropomyosin I (TPM1), gap junction protein alpha 1/Cx43 (GJA1/Cx43), and myocyte enhancement factor 2C (MEF2C). (Figure 3.1) NCSC-derived cardiomyogenic cells (NCSC-CMs) also stained positive for

cardiomyocyte-specific proteins, cardiac troponin I (cTnI) and skeletal muscle actin (α -SMA), and showed greater expression and translocation of MEF2C. (Figure 3.2) Cells that were not incubated with the growth factor cocktail stained negative for these sarcomeric proteins.

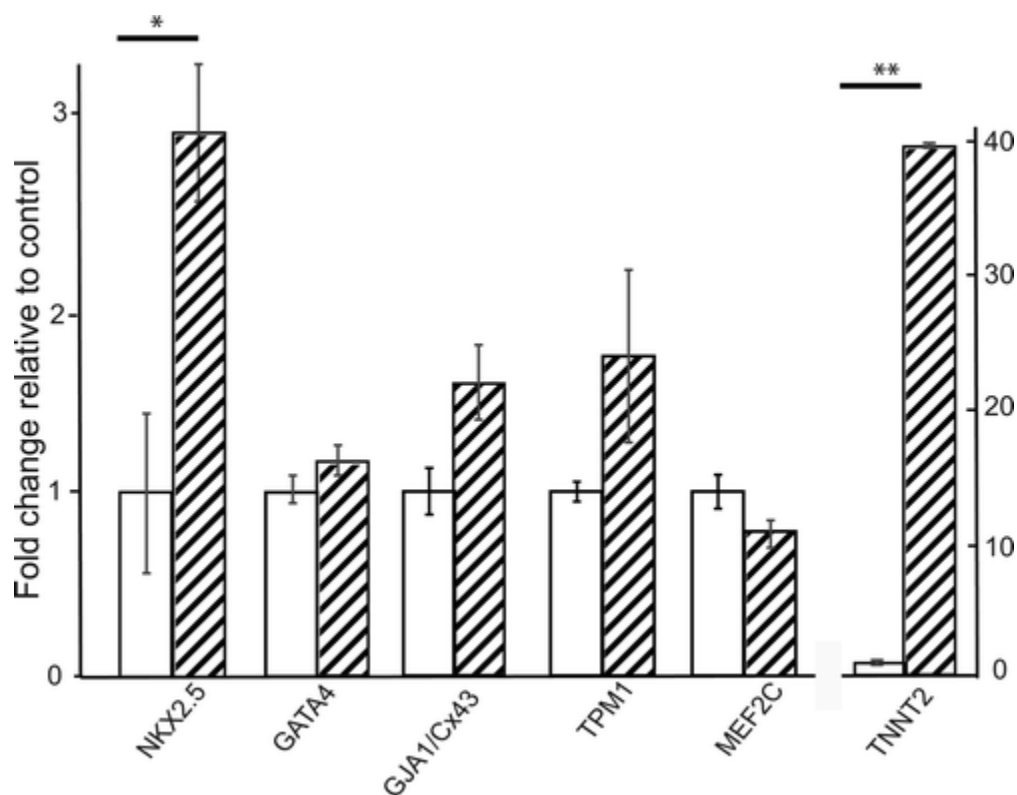


Figure 3.1 - Gene expression. Significant upregulation seen in the early cardiomyocyte-specific transcription factor, NKX2.5 ($p < 0.05$), and cardiac troponin T type 2 (** $p < 0.01$). Also seen is an upregulation, although not statistically significant in gap junction protein alpha 1/Cx43, tropomyosin 1, and a small increase in the cardiomyocyte-specific transcription factor, GATA4.*

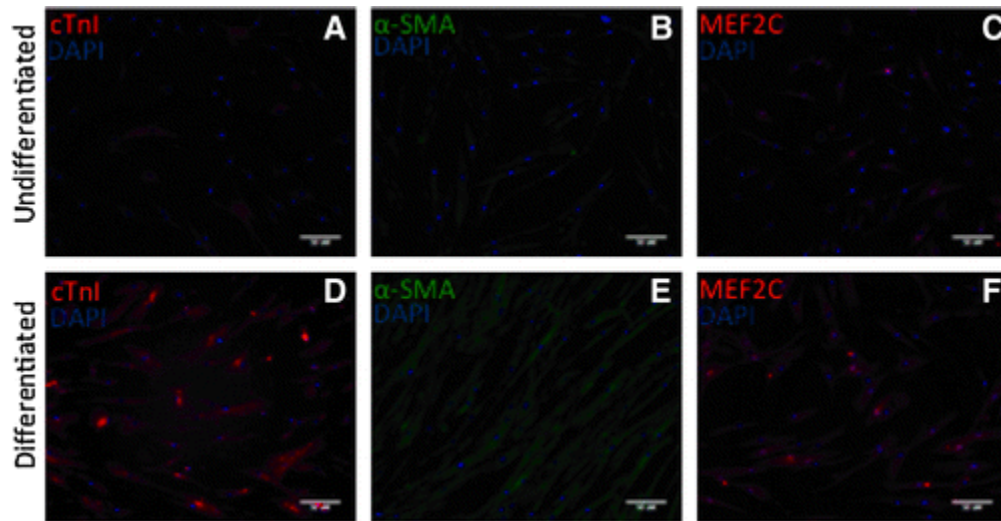


Figure 3.2 - Immunohistochemical analysis of two important proteins: the sarcomeric proteins, cardiac troponin I (cTnI) and skeletal muscle actin (α -SMA), in NCSC-CMs after completion of the 2-week growth factor cocktail regime. Control cells grown under identical conditions, except for the addition of growth factors, do not express skeletal muscle actin or cardiac troponin I (A, B). However, the NCSC-CMs showed a robust expression of the two proteins (D, E). Differentiated cells also show increased expression and translocation of MEF2C (C, F). NCSCs, neural crest stem cells-derived cardiomyogenic cells.

Cardiomyocytes derived from NCSCs are excitable

Multiple studies have shown that infrared stimulation leads to an intracellular Ca^{2+} response and contraction in cardiomyocytes (128, 129, 131, 132). In the present study, we analyzed if IR also elicits similar contraction of aggregate cardiospheres.

First, we sought to determine whether differentiated cells possessed stores of Ca^{2+} , which could be stimulated for release. Intracellular Ca^{2+} transients in NCSC-CMs were monitored with Ca^{2+} -sensitive Ca 520 AM dye. Ca^{2+} ionophore ionomycin was used to determine whether NCSC-derived cardiomyocytes possessed stores of Ca^{2+} . Ionomycin depletes intracellular Ca^{2+} stores, leading to a rapid increase in cytosolic Ca^{2+} reflected on a significant increase in Ca^{2+} fluorescence. As expected, addition of ionomycin led to a large increase in normalized fluorescence lasting for a few minutes (Figure 3.3).

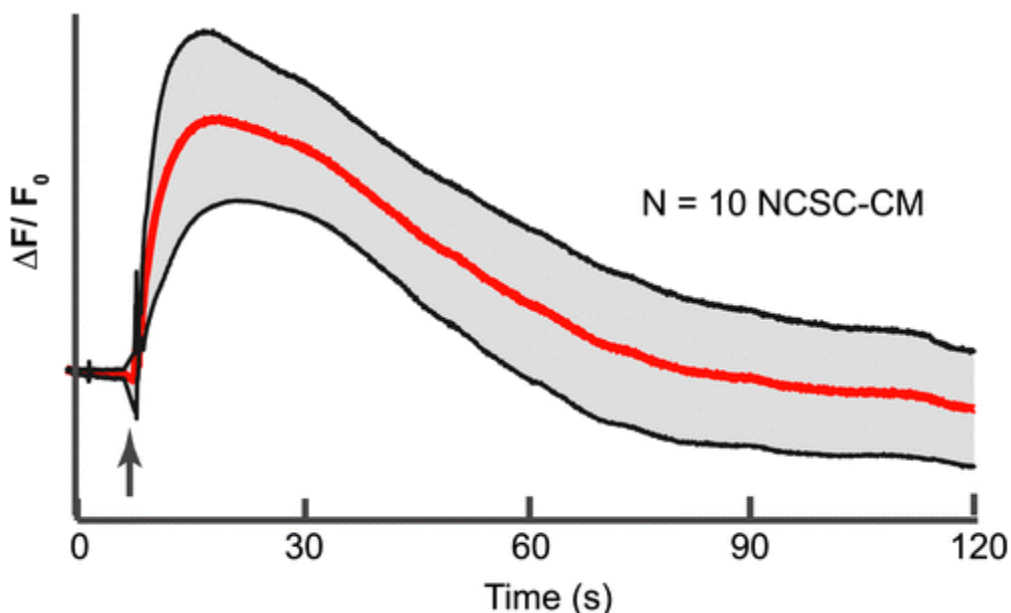


Figure 3.3 - NCSC-CM response in Ca 520 AM fluorescence to ionomycin. Ionomycin is an ionophore-depleting intracellular Ca^{2+} store. As expected, addition of $1\ \mu\text{M}$ ionomycin induced a transient rise in normalized fluorescence in NCSC-CMs, lasting for a few minutes. The arrow indicates addition of ionomycin. Data depicted as mean (red line) \pm 95% CI (gray area bounded by black lines) for $N = 10$ NCSC-CMs.

IR stimulation (0.25–2 pps, 2 ms, $661\ \text{mJ}/\text{cm}^2$) delivered to NCSC-CM aggregates ($N = 5$, $k = 2$) elicited visible contractile behavior. Contraction was measured using PIV analysis (Figure. 3.4). The overall net direction of contraction is away from the IR source, which implies that distance from the IR source affects the velocity of induced contraction. To determine the spatial effects, mean velocity for the three frequencies studied was compared to the distance from the IR source. Data shown are from one trial for comparison purposes. Average velocity of contraction was larger near the bottom of the aggregate, which correlates with being spatially closer to the IR source, and declined as distance from the IR source increased (Figure 3.5). This was also true for the relaxation vector. The mean velocities at the frequencies tested were $3.74 \pm 1.59\ \mu\text{m}/\text{s}$ ($n = 12$) at 0.5 Hz, $6.34 \pm 1.81\ \mu\text{m}/\text{s}$ ($n = 30$) at 1 Hz, and $11.5 \pm 3.82\ \mu\text{m}/\text{s}$ ($n = 60$) at 2 Hz. In the absence of applied stimulation, contractile behavior ceased.

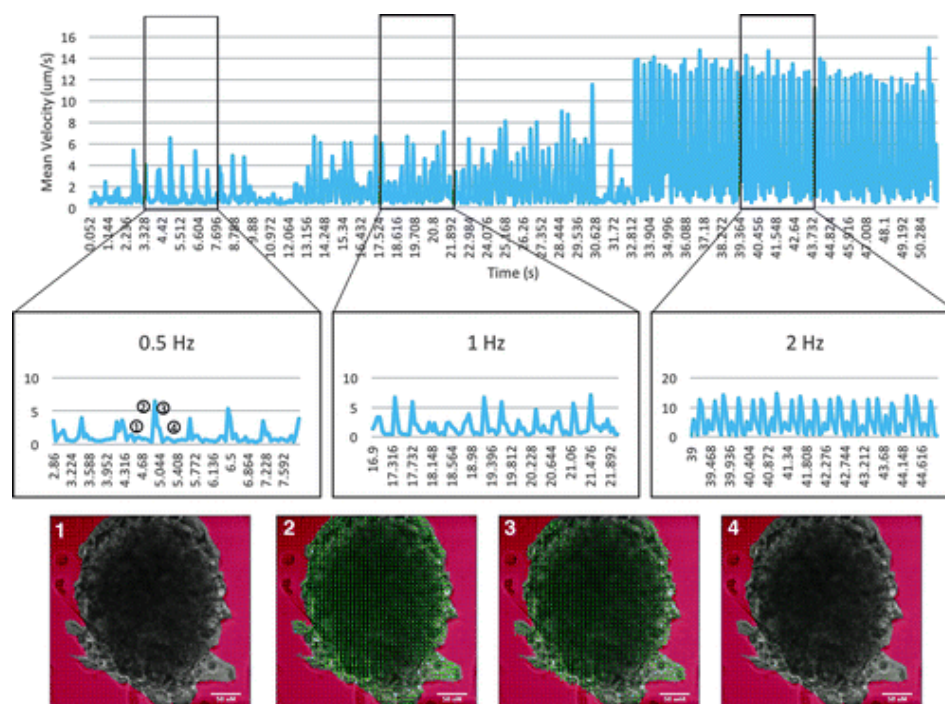


Figure 3.4 - PIV of NCSC-CM cardiosphere. Within NCSC-CM cardiospheres, visible contraction could be observed. Representative velocity vectors of an NCSC-CM cardiosphere undergoing IR-induced contraction (point 2) and relaxation (point 3) were computed using PIV analysis. Both contraction and relaxation are of larger magnitude on the periphery of the aggregate and close to the optical fiber. Images represent sample PIV results of aggregates before contraction (1), during contraction (2), during relaxation (3), and immediately after relaxation (4). IR, infrared radiation; PIV, particle image velocimetry.

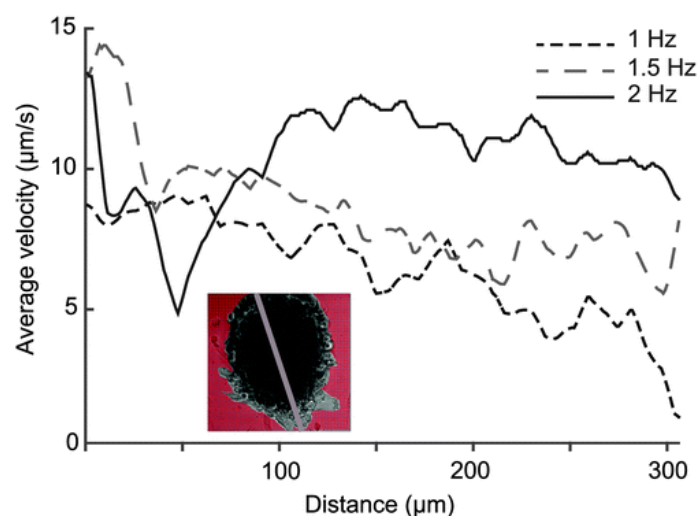
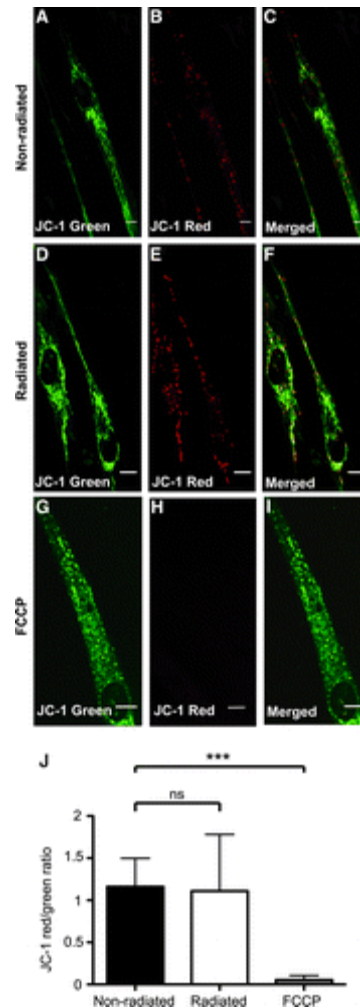


Figure 3.5 - Analysis of spatial effects: average velocity of contraction was measured along the beam path of the IR. The inset shows an NCSC-CM aggregate (the IR source was located in the lower right hand corner). Along the line from the source to the other side of the aggregate, the amplitude of the velocity vector decreased. Additionally, as frequency of stimulation is increased, the magnitude of the velocity of contraction increased.

Long-duration stimulation with IR

Previous studies have shown that the response to IR is dependent on mitochondrial Ca^{2+} cycling. We postulated that IR-induced Ca^{2+} cycling in NCSC-CMs would lead to excessive mitochondrial Ca^{2+} uptake, which may lead to membrane depolarization and permanent opening of the mitochondrial transition pore releasing apoptotic components to the cytosol (cytochrome *c*, smac Diablo, and ROS) (134). To determine if a long period of IR stimulation would cause irreversible damage to the NCSC-CMs, we tested the efficacy of these cells to respond to and survive during long-duration stimulation. Mitochondrial function was assessed by investigating the state of mitochondrial membrane polarization. The NCSC-CMs were radiated for 10 min, and then incubated for 24 h before JC-1 staining. FCCP, a mitochondrial decoupling agent, was used as a positive control for these experiments. JC-1 red aggregates indicating normal resting values of membrane potential could be observed in both radiated ($N=18$ cells) and nonradiated ($N=13$) NCSC-CMs belonging to the same membrane with no significant difference ($p > 0.05$). As expected, FCCP ($N=16$) led to a shift in JC-1 fluorescence emission to green, indicating loss of membrane potential ($p < 0.001$) (Figure 3.6).



*Figure 3.6 - JC-1 staining of NCSC-CMs after long-term IR stimulation. To test whether applied radiation causes permanent mitochondrial membrane depolarization, three different groups were tested using JC-1, a fluorescent sensor of mitochondrial membrane potential. (A–C) NCSC-CMs that were not exposed to any radiation; (D–F) NCSC-CMs grown on the same membrane as (A–C), but exposed to IR (30 pps, 1 ms, 661 mJ/cm²) for 10 min, and cultured for 24 h; (G–I) NCSC-CMs incubated with 10 μM FCCP, a mitochondrial oxidative phosphorylation inhibitor. Both radiated and nonradiated NCSC-CM mitochondria still fluoresce red, an indication that pulsed IR did not induce permanent mitochondrial depolarization in these experimental settings. In NCSC-CMs pretreated with FCCP, JC-1 red aggregates were absent, indicating loss of membrane potential. (J) Representation of JC-1 red/green signal ratios (mean ± SD). Red/green signal ratios were computed in ImageJ for the nonradiated (N = 13), radiated (N = 18), and FCCP-treated (N = 16) NCSC-CMs. Significant difference (***) $p < 0.001$ was observed when comparing both radiated and nonradiated with FCCP-treated NCSC-CMs, but not between radiated and nonradiated (ns, $p > 0.05$). SD, standard deviation.*

Discussion

This study shows the potential of NCSCs for cardiomyogenic application and the applicability of IR stimulation to generate contractile behavior in quiescent cell populations as we were able to engineer contracting tissue that expresses cardiac troponin and skeletal muscle actin. In addition, we show significant upregulation of NKX2.5, which is one of the earliest known markers of cardiac lineages (135). Additionally, NKX2.5 is known to interact with GATA4, which although not statistically significant, we do see a small upregulation of (115, 135). The smaller than expected increase is not surprising as cells of the migrating neural crest origin are known to also express GATA4 (136). This is also true of MEF2C; however, the translocation into the nucleus may show activation of the transcription factor (137). The smaller increase in GJA1/Cx43 is likely a result of our cells being selected on expression of connexin 43. Thus, with the increase in NKX2.5 coupled with the large increase in TNNT2 expression and immunohistochemical data, we hypothesize that NCSC-derived cardiomyocytes are similar to that of other MSCs where differentiated cells demonstrate upregulation of cardiomyocyte-specific genes and proteins, but do not exhibit cardiomyocyte functionality (72). To our knowledge, we are the first group to demonstrate *in vitro* differentiation of NCSCs and show that IR stimulation can initiate contractile behavior in stem cell-derived cardiomyogenic cells.

Currently, one of the largest risks associated with cellular cardiomyoplasty procedures is the formation of arrhythmia (111). Current research suggests that transplanted cells lack proper gap junctions necessary for myocardial coupling. This in turn leads to transplanted cells becoming electrically isolated from the host myocardium and the generation of arrhythmia (126). As the most abundant gap junction in the myocardium is Cx43, it is

possible that the neural crest cells isolated by our group may help to diminish this risk of arrhythmia. Overexpression of Cx43 in myoblasts has been investigated as a potential solution to the risk of arrhythmia formation (138-140). Roell *et al.* demonstrated that genetically engineered overexpression of Cx43 in skeletal myoblasts leads to protection against induced ventricular tachycardia in a murine infarct model (140). Fernandes *et al.* meanwhile report that genetically engineered myoblasts improved intracellular electrical coupling of myoblasts and cardiomyocytes (139). Preconditioning cells with IR stimulation may further reduce the risk of arrhythmia formation; however, it is also possible that transplantation of contracting cells may increase the risk of electrically isolated cells. This may be further evidenced by the increase in contraction velocity as the frequency is increased. We hypothesize that the additional energy leads to increased cellular recruitment, which may be a result of Cx43 selection.

Optical stimulation is advantageous as it does not require direct contact with cells, is spatially precise, and does not produce any stimulation artifact and, as shown in the study, can be applied for long durations without damaging the cells (128). Owing to these advantages, other approaches using optical stimulation have been investigated. This includes modifying the tissue to express photosensitive proteins (optogenetics) and controlling excitation and contraction by light (141, 142), although it is likely that the required genetic manipulation has other deleterious effects.

Our results are qualitatively similar to Dittami *et al.* who show a rapid increase in intracellular Ca^{2+} as a result of IR stimulation and contraction of neonatal cardiomyocytes. Neonatal cardiomyocytes are known to qualitatively differ from the adult myocyte in Ca^{2+} handling and special arrangement of sarcoplasmic reticulum (the primary site of

Ca²⁺ storage in the myocyte) and mitochondria (128, 143). Furthermore, Dittami *et al.* did report that in spontaneously contracting cells, IR stimulation caused a cessation of spontaneous events and return of Ca²⁺ to baseline levels. They hypothesize that this response may be the result of the action of IR stimulation on the mitochondrial calcium uniport (mCU) to clear Ca²⁺. These data were further verified by the inhibition of IR-evoked responses in the presence of Ruthenium Red, an inhibitor of the mCU. Pulsed IR is also known to cause a capacitive photothermal membrane current (144-146). However, the relatively small amplitude depolarization reported would not be sufficient to trigger the responses observed here. Pulsed IR clearly evokes large changes in the intracellular calcium in cultured spiral and vestibular ganglion neurons (127). This is in agreement with previous studies reporting that IR applied to the cell body modulates intracellular (Ca²⁺) and that this signaling plays a major role in somatic IR excitability (132, 147). Previous results have shown that inhibition of transmembrane Ca²⁺ channels or removal of extracellular Ca²⁺ did not impact the response to IR (127). This is further evidenced as all our stimulation experiments were performed in Ca²⁺-free buffer. Pharmacological data from this study showed that IR likely activates the endoplasmic reticulum (ER) Ca²⁺ release with a dependence on mitochondrial Ca²⁺ cycling (127, 128). In unpublished recent studies, we have observed that IR may induce Ca²⁺ releases from the ER in neurons by activating IP₃, ryanodine receptor channels, and/or through a mechanism that increases the probability of opening of these channels such as the degree of Ca²⁺ loading into the ER. The Ca²⁺ release from the ER was fully reversible and completely blocked by application of caffeine, indicating that IP₃ and/or ryanodine channels are necessary for its release. Additionally, mitochondria close to endoplasmic or sarcoplasmic Ca²⁺ release sites (e.g.,

ryanodine receptors, RyRs) are exposed to higher Ca^{2+} , making them likely to have higher rates of Ca^{2+} uptake (148). It is possible that IR modulates the $\Delta\Psi_m$ component of the electrochemical gradient potential that drives mitochondrial Ca^{2+} uptake (127, 149). However, the mechanisms by which pulsed IR modulates mitochondrial membrane potential, Ψ_m , plasma membrane potential, Ψ_p , or significant changes in cytosolic Ca^{2+} and the events controlling the IR effects on cells remain to be fully elucidated.

It could also be hypothesized that IR-induced contraction is related to thermal effects elicited by stimulation as has been shown (150). It has been shown that pulsed IR induces a transient increase in temperature up to $\sim 22.2^\circ\text{C}$ for a 10-ms pulse (7.3 mJ, 5.8 J/cm) (146). In the current study, the maximum radiant energy was 0.839 mJ, far less than that reported in previous studies investigating IR-evoked temperature transients. Coupled with previous results, which have shown that cooling or heating extracellular fluid does not alter the observed Ca^{2+} transients, we do not believe that the observed contractions are a result of temperature transients induced by IR stimulation (127, 128).

CHAPTER 4. PLURIPOTENT STEM CELL DERIVED MODEL

Motivation

Nicotine usage among pregnant women represents a significant health concern. According to data from the CDC, the overall smoking rate at any time during pregnancy was 8.4%. Of those who smoked during the first and second trimester, 20.6% quit by the third (11). This provides little solace in regards to heart development as the heart is the first organ in the fetus to fully develop and function with the heart tube fusing at approximately day 21 of development and the first beat occurring at day 23 (12). Nicotine rapidly crosses the placental barrier and nicotine concentrations in the fetus can be 15% higher than maternal levels (10). Nicotine exposure in the first trimester lead has been previously linked to increased spontaneous abortions and during the third trimester increased premature delivery rates, and decreased birth weights (10). Specifically, in regards to the heart, numerous studies have shown that nicotine usage among pregnant women is linked to increased blood pressure in infants (13, 14). Nicotine usage during pregnancy does not only effect an individual for the first few months-year of life, but also increases the risk of many diseases including cardiovascular disease later in life (15). Despite this, the molecular effects of nicotine on cardiomyocyte development remain largely unknown.

The development of the heart is a complex process that begins early in human gestation that involves many pathways. In order to populate the growing myocardium, cardiomyocytes actively proliferate during development, however in mammals, cardiomyocytes exit the cell cycle shortly after birth (151). In addition to cardiomyocyte proliferation, resident cardiomyocytes also undergo hypertrophic growth to populate the expanding chambers of the heart. Classical theory of heart development suggest that blood

flow and cardiac contraction are key initiators of cardiac hypertrophy (34), however new evidence suggests that intracellular cycling of Ca^{2+} as a secondary messenger is crucial to the overall development of the myocardium. Andersen et. al. recently showed that ventricular hypertrophy that is necessary to populate the developing myocardium during gestation is dependent on Ca^{2+} cycling (33). Even in absence flow or contraction, developmental ventricular myocyte hypertrophy was correlated with the amount of Ca^{2+} influx through L-type voltage gated calcium channels, indicating Ca^{2+} influx is the key regulator of ventricular hypertrophy. As a response to neurohormonal or biomechanical stress, cardiomyocytes may also revert to a fetal like state to induce hypertrophic growth of myocytes (47). Post-natal hypertrophy is often pathological and can lead to thinning of the heart wall as seen in dilated cardiomyopathy and unregulated cardiomyocyte hypertrophy can ultimately lead heart failure.

Owing to its importance, the flow of Ca^{2+} ions in cardiomyocytes is under tight control by the cell. Contraction of cardiomyocytes is a result of excitation contraction coupling and calcium induced calcium release. Briefly, action potentials induce opening of voltage gated calcium channels, which induces release of Ca^{2+} from stores in the sarcoplasmic reticulum. Release of Ca^{2+} stores induces contraction of muscle fibers, and following contraction, Ca^{2+} stores in the SR are refilled primarily through Sarco(endo)Plasmic Reticulum Ca^{2+} ATPases. Many of the proteins involved in this signaling cascade are directly regulated by kinases or are associated with other regulatory proteins. One of the key sensors and regulators in mediating intracellular Ca^{2+} cycling in cardiomyocytes is CaMKII. CaMKII can be activated by increased intracellular calcium loads, thus its sensor function. Once activated CaMKII can alter gene expression patterns, and induce

phosphorylation of proteins that directly control Ca^{2+} cycling including VDCCs, RyR2 channels, and phospholamban a key regulator in the reuptake of calcium into the SR (19). CaMKII activity has also been shown to be increased in hypertrophied and failing hearts (40).

Nicotinic acetylcholine receptors are a highly conserved class of ligand gated ion channels and are the molecular target of nicotine *in vivo*. nAChR's are pentameric channels that can be comprised of 16 different subunits, and subunit composition decides the affinity of each receptor to various ions. The $\alpha 7$ homopentameric (all 5 subunits being $\alpha 7$) are considered the most permeable to Ca^{2+} ions (87). Studies have shown that human embryonic stem cells (ESCs) express genes for all nAChR, but at the protein level only $\alpha 3$ and $\alpha 7$ nAChR's are present (92). Until this study, the expression on human iPS cells remained unknown, but murine iPS cells have been shown to express $\alpha 4$ and $\alpha 7$ channels (94). In these studies we hypothesize that Ca^{2+} entry through $\alpha 7$ nAChR may induce hypertrophy through CaMKII signaling.

Studies looking at the role of nicotine and nAChR's in cardiac development are few and far between. Ishizuka *et. al.* exposed murine iPS cells to 300 nM nicotine and showed that exposure induced significantly increased DNA synthesis in both naïve iPS cells and iPS derived mesodermal progenitor cells. This result could be inhibited by pretreatment with dihydro- β -erythrodine (DH β E), a specific $\alpha 4$ nAChR antagonist, a-bungarotoxin, a specific $\alpha 7$ nAChR antagonist, or KN-93 a CaMKII inhibitor (28). Another recent study was conducted that looked at the exposure of zebrafish to tobacco smoke and e-cigarette extract and the associated effects on cardiac development. In zebrafish, following 72 hour exposure of 6.8, 13.7, and 34 μM of nicotine, the 34 μM showed 0% survival and therefore

the effect on cardiac development was not assayed. Of those that were assayed cardiac development displayed increased defects in a dose dependent manner for the groups receiving cigarette smoke extract and e-cigarette extract, but interestingly not for those that received nicotine alone. Following 24 hour exposure, both the tobacco group and e-cigarette group showed decreases in the contractile genes CMLC2, and TNNT2, the transcription factor MEF2CA and the major gap junction in the myocardium GJA1. Additionally observed was increase in the cardiac homeobox gene NKX2.5, but only in the tobacco cigarette group (100).

In the studies presented, we successfully differentiated human iPS cells to a cardiomyocyte lineage that spontaneously contracts, and showed that iPS-CM contain functional calcium stores in the sarcoplasmic reticulum (SR) and intracellularly cycle calcium as would be expected of mature cardiomyocytes. Additionally, we show the expression of $\alpha 7$ nAChR's on the surface of human iPS cells. After 21 days of exposure we performed gene expression analysis and show that nicotine induces cells to revert to a fetal gene program, a pattern indicative of cardiomyocyte hypertrophy. Using protein analysis, we show an increase in CaMKII activity, and using IonOptix to study intracellular calcium cycling we show that iPS-CM exposed to nicotine have increased intracellular calcium loads, and altered Ca^{2+} release kinetics.

Materials and Methods

iPS Cell Culture and Differentiation

Human sendai virus reprogrammed cardiac fibroblast derived induced pluripotent stem cells were purchased American Type Culture Collection (ATCC ACS-1021, Manassas, VA). Cells were grown on Geltrex (Life Technologies, Grand Island, NY) coated

polystyrene dishes in Essential 8 medium (E8, Life Technologies). Cells were passaged non-enzymatically using 5 mM EDTA in phosphate buffered saline (PBS, Life Technologies) and mechanical disruption. For 24 hours after passaging cells were cultured in E8 supplemented with 10 μ M Y27632, followed by growth in E8 medium. Differentiation was carried out over a period of 21 days using modification of canonical wnt signaling as first described by Lian et. al. with slight modification (Figure 4.1) (152). Briefly cells were grown to approximately 90% confluence on Geltrex coated polystyrene dishes. On day 0, media was replaced with RPMI-1640 (Life Technologies) supplemented with 25x B27 supplement minus insulin (Life Technologies) and 6 μ M GSK3 synthase inhibitor CHIR-99021 (Sigma Aldrich, St. Louis, MO). After 2 days media was replaced with RPMI-1640 supplemented with 25x B27 supplement minus insulin. On Day 3 media was replaced with RPMI-1640 supplemented with 25x B27 and 5 μ M wnt inhibitor IWP-2 (Sigma Aldrich). On day 5, media was replaced with RPMI-1640 supplemented with 25x B27 supplement minus insulin. On day 7, media was replaced with RPMI-1640 supplemented with 25x B27 supplement (Life Technologies). On Day 10, non-myocytes are depleted by culturing cells in RPMI 1640 (-Glutamine) (Life Technologies) supplemented with 25x B27. On Day 13, and every 3 days after media is replaced with RPMI-1640 supplemented with 25x B27 supplement. Cells were allowed to differentiate for 21 days at which point they were used for data analysis.

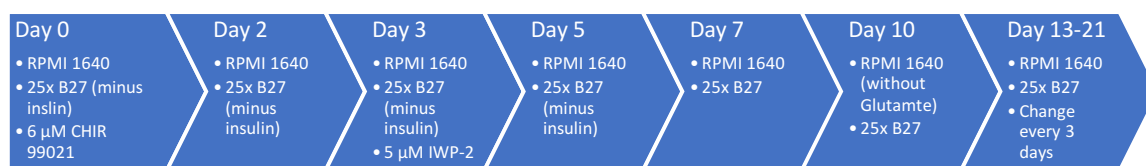


Figure 4.1 - Schematic of iPS stem cell differentiation

Nicotine and Pharmacological Inhibitors

Pure nicotine (Sigma Aldrich) was diluted to a concentration of 1 mM in 100% ethanol (Sigma Aldrich), and diluted 1:1000 at each media change to achieve a final concentration of 1 μ M. Nicotine concentrations were selected based on physiological relevance and previously published results from our laboratory (153, 154). For pharmacological studies, cells were incubated for 30 min in media containing pharmacological agents prior to nicotine addition. α -bungarotoxin (α btx, R&D Systems, Minneapolis, MN) an irreversible selective antagonist of α 7 nAChRs was reconstituted in PBS to a concentration of 10 μ M in PBS and stored at -20°C until use. On day of use α btx was diluted 1:1000 in cell culture media. Mecamylamine (MCA, R&D Systems), a non-competitive, non-selective antagonist of nAChRs was reconstituted to 10 μ M in PBS and stored at -20°C until use. On day of use MCA was diluted 1:1000 in cell culture media. KN-93 (R&D Systems) a selective inhibitor of CaMKII was reconstituted to a concentration of 500 μ M in Dimethyl Sulfoxide (DMSO, Sigma Aldrich, St. Louis, MO) and stored at -20°C until use. On day of use KN-93 was diluted 1:5000.

Immunostaining

iPS cells were grown to \sim 70% confluence and fixed in 10% neutral buffered formalin (VWR). Cells were then blocked for one hour in PBS supplemented with 20 mg/mL bovine serum albumin (BSA, Sigma Aldrich, St. Louis, MO) 1% Fetal Bovine Serum (FBS,

Atlanta Biologicals, Flower Branch, GA), and 0.05% Tween-20 (Sigma Aldrich, St. Louis, MO). Following blocking cells were incubated in PBS containing 1% BSA and 1: 100 primary antibody against $\alpha 7$ nAChR (ab10096, Abcam, Cambridge, MA) at 4°C overnight with gentle agitation. The following day, cells were washed 3 times in PBS, and incubated in 1% BSA containing 1:500 goat anti rabbit Alexafluor 546 (Life Technologies) for 2 hours at room temperature with gentle agitation. Following incubation with secondary antibodies cells were washed an additional three times and mounted using slow fade mounting media containing DAPI (Life Technologies). Cells were imaged on a Zeiss LSM 700. Post processing of images was done using ImageJ (NIH, Bethesda, MD).

Gene Expression

Total RNA was isolated by means of TRIzol reagent (Life Technologies) following the manufacturers' recommended protocol and resuspended in RNase- and DNase-free water. The RNA suspension was then frozen at -80°C overnight and quantified using a NanoDrop[®] spectrophotometer (Nanodrop Products, Wilmington, DE).

Reverse transcription of RNA to cDNA was performed by means of the High-Capacity cDNA Reverse Transcription Kit (Applied Biosystems, Grand Island, NY) as per the manufacturer's recommended protocol. Briefly, 1 μg of RNA for each sample was converted to cDNA and then diluted to a final concentration of 10 ng/ μL of PCR-grade water and used for gene expression analysis.

Real-time PCR was carried out using SYBR Green PCR Master Mix (Applied Biosystems) and custom-designed primers (Table 4.1) (Eurofins MWG Operon, Louisville, KY). For all the genes, 20 ng of cDNA was used for each reaction. The reactions were performed using an Agilent Technologies Stratagene Mx3000p real-time PCR system.

Each reaction was run in triplicate for each assay and gene expression quantification was carried out by means of the comparative Ct method with GAPDH used as an endogenous control (133).

Table 4.1 - Primers for gene expression analysis

Gene	Forward Primer (5'-3')	Reverse Primer (5'-3')	Accession Number
MYH7	GCTCTACAACCTCAA GGAT	TTGACGGTGACACAG AAG	NM_000257.3
NKX2.5	CTAGAGCCCGAAAAG AAAG	AGCATTTGTAGAAAG TCA	NM_001166175. 1
TNNT2	GGTTACATCCAGAAG ACAGA	TCCTCTCAGCCAGAA TCT	NM_000364.3
RYR2	GGAGATGCTGGCTAA CAC	GATGACCACCACCTT GAG	NM_001035.2
PLN	TTAATATGTCTCTTGC TGAT	GGAAGTGGTCTGTTA TAC	NM_002667.4
ATP2A1	CTACCTCATTTCTCC AA	CACCAAGTTCACCCC ATAG	NM_001286075. 1
NPPA	ACACGCTTCCGGTAC TGAAGATAA	CCATGGCAACAAGA TGACACA	NM_006172.3
NPPB	GATCCCCAGACAGCA CCTTC	GTTGCGCTGCTCCTG TAAC	NM_002521.2
CASQ2	CGAACGCATTGAAGA CTA	GATGTAAGGCTGGA AGTG	NM_001232.3

Western Blot

For protein analysis at the time of collection cells were washed 1x in ice cold PBS, and incubated on ice for 10 min in RIPA buffer (ThermoFisher Scientific, Waltham, MA) containing protease/phosphatase inhibitor cocktail. Following 10 min, cells were mechanically disrupted using a cell scraper. Resultant lysate was centrifuged at 14000 RPM for 10 min and the supernatant collected. 15 µg of total protein was mixed with 6x Lamelli sample buffer (VWR), and boiled for 5 min. Gels were loaded and resolved at 150 V for approximately 45 min in 4-20% polyacrylamide polyprecast gels (Biorad, Hercules, CA). Gels were transferred using a TransBlot® Turbo™ and TransBlot® Turbo™ transfer

packs (Biorad). Following transfer, membranes were cut and blocked for 30 min at room temperature in 1% BSA in TBS containing 0.05% Tween-20 (TBS-T, VWR). Following blocking, blots were washed 2x in TBS-T, and then incubated at 4°C overnight in TBS-T containing 1% BSA and primary antibody (Table 4.2). After overnight incubation, blots were washed 3x in TBS-T and incubated for an additional 2 hours in TBS-T containing 1% BSA and 1:2000 secondary antibody to either mouse or rabbit, respectively, conjugated with horseradish peroxidase (HRP). (BioRad) Following incubation in secondary antibody, blots were washed three additional times in TBS-T. Bands were detected using chemiluminescence with Clarity ECL Western Blotting Substrate (BioRad). Blots were imaged on a Biorad ChemiDoc MP Imaging System (BioRad). Densitometric analysis was performed using ImageJ on a computer running Mac OS X.

Table 4.2 - Primary antibodies for western blots

<i>Protein</i>	<i>Dilution</i>	<i>Supplier/Part Number</i>
PLN	1:1000	Abcam ab2865
Thr ¹⁷ PLN	1:1000	Badrilla A010-13AP
CaMKII	1:1000	Cell Signaling #3362
Thr ²⁸⁶ CaMKII	1:1000	Cell Signaling #12716
β-actin	1:2000	Sigma Aldrich A5316

IonOptix Calcium and Contractility Assay.

Human iPSC-derived cardiomyocytes were placed in a perfusion chamber adapted to the stage of an inverted Nikon eclipse TE2000-U fluorescence microscope. Cells were superfused with a Tyrode's buffer containing (in mM): 144 NaCl, 1 MgCl₂, 10 HEPES, 5.6 glucose, 5 KCl, 1.2 NaH₂PO₄, and 1.8 CaCl₂, adjusted to a pH 7.4 with NaOH.

Intracellular Ca^{2+} was measured using the Ca^{2+} -sensitive dye Fura-2 and a dual-excitation (340/380 nm) spectrofluorometer (IonOptix LLC, Milton, MA, USA). First, cardiomyocytes were incubated with 5 μM Fura-2 for 30 minutes at room temperature and then washed with fresh regular Tyrode's solution for at least 10 minutes. All Ca^{2+} measurements were performed at 37°C. SR Ca^{2+} content was assessed by caffeine challenge. Briefly, the regular Tyrode's solution was switched for a $0\text{Na}^+/0\text{Ca}^{2+}$ Tyrode's buffer containing (in mM): 144 LiCl, 1 MgCl_2 , 10 HEPES, 5.6 glucose, 5 KCl, 10 EGTA, adjusted to a pH 7.4 with LiOH). Once the cardiomyocytes stopped beating, $0\text{Na}^+/0\text{Ca}^{2+}$ Tyrode's buffer containing 20 mM caffeine was rapidly applied. SR Ca^{2+} contents were calculated considering that SR represents 3.5% and cytosol 65% of the myocyte volume as previously described by Shannon et. al. (155). The following equation from Shannon et al. was used:

$$[\text{Ca}^{2+}]_{\text{SR}} = [\text{Ca}^{2+}]_{\text{caff}} + \frac{\beta_{\text{max-SR}} \times [\text{Ca}^{2+}]_{\text{caff}}}{[\text{Ca}^{2+}]_{\text{caff}} + K_{\text{d-SR}}}$$

$[\text{Ca}^{2+}]_{\text{SR}}$ is the SR Ca^{2+} content, $[\text{Ca}^{2+}]_{\text{caff}}$ is the SR Ca^{2+} released by caffeine, $\beta_{\text{max-SR}}$ and $K_{\text{d-SR}}$ are the usual Michaelis parameters for SR Ca^{2+} binding.

The calibration was performed *in-vivo* in cardiomyocytes by superfusing a free Ca^{2+} and then a Ca^{2+} saturating (5 mM) solutions, both containing 10 μM ionomycin (Sigma, St. Louis, MO) until reaching a minimal (R_{min}) or a maximal (R_{max}) ratio values, respectively. $[\text{Ca}^{2+}]_i$ was calculated as described previously using the following equation (156):

$$[\text{Ca}^{2+}]_i = K_d \times \frac{S_{f2}}{S_{b2}} \times \frac{(R - R_{\text{min}})}{(R_{\text{max}} - R)}$$

K_d (dissociation constant) was taken as 224 nmol/L. The scaling factors S_{f2} and S_{b2} were extracted from calibration as described by Grynkiewicz et al. (157) $\Delta[Ca^{+2}]_i$ amplitude was considered as: peak $[Ca^{+2}]_i$ – resting $[Ca^{+2}]_i$.

Statistics

The data are expressed as mean \pm SD unless otherwise indicated. Analysis was performed using students t-test between groups with $p < 0.05$ considered significant using Microsoft Office Excel 2016 Microsoft Office Excel 2016 for Mac OS X.

Results

Human iPS cells express the $\alpha 7$ nAChR and can be differentiated to a cardiomyogenic lineage

Immunostaining of non differentiated human iPS cells showed that non differentiated iPS cell colonies express the $\alpha 7$ nAChR in relative abundance (Figure 4.2). Following 21 days of differentiation, robust contraction of cardiomyocytes was observed (Supplemental Video 1). After 21 days of differentiation appropriate calcium handling including sarcoplasmic reticulum handling was verified through the use of pharmacological agents and IonOptix. iPS-CM responded to electrical field stimulation by contracting in response to field stimulation. Contraction could be inhibited with the removal of extracellular Ca^{2+} indicating functional ECC (Figure 4.3 and Figure 4.4). We also tested to determine whether functional sarcoplasmic calcium storage was occurring. As expected, 20 mM caffeine elicited a rapid rise in intracellular calcium levels through the release of Ca^{2+} from stores in the SR (Figure 4.4). We also used a pharmacological panel of inhibitors to determine that CICR was occurring as expected, and that the SR contained functional SERCA channels were able to refill the SR Ca^{2+} stores following contraction. 10 μ M Ryanodine

proved effective in inhibiting contraction by blocking the release of Ca^{2+} from stores in the SR through RyR2 channels (Figure 4.5). Lastly, 10 μM thapsigargin, an inhibitor of SERCA channels was effective in slowing calcium decay in cardiomyocytes as would be expected in a mature cardiomyocyte (Figure 4.6).

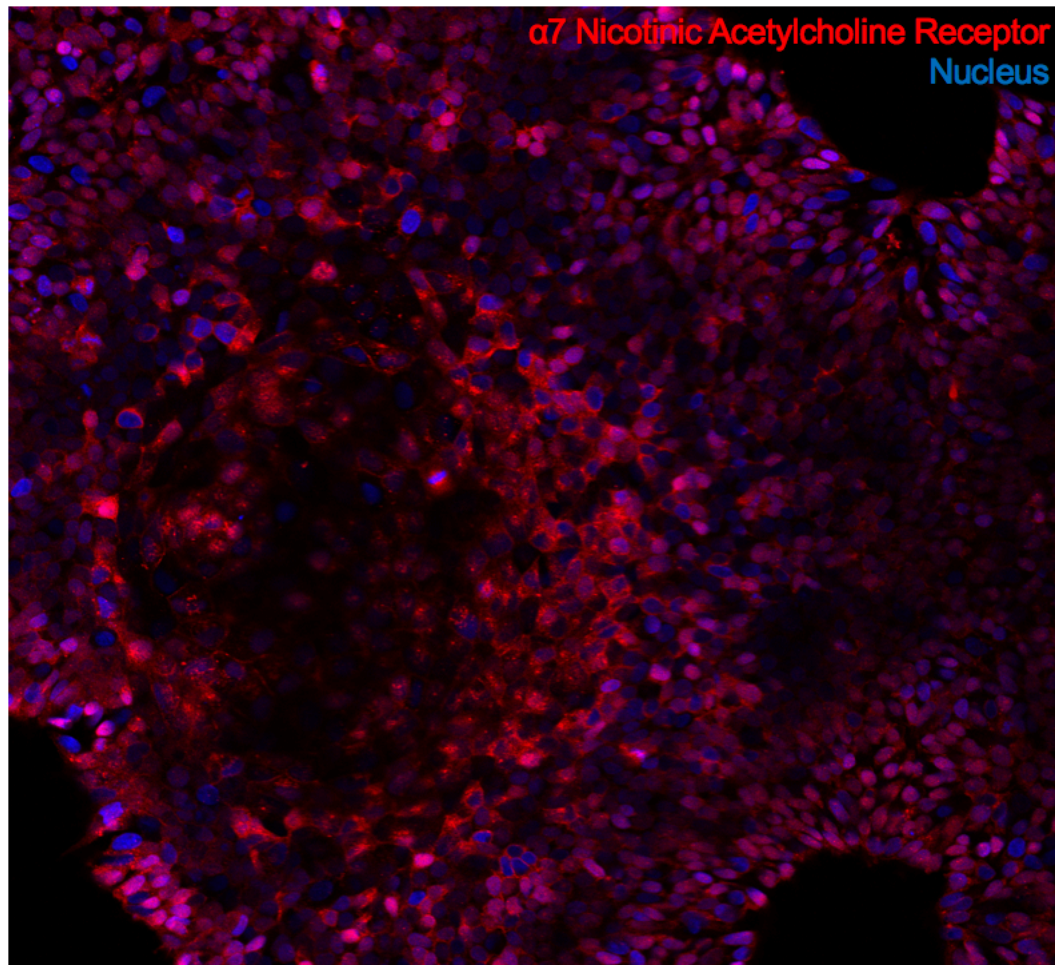


Figure 4.2 - Immunohistochemical staining of $\alpha 7$ nicotinic acetylcholine receptor on naive human induced pluripotent stem cell

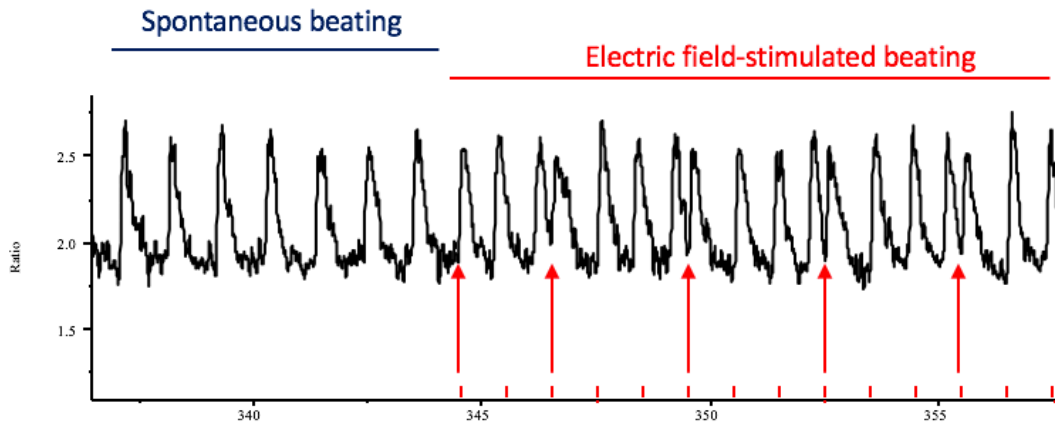


Figure 4.3 - *iPS-CM* respond to electrical field stimulation

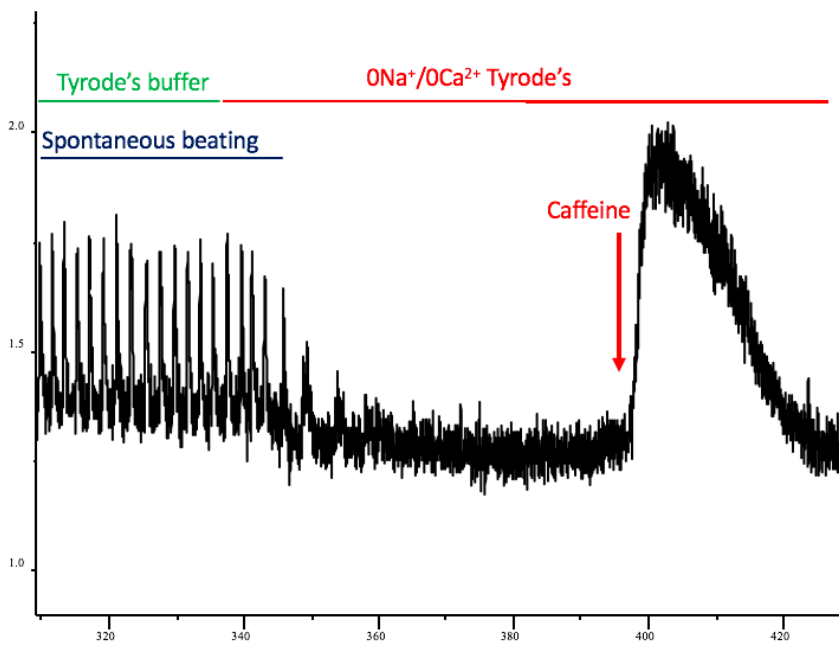


Figure 4.4 - 20 mM Caffeine elicits a rapid release of calcium from intracellular SR stores

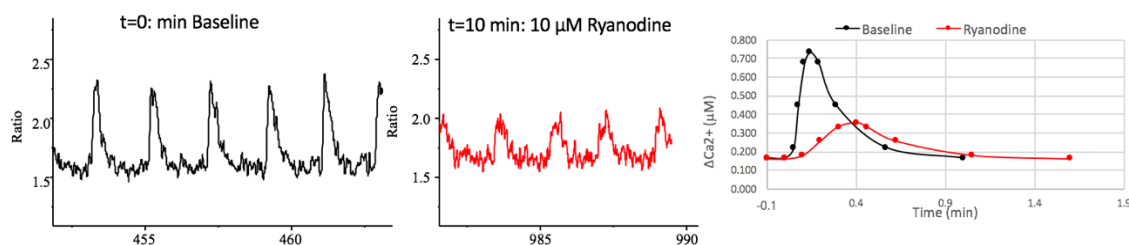


Figure 4.5 - Ryanodine inhibits iPS-CM contraction by inhibiting intracellular SR calcium cycling by blocking RyR2 channels in the SR

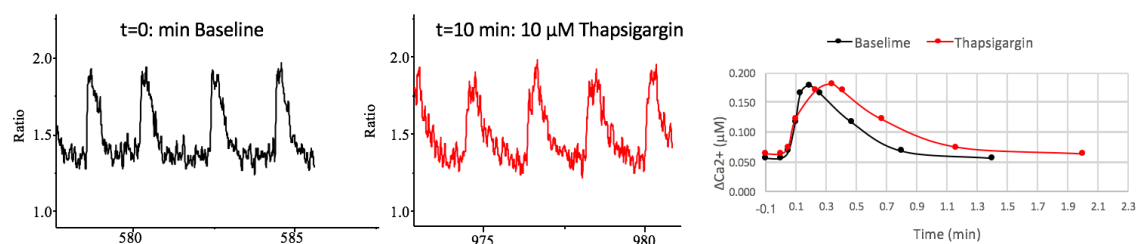


Figure 4.6 - Thapsigargin slows iPS-CM contraction by inhibiting intracellular SR calcium cycling by blocking reuptake of Ca^{2+} into the SR via SERCA channels

Nicotine effects intracellular calcium cycling of iPS-CM

After 21 days of differentiation traces of intracellular calcium cycling were collected using the IonOptix imaging modality. Under spontaneous contraction we observed that the intracellular calcium load was increased in groups treated with 1 μM nicotine over control. Both ωbtx and KN-93 were able to restore calcium levels to near baseline levels however MCA treated groups showed increased Ca^{2+} loads above even that of nicotine. When groups were subject to electrical stimulation at 1 Hz, nicotine still induced increased calcium loads but ωbtx and KN-93 were not as efficacious in inhibiting this increased load. We continue to observe calcium loads above all other groups in the MCA treated groups. (Figure 4.8)

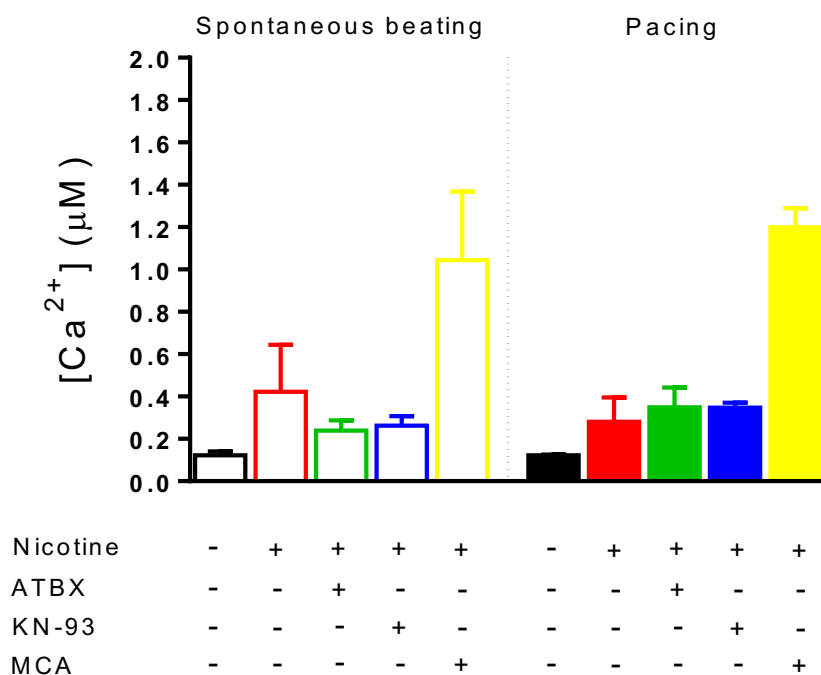


Figure 4.7 - Nicotine induces increased calcium load in iPS-CM. While undergoing spontaneous contraction, calcium levels could be reduced to near baseline levels with pretreatment with α btx or KN-93, however MCA increased calcium load above all other groups including nicotine (left). While undergoing electrically stimulated contraction, calcium levels could not be reduced to near baseline levels with pretreatment with α btx or KN-93. MCA continued to increase calcium load above all other groups including nicotine ($n=2$).

We also used IonOptix imaging to investigate changes in iPS-CM calcium cycling kinetics induced by 1 μ M nicotine. While undergoing spontaneous contraction, nicotine appears to induce a decreased time to peak Ca^{2+} , as well as decreased Ca^{2+} decay following contraction. This change could be partially rescued by treatment with α btx or KN-93. Similar to the measurements of Ca^{2+} SR load, MCA lead to the fastest time to peak and fastest clearance of Ca^{2+} following contraction. (Figure 4.8). When iPS-CM were subject to electrical stimulation at 1 Hz similar results were obtained with nicotine inducing decreased time to peak and decreased clearance of Ca^{2+} following contraction. Similar

to measurements of Ca^{2+} load, inhibitors were not effective in returning time to peak and decay time to control levels while undergoing electric field stimulation. (Figure 4.9)

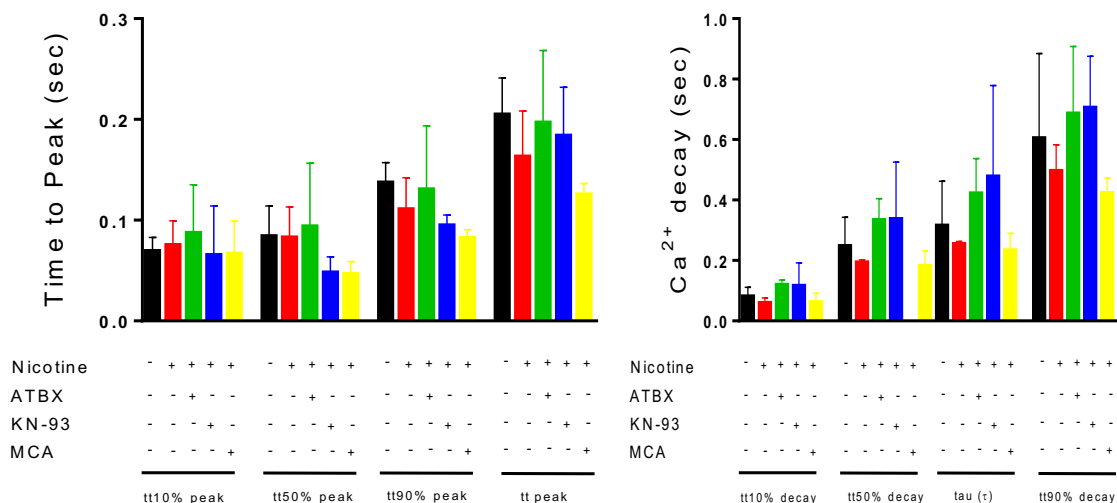


Figure 4.8 - While undergoing spontaneous contraction iPS-CM reach peak calcium levels quicker and are also faster to reuptake Ca^{2+} post contraction. Similar to Ca^{2+} load this effect could be brought back to baseline values with pretreatment with αbtx or KN-93, but Mecamylamine groups reach peak faster than any other group and also cleared calcium the fastest following contraction ($n=2$).

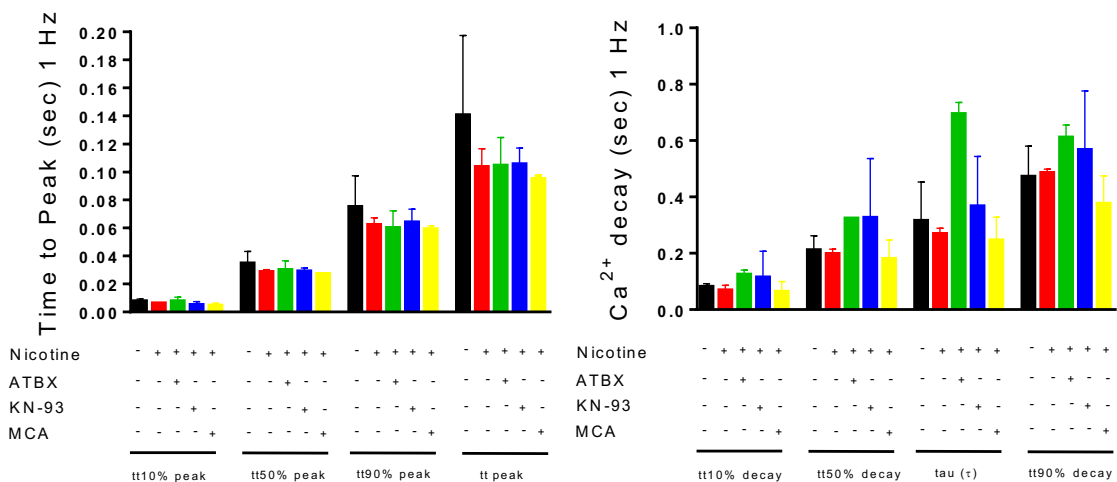


Figure 4.9 - While being electrically paced, groups treated with nicotine reach peak calcium levels faster than control, but reuptake does not appear to be effected by nicotine. Similar to Ca^{2+} load when being electrically paced even groups pretreated with inhibitors did not return to baseline levels ($n=2$).

Nicotine increases the activity of CaMKII and Thr²⁸⁶CaMKII.

Previous studies using murine iPS cells have suggested that the effects of nicotine are modulated through CaMKII signaling pathways. To evaluate whether the same was true in human iPS cells we performed western blots of CaMKII and Thr²⁸⁶CaMKII. Groups treated with nicotine showed an increase in the amount of CaMKII present which could be reduced with the use of α -bungarotoxin. Mecamylamine and KN-93 were not effective in inhibiting the increased CaMKII levels over control (Figure 4.10). Increased levels of Ca²⁺ are also known to induce autophosphorylation of CaMKII at the Thr286 site which can increase the activity of CaMKII. Groups treated with nicotine showed a modest increase in Thr²⁸⁶CaMKII which could be ameliorated by pretreatment with abtx but not mecamylamine or KN-93 (Figure 4.11).

Phospholamban is a reversible regulator of SERCA activity in the SR and a substrate of CaMKII. When phosphorylated by Protein Kinase A at the Ser16 residue or CaMKII at the Thr17 site, phospholamban disassociates from SERCA channels and allows for greater reuptake of Ca²⁺ into the SR. We hypothesized that increased CaMKII activity, as a result of activation of nAChRs, would also induce increases in the phosphorylation of PLN. Treatment with 1 μ M nicotine showed an increase in the amount of phosphorylated phospholamban protein. Phosphorylation could be partially reduced with pretreatment of KN-93 or abtx. Mecamylamine did not appear to reduce the phosphorylation rate of PLN at the Thr17 site (Figure 4.12).

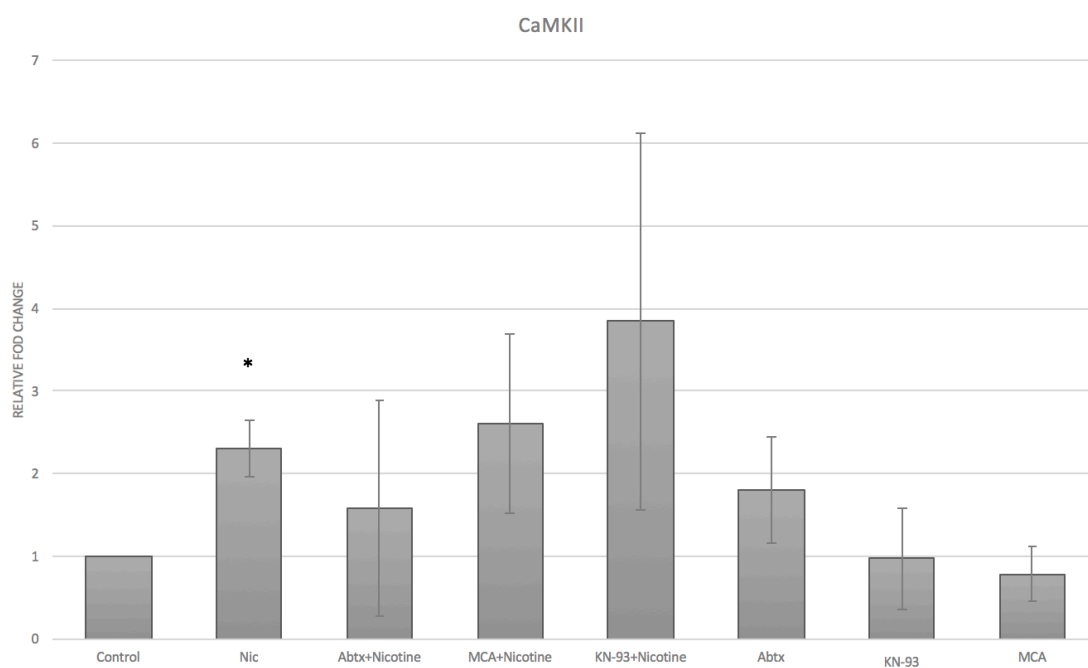
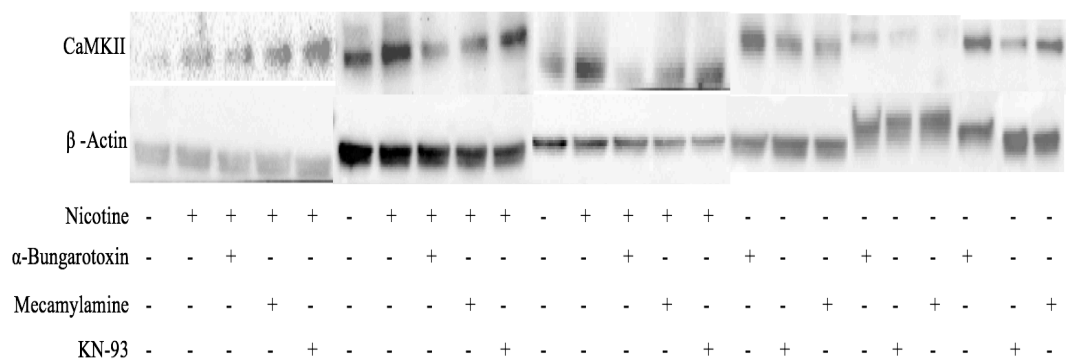


Figure 4.10 - $1 \mu\text{M}$ Nicotine induces an increase in protein expression of CaMKII ($n=3$, * $p < 0.05$)

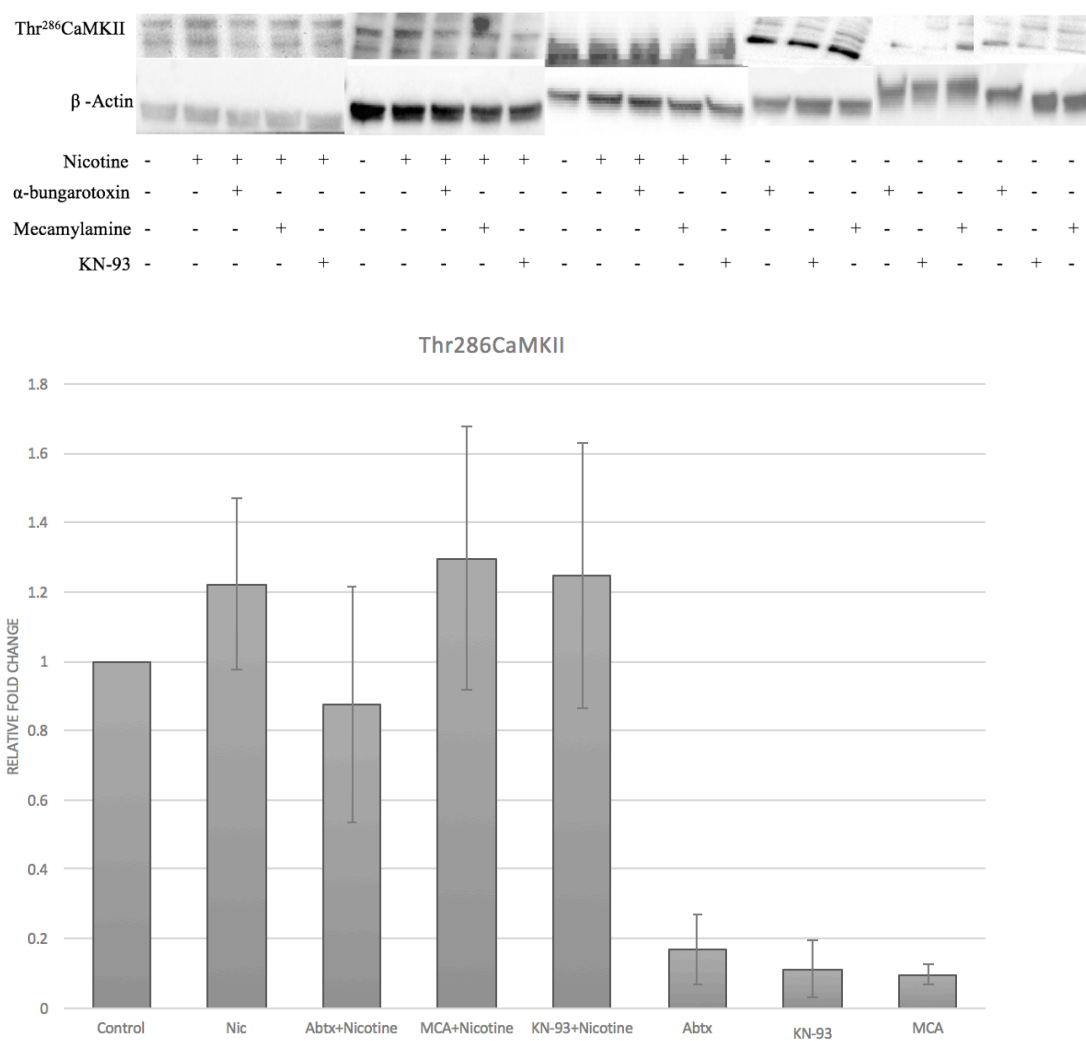


Figure 4.11 - 1 μ M Nicotine induces an increase in protein expression of Thr²⁸⁶CaMKII ($n=3$)

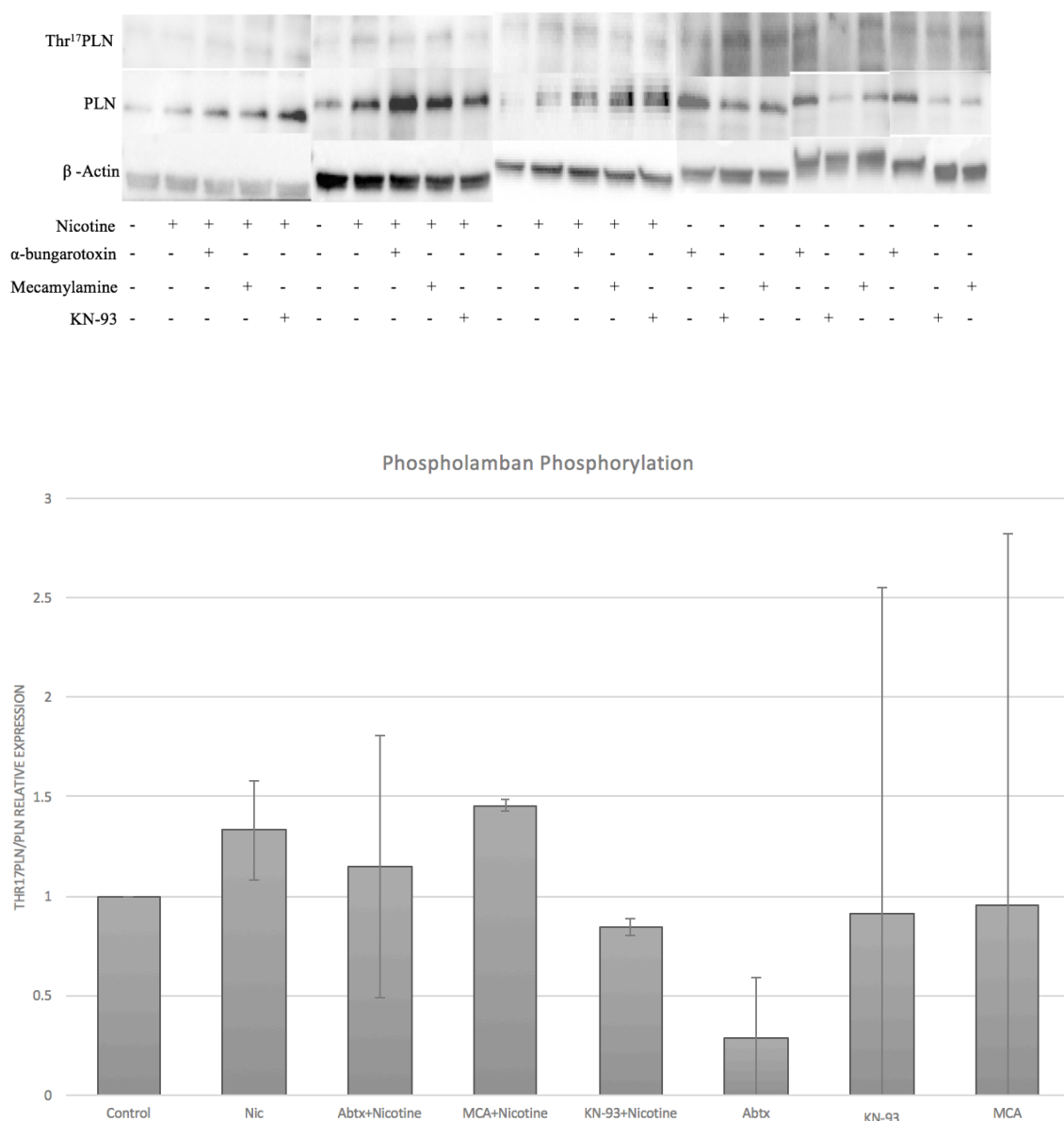


Figure 4.12 - 1 μ M Nicotine increases in the ratio of Thr¹⁷Phospholamban relative to total phospholamban (n=3)

Reversion to a fetal gene like pattern is a hallmark characteristic of cardiomyocyte hypertrophy. Following 21 days of differentiation with or without exposure to nicotine cells were collected for gene expression analysis. The first set of genes analyzed were transcription factors, sarcomeric genes associated with differentiation of stem cells to cardiomyocytes, and hypertrophic markers. These include NK homeobox 2 locus 5

(NKX2.5), myosin heavy chain β (MYH7), and cardiac muscle troponin T (TNNT2), natriuretic peptide A (NPPA), and natriuretic peptide B (NPPB). (Figure 4.13-17). NKX2.5 disruption in mice has been shown to cause embryonic lethality due to arrested morphogenesis of the myocardium in mice. (158) NKX2.5 has also been shown to play a role in the homeostasis of adult myocytes in mice, and upregulation in adult hearts is associated with hypertrophy. (158, 159) In these studies we observed a small increase in the expression of NKX2.5 in groups subject to nicotine treatment. MYH7 is a gene that is expressed in the fetal heart under the control of NKX2.5 and other early cardiac regulatory transcription factors such as GATA4, and MEF2C. In the adult myocardium, thyroid hormone inhibits the expression of MYH7; however, in the hypertrophic fetal like state, MYH7 expression is reactivated (160). In our studies nicotine induced a significant increase in MYH7 expression which could be inhibited through any of the pharmacological agents employed. Mutations of MYH7 and TNNT2 have been linked to the development of hypertrophic cardiomyopathy in the clinic (161). Similar to MYH7, nicotine induced a significant increase in the expression of TNNT2 that could be inhibited with the use of any of the pharmacological agents used in these studies. During development NPPA and NPPB are expressed relatively high levels that are downregulated in the adult myocardium. expression has also been shown strongly increase in hypertrophy and heart failure (162). In the present studies NPPA was increased in the nicotine treated group. Similar to MYH7 and TNNT2 this upregulation could be inhibited by treatment with any of the pharmacological inhibitors investigated. NPPB on the other hand did not show changes upon stimulation with nicotine.

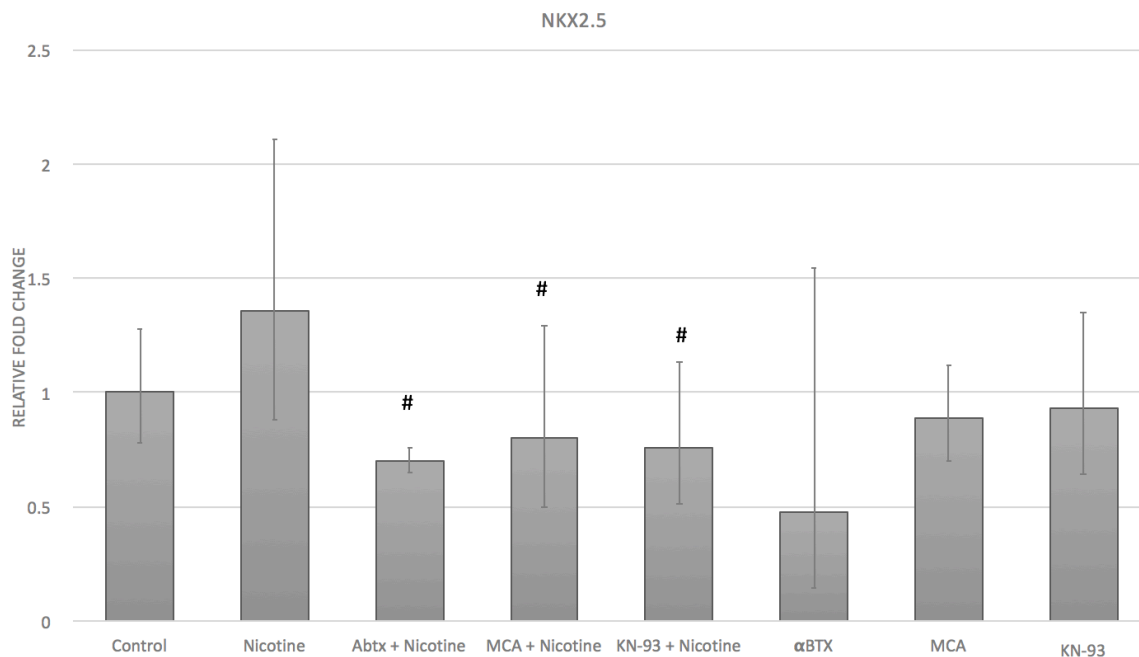
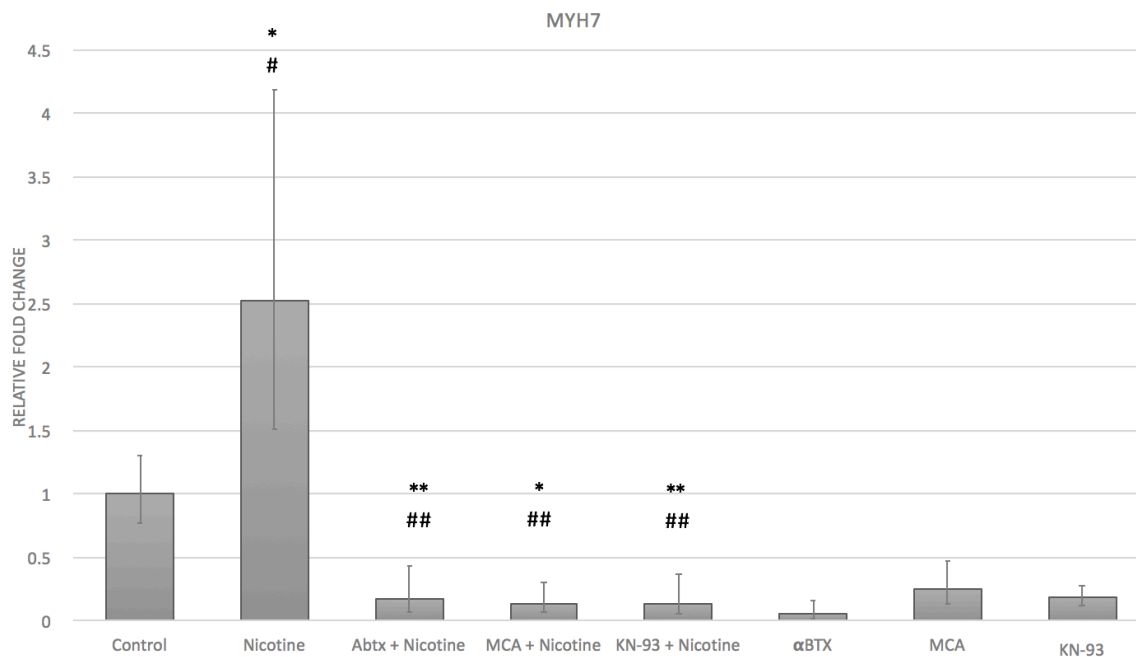
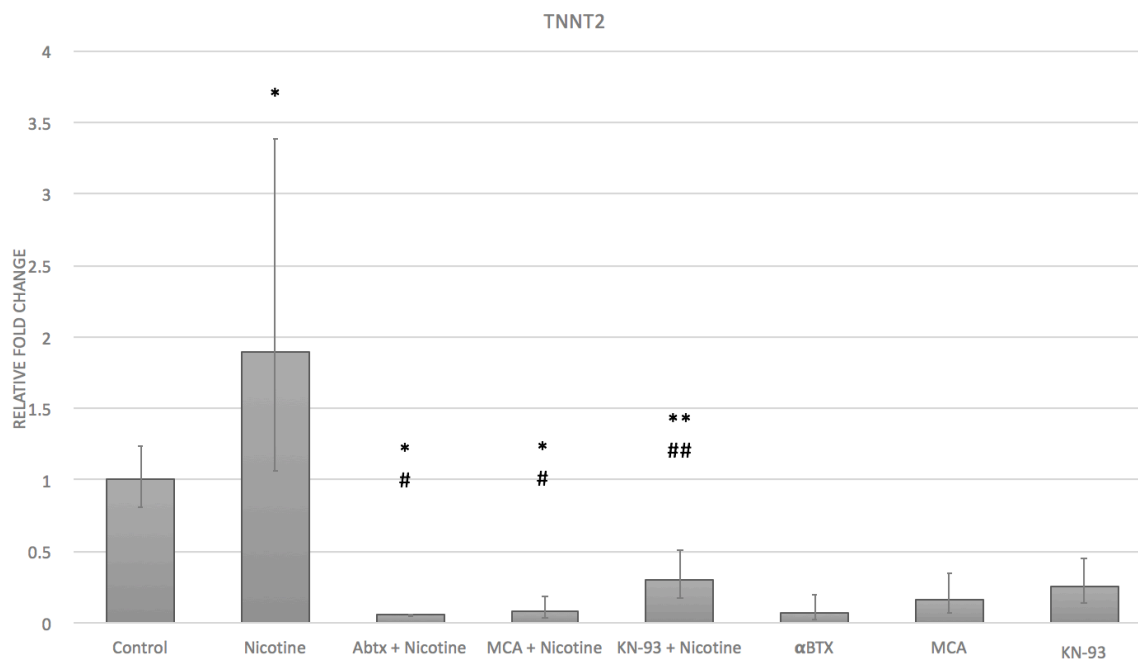


Figure 4.13 - Genetic expression analysis for NK Homeobox 2 locus 5 (NKX2.5) following treatment with 1 μ M nicotine with and without pretreatment of pharmacological agents. NKX2.5 is upregulated in the presence of nicotine, an indicator of a reversion to fetal like gene expression pattern observed in cardiomyocyte hypertrophy. Inhibition of increased expression is observed with all pharmacological agents used in these studies (n=3, # p<0.05 with respect to nicotine)



*Figure 4.14 - Genetic expression analysis for myosin heavy chain β (MYH7) following treatment with 1 μ M nicotine with and without pretreatment of pharmacological agents. MYH7 is upregulated in the presence of nicotine, an indicator of a reversion to fetal like gene expression pattern observed in cardiomyocyte hypertrophy. Inhibition of increased expression is observed with all pharmacological agents used in these studies. (n=3, * $p < 0.05$ with respect to control, # $p < 0.05$ with respect to nicotine, ** $p < 0.01$ with respect to control, ## $p < 0.01$ with respect to nicotine)*



*Figure 4.15 - Genetic expression analysis for cardiac muscle troponin T (TNNT2) following treatment with 1 μ M nicotine with and without pretreatment of pharmacological agents. TNNT2 is upregulated in the presence of nicotine, an indicator of a reversion to fetal like gene expression pattern observed in cardiomyocyte hypertrophy. Inhibition of increased expression is observed with all pharmacological agents used in these studies. $n=3$, * $p<0.05$ with respect to control, # $p<0.05$ with respect to nicotine, ** $p<0.01$ with respect to control, ## $p<0.01$ with respect to nicotine)*

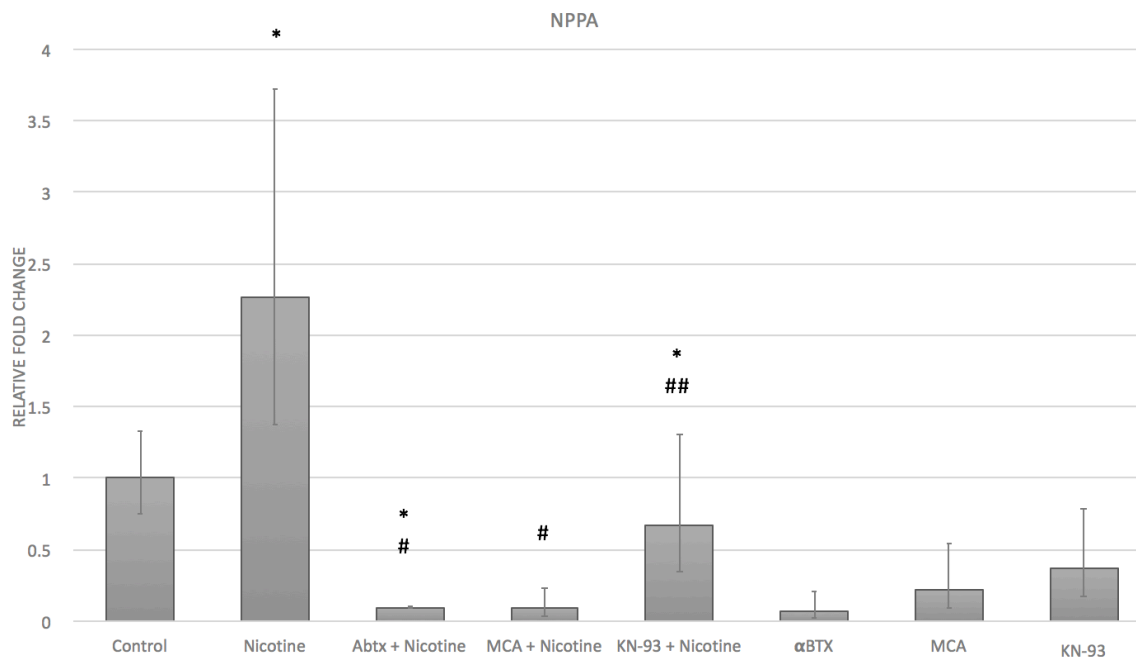


*Figure 4.16 - Genetic expression analysis for natriuretic peptide A (NPPA) following treatment with 1 μ M nicotine with and without pretreatment of pharmacological agents. NPPA is upregulated in the presence of nicotine, an indicator of a reversion to fetal like gene expression pattern observed in cardiomyocyte hypertrophy. Inhibition of increased expression is observed with all pharmacological agents used in these studies. (n=3, n=3, * p <0.05 with respect to control, # p <0.05 with respect to nicotine, ## p <0.01 with respect to nicotine)*

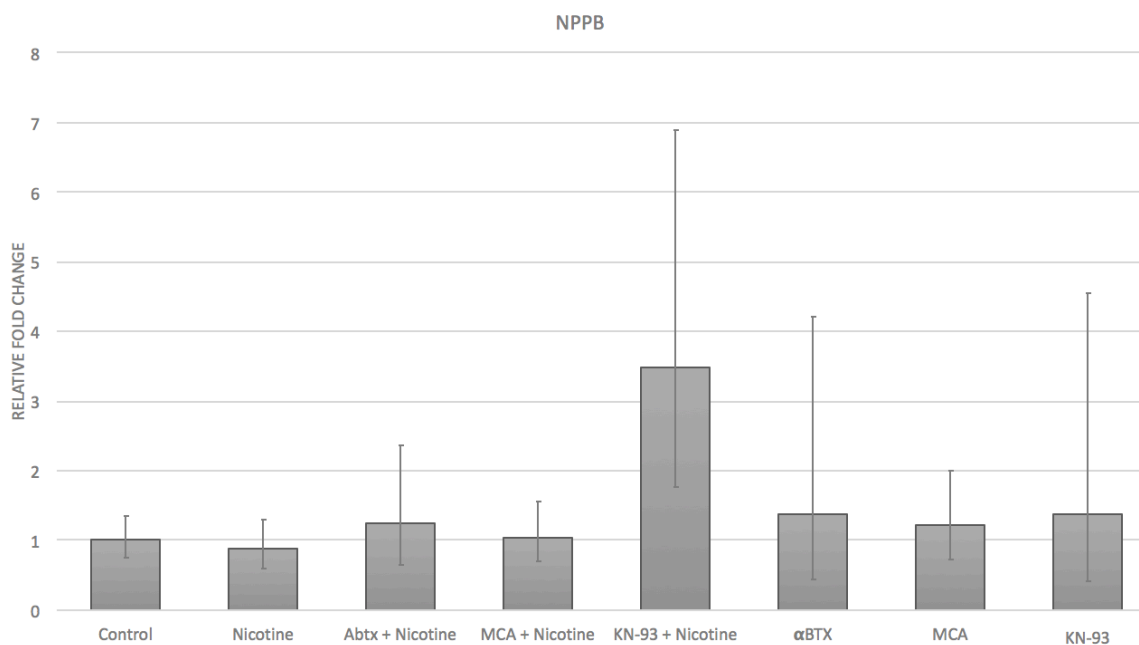


Figure 4.17 - Genetic expression analysis for natriuretic peptide B (NPPB) following treatment with 1 μ M nicotine with and without pretreatment of pharmacological agents. Expression patterns of NPPB do not appear altered in the presence of nicotine. (n=3)

In addition, we also analyzed a panel of calcium cycling genes including RYR2, CASQ2, PLN, and ATP2A1 (Figure 4.18-21). RYR2 mediates calcium release from the sarcoplasmic reticulum. Previous studies have shown that nicotine upregulates RYR2 in neurons and induces long lasting reinforcement of Ca^{2+} signaling via CICR (163). Our results are consistent with these findings and show that nicotine induces upregulation of RYR2 gene. Further, we show that inhibition with pharmacological agents was successful in inhibiting this observed change. CASQ2 is a protein in the SR which binds calcium ions following contraction. ATP2A1 is the gene which encodes for SERCA channels that are responsible for refilling stores of Ca^{2+} following contraction. We did not observe significant changes in either of these genes. Lastly we also investigated the genetic form of phospholamban and observed that nicotine induced an upregulation in the gene for PLN.

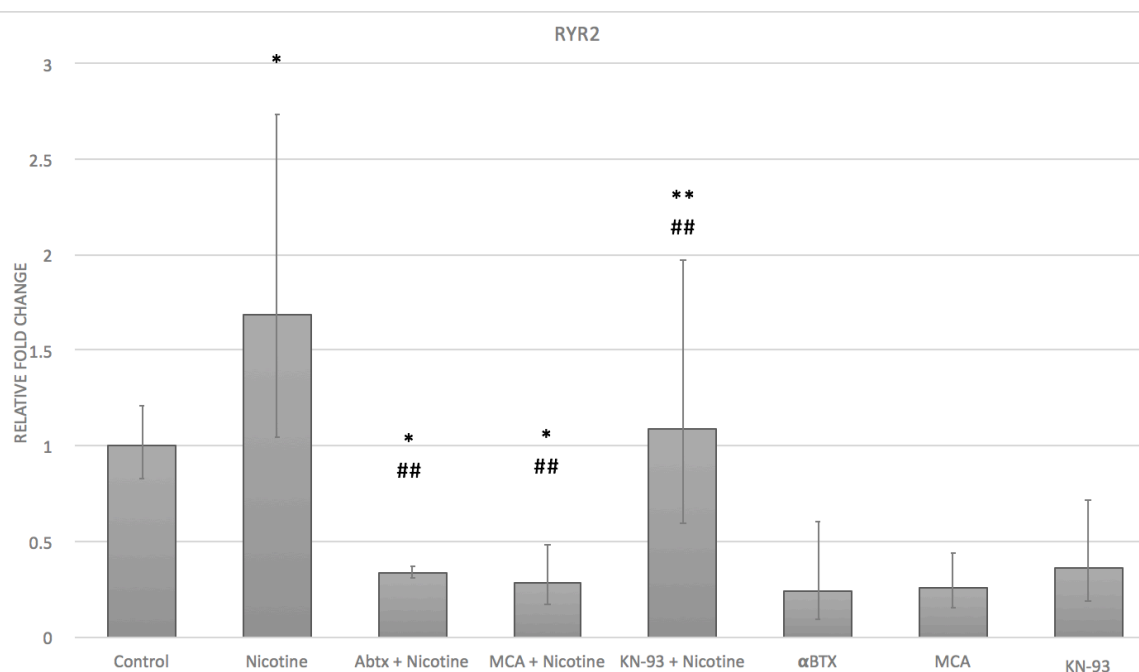


Figure 4.18 - Genetic expression analysis for ryanodine receptor 2 (RYR2) following treatment with 1 μ M nicotine with and without pretreatment of pharmacological agents. RYR2 is upregulated in the presence of nicotine. Inhibition of increased expression is observed with all pharmacological agents used in these studies. ($n=3$, * $p<0.05$ with respect to control, # $p<0.05$ with respect to nicotine, ** $p<0.01$ with respect to control, ## $p<0.01$ with respect to nicotine)

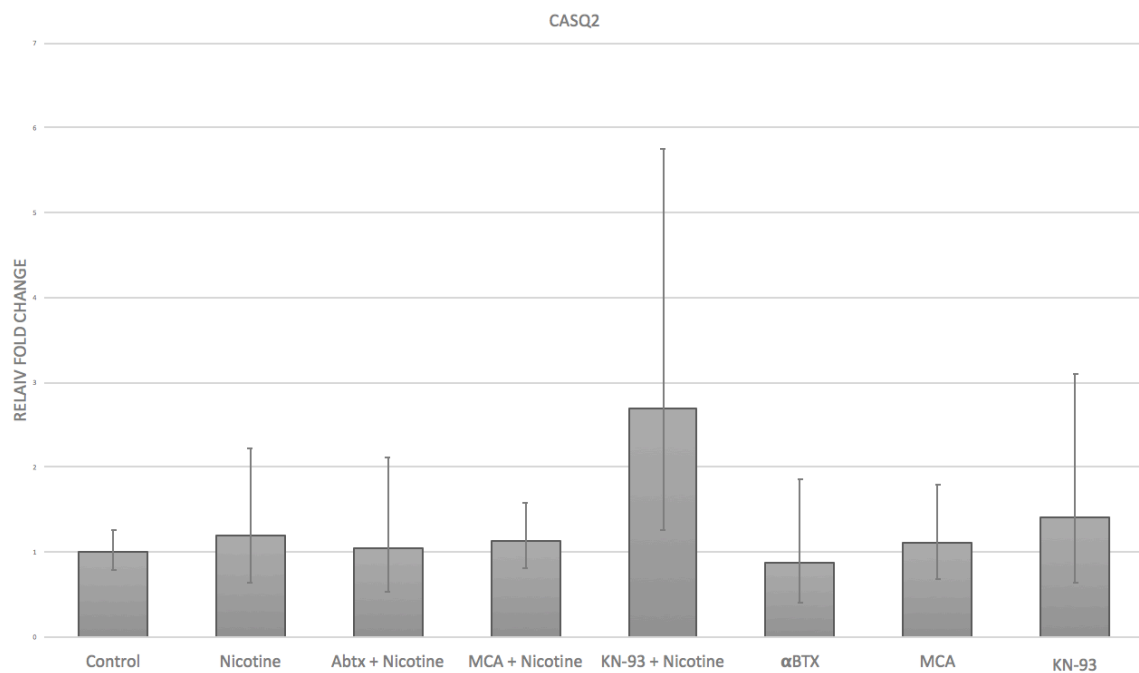


Figure 4.19 - Genetic expression analysis for calsequestrin (CASQ2) following treatment with 1 μ M nicotine with and without pretreatment of pharmacological agents. Expression patterns of CASQ2 do not appear altered in the presence of nicotine. (n=3)

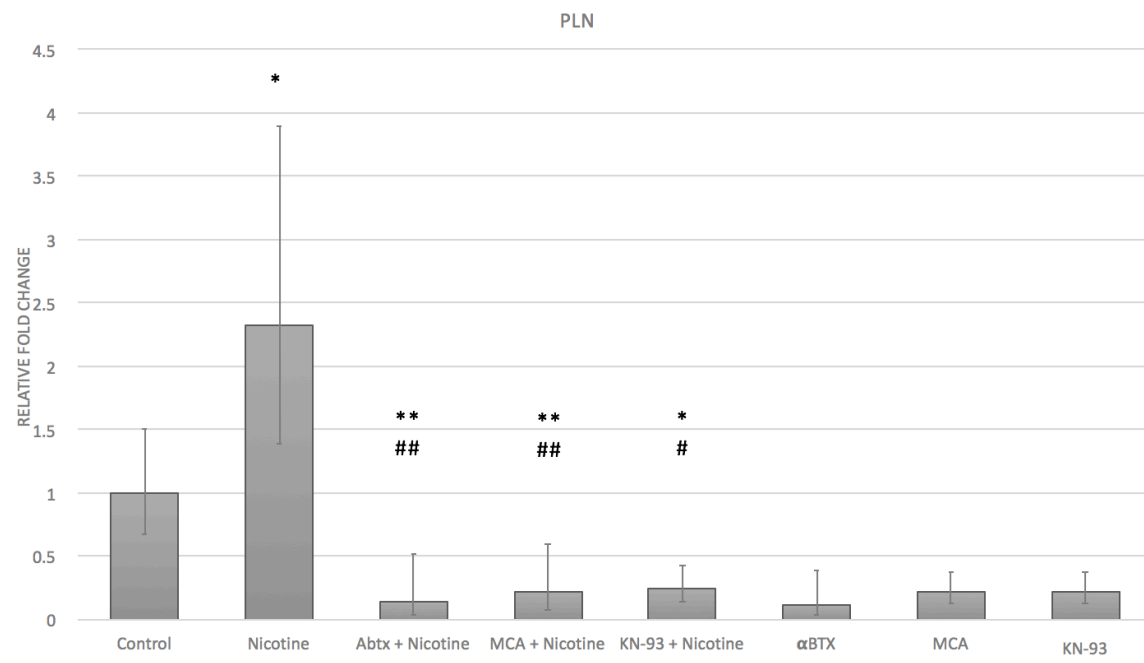


Figure 4.20 - Genetic expression analysis for phospholamban (PLN) following treatment with 1 μ M nicotine with and without pretreatment of pharmacological agents. PLN is upregulated in the presence of nicotine. Inhibition of increased expression is observed with all pharmacological agents used in these studies. ($n=3$, $n=3$, * $p<0.05$ with respect to control, # $p<0.05$ with respect to nicotine, ** $p<0.01$ with respect to control, ## $p<0.01$ with respect to nicotine')

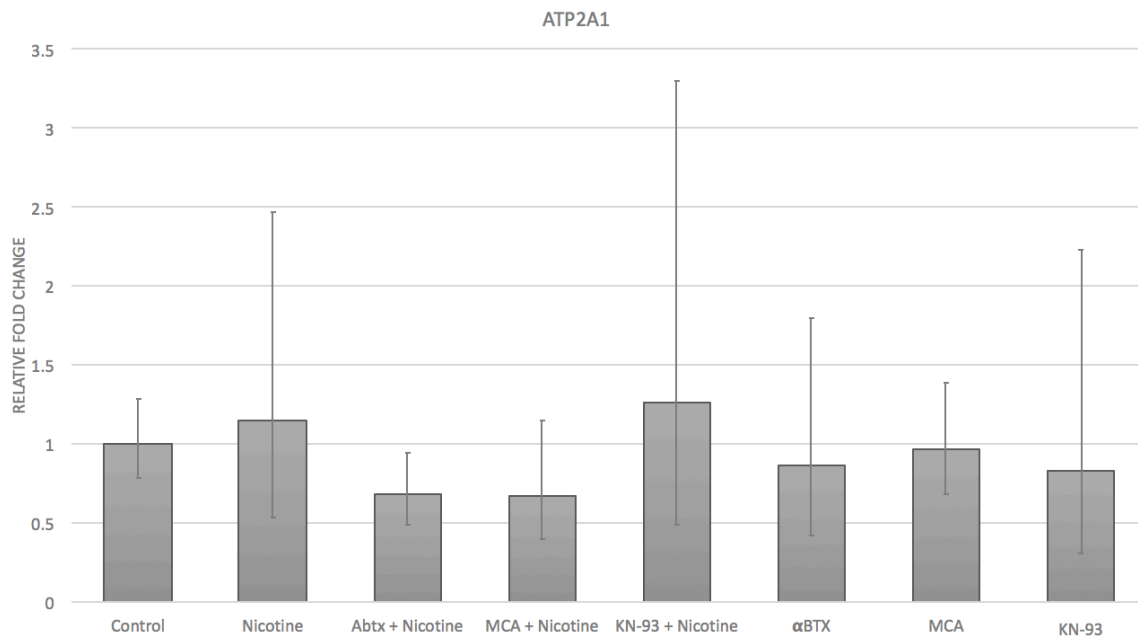


Figure 4.21 - Genetic expression analysis for Sarcoplasmic/Endoplasmic Reticulum Calcium ATPase 1 (ATP2A1) following treatment with 1 μ M nicotine with and without pretreatment of pharmacological agents. Expression patterns of ATP2A1 do not appear altered in the presence of nicotine. (n=3)

Discussion

To our knowledge we are the first to show that nicotine can affect CaMKII signaling and can induce hypertrophic signaling in iPS derived cardiomyocytes. We use IonOptix studies to show increased calcium loads in iPS-CM that were subject to 1 μ M nicotine treatment at every media change during differentiation. Using pharmacological agents, we show that this it is likely that increased calcium loads are induced by the activation of $\alpha 7$ nAChR present on naïve iPS cells. Further, we show this increased calcium load induces increased CaMKII activity which leads to changes in gene expression indicative of cardiomyocyte hypertrophy.

Gene expression patterns observed in these studies show that cells subject to nicotine exposure present fetal like gene program, as would be expected in cardiomyocyte hypertrophy. The concept of hypertrophy is commonly associated with a reversion to fetal

like growth program to compensate for increased demands, hence the reversion to fetal like gene programs. It remains to be seen in our studies whether these cells are arrested in a fetal like state during development, or cells mature and then revert to a fetal like state through continued maturation. Recent studies suggest that NPPA downregulation, more so than NPPB downregulation, is indicative of that post-natal phenotype in cardiomyocytes which may represent why NPPB was not upregulated to the extent of NPPA (164). This may also suggest that the cells are arrested in fetal like state do not mature fully. Had cells been allowed to mature we may also observe increases in NPPB consistent with that of NPPA. Based on gene expression analysis it would also appear that signaling through the nAChR play a crucial role in the development of cardiomyocytes. In the mature heart acetylcholine regulates the minute-to-minute contractility, and Roy et. al. show that autocrine acetylcholine stimulation from cardiomyocytes as well as parasympathetic innervation affect ACh concentrations (165). It would follow then that ACh signaling pathways also play key roles in the development of the heart, and may warrant further investigation.

α -bungarotoxin, the selective $\alpha 7$ inhibitor was effective in reducing the Ca^{2+} loads; however, mecamylamine, a general nAChR inhibitor appears to increase the intracellular calcium levels more than nicotine alone. One possible explanation for this may be a result of nicotine induced upregulation of nicotine receptors, a phenomenon that has been observed in the brain (166), and the kinetics of antagonist binding to nAChRs. α -bungarotoxin is known to bind relatively irreversibly to the $\alpha 7$ nAChR whereas mecamylamine inhibition can be reversed. It is possible that during long term culture, mecamylamine dissociates and due to nicotine induced upregulation, increased

concentration of uninhibited nAChRs responsible for the increased Ca^{2+} loads. Future studies should look at expression level of nAChR's at several points during differentiation to determine if this is indeed true. IonOptix data regarding kinetics appears to support our hypothesis that nicotine induces increased CaMKII activity. Ziolo et. al. have shown that under high systolic intracellular Ca^{2+} levels, calcium transients are faster, and the authors hypothesize that the faster time to peak is mediated by CaMKII signaling (167). Our results are consistent with this finding in showing that groups subject to 1 μM nicotine showed faster time to peak Ca^{2+} levels, and that this could be attenuated with the pretreatment using αbtx or KN-93.

Our data also shows that nicotine induces increased CaMKII activity as well as autophosphorylation of the Thr286 site of CaMKII. Autophosphorylation of CaMKII has the effect of reducing likelihood of Ca^{2+} dissociation from CaMKII, and increasing the affinity of the protein by 10^5 (40). The data presented herein also seems to support the hypothesis that increased CaMKII activity as a result of nAChR activation induces Thr17 phospholamban phosphorylation. In addition to PLN, CaMKII has many targets in cardiomyocytes to effect Ca^{2+} cycling regulation and it is important to keep these in mind. The scope of this study was to establish the link of CaMKII signaling and nicotine, and future studies should seek to look at the effects of nicotine on other targets of CaMKII signaling.

In addition to direct Ca^{2+} entry through $\alpha 7$ nAChR It is highly likely that nicotine also induces changes in other Ca^{2+} signaling pathways which have a contributory effect to CaMKII activity and intracellular calcium levels. In a mouse model, Li et. al. suggest that nicotine primarily induces hypertrophy through TRPC channels (25). TRPCs are

transmembrane channels that are traditionally found on lipid rafts in the plasma membrane, but have also been observed in the membranes of golgi and ER/SR where they function to refill stores. TRPCs are glycosylation-dependent proteins that similar to nAChRs once activated gate for Ca^{2+} . The exact role of TRPCs is still unknown, however it is believed that TRPCs control Ca^{2+} microdomain signaling and it has also been hypothesized that TRPCs interact directly with Ca^{2+} regulator proteins, such as phospholamban, and Cav1.2 protein, a calcium channel subunit of VDCCs (168). The associations between TRPC signaling activation and pathological cardiomyocyte hypertrophy have been previously described by Eder *et. al.* (169). The interaction between TRPC and nAChRs however is not entirely clear. A 2006 study by Feng *et. al.* developed a model of nicotine dependence in *C. Elegans* to determine the genetic underpinning of behavioral response changes elicited by nicotine. This study showed that nicotine responses require nAChRs, but interestingly mutant worms lacking TRPC channels were defective in their response to nicotine, thus highlighting the role of TRPC channels in regulating nicotine induced behavioral changes, and perhaps suggesting a role of TRPC in the changes observed in our studies (170).

CHAPTER 5. CONCLUSIONS AND FUTURE WORK

This project explores the development of a model of cardiomyocyte calcium cycling from stem cells, and uses the model to determine the effects of nicotine on cardiomyocyte differentiation and function. Both adult stem cells and induced pluripotent stem cells were investigated as potential models. While adult stem cells would be an ideal model due to their easy isolation and potential use for autologous transplantation, functional maturation of these cells to continuously beating myocytes was not observed in the studied model. Induced pluripotent stem cells were capable of differentiation to a functionally mature cardiomyocyte which spontaneously contracted through sarcoplasmic reticulum calcium cycling. With the development of the model, nicotine was added during differentiation to determine the mechanism of nicotine induced cardiac dysfunction. Through gene expression, protein expression, and calcium imaging it was determined that nicotine, through $\alpha 7$ nAChR, induces increased calcium load in iPS-CMs. Increased calcium loads in iPS-CM then activate CaMKII signaling pathways which alter intracellular calcium cycling pathways in iPS-CMs. iPS-CMs subject to nicotine exposure also displayed a reversion to a fetal like gene program which is commonly associated with cardiomyocyte hypertrophy.

Calcium cycling is highly regulated in cardiomyocytes and dysfunction of this pathway is linked to overall poor myocardial differentiation during development and pathological conditions in adults. While our studies were limited to the developing myocytes, it is likely that nicotine acts in similar ways in adult myocytes. The expression of nAChR on adult myocytes has been established and the role of CaMKII signaling is well established suggesting a likely corollary exists (171). Smoking induced cardiac hypertrophy is a well-

established clinical issue and the data presented here in presents options for new targets for therapeutics for smoking induced cardiac hypertrophy (172).

The obvious first potential targets to investigate would be the $\alpha 7$ nAChR. Targeting of $\alpha 7$ nAChR is already occurring in the clinic with $\alpha 7$ antagonists being prescribed for the treatment of Alzheimer's and schizophrenia. It is believed that $\alpha 7$ antagonists function in these conditions by reducing inflammation (173). $\alpha 7$ antagonism has also been suggested for use in cancer therapeutics, and treatment with α btx has shown promising effects in cell models of lung, bladder, and colon cancer cells (174). Another obvious potential target for innervation that the data may suggest is CaMKII. A 2010 report by Sossalla et al. has shown that in myocytes isolated from failing human myocardium, inhibition of CaMKII signaling could functionally improve contractility and suggest that further studies of CaMKII in heart failure patients are warranted (175). CaMKII inhibition has also been effectively used as a neuroprotective for brain ischemia following cardiac arrest (176) suggesting that CaMKII inhibition may be a potential innervational strategy. Lastly, VDCC's may represent an interesting target in this mechanism. VDCC's are known to be modulated by CaMKII signaling. VDCC's also represent the first site in CICR for regulation. The amount of Ca^{2+} which enters through VDCC's is directly correlated with the strength of that contraction. Modulation of VDCC signaling has already been successfully employed in the clinic with nifedipine being used to treat hypertension. It could be suggested modulation of intracellular calcium influx through VDCC channels may ameliorate the effects of nicotine on cardiomyocytes (177).

Future Directions

The results of these studies open the door for many future basic science studies based off the knowledge obtained herein. First would be to investigate changes at the epigenetic level following exposure of stem cells to nicotine. Recent work by Jung et al. has shown that nicotine effects neurological development through an epigenetic mechanism. Similar to heart development, *in utero* nicotine exposure is known to cause changes to neuron morphology and can ultimately lead to learning defects and psychiatric issues later in life. In these studies, Jung et al. used microarrays to show that nicotine induced activation of ash2l, a component of the histone methylation complex. Action of ash2l increased trimethylation of histone 3, lysine 4 (H3K4me3) at promoter regions associated with development and maintenance of synapses, including the MEF2C site (178). In addition to its role in neural development, MEF2C is an important transcription factor involved in heart development, including differentiation of cardiomyocytes, and hypertrophy (179, 180). High levels of H3k4me3 indicates transcriptionally active sites, and changes in these epigenetics marks has been linked to cardiomyocyte hypertrophy and heart failure (181). In addition to this specific site marks at H3k9, have also been linked to heart failure (179). Based on this discussion, it is possible that nicotine may be inducing epigenetic marks similar to those in neurons and indicated in heart failure and that these marks could offer potential sources of new drug targets.

The other potential avenue that this data may lead is in the effects of nicotine in cells isolated from schizophrenic patients. Neurons are another cell type which use regulation of Ca^{2+} to achieve effector functions. Many of the regulatory proteins involved in cardiomyocytes Ca^{2+} regulation are known to be expressed and active in neurons as well.

A 2014 review even highlights the emerging role of CaMKII in neuropsychiatric disease (182). Epidemiological studies have shown that schizophrenic patients smoke more heavily than the general population. Nicotine has been reported to decrease the side effects of antipsychotics, and alleviating feelings of anxiety, depression, anhedonia, and amotivation in schizophrenic patients (183). The exact cause of schizophrenia remains unknown; however, it is becoming increasingly clear that $\alpha 7$ nAChR are related to the pathophysiology of schizophrenia (183). The ability to generate pluripotent stem cells from somatic cells allows for the development of a model of neurons from schizophrenic patients. Using these cells we can then model the effects of nicotine to help determine the molecular role of $\alpha 7$ nAChR in neurons derived from schizophrenic patients, and changes in calcium cycling in diseased patients.

REFERENCES

1. Mullin R. Tufts study finds big rise in cost of drug development. *Chemical & Engineering News*. 2014.
2. Bowes J, Brown AJ, Hamon J, Jarolimek W, Sridhar A, Waldron G, et al. Reducing safety-related drug attrition: the use of in vitro pharmacological profiling. *Nat Rev Drug Discov*. 2012;11(12):909-22.
3. Nguyen N, Nguyen W, Nguyenton B, Ratchada P, Page G, Miller PE, et al. Adult human primary cardiomyocyte-based model for the simultaneous prediction of drug-induced inotropic and pro-arrhythmia risk. *Front Physiol*. 2017;8:1073.
4. Milani-Nejad N, Janssen PM. Small and large animal models in cardiac contraction research: advantages and disadvantages. *Pharmacol Ther*. 2014;141(3):235-49.
5. Ramalho-Santos M, Willenbring H. On the origin of the term "stem cell". *Cell Stem Cell*. 2007;1(1):35-8.
6. Thomson JA, Itskovitz-Eldor J, Shapiro SS, Waknitz MA, Swiergiel JJ, Marshall VS, et al. Embryonic stem cell lines derived from human blastocysts. *Science*. 1998;282(5391):1145-7.
7. The health consequences of smoking-50 years of progress: a report of the surgeon general. In: U.S Department of Health and Human Services, National Center for Chronic Disease Prevention and Health Promotion. Atlanta, GA2014.
8. How tobacco smoke causes disease: the biology and behavioral basis for smoking-attributable disease: a report of the surgeon general. *Publications and Reports of the Surgeon General*. Atlanta (GA)2010.
9. Wickstrom R. Effects of nicotine during pregnancy: human and experimental evidence. *Curr Neuropharmacol*. 2007;5(3):213-22.
10. Lambers DS, Clark KE. The maternal and fetal physiologic effects of nicotine. *Semin Perinatol*. 1996;20(2):115-26.
11. Curtin SC, Matthews TJ. Smoking prevalence and cessation before and during pregnancy: data from the birth certificate, 2014. *Natl Vital Stat Rep*. 2016;65(1):1-14.
12. Martinsen BJ, Lohr JL. Cardiac Development. In: Iaizzo PA, editor. *Handbook of cardiac anatomy, physiology, and devices*. Cham: Springer International Publishing; 2015. p. 23-33.
13. Beratis NG, Panagoulas D, Varvarigou A. Increased blood pressure in neonates and infants whose mothers smoked during pregnancy. *J Pediatr*. 1996;128(6):806-12.

14. Blake KV, Gurrin LC, Evans SF, Beilin LJ, Landau LI, Stanley FJ, et al. Maternal cigarette smoking during pregnancy, low birth weight and subsequent blood pressure in early childhood. *Early Hum Dev.* 2000;57(2):137-47.
15. Bruin JE, Gerstein HC, Holloway AC. Long-term consequences of fetal and neonatal nicotine exposure: a critical review. *Toxicol Sci.* 2010;116(2):364-74.
16. Baumeister RF. Addiction, cigarette smoking, and voluntary control of action: do cigarette smokers lose their free will? *Addict Behav Rep.* 2017;5:67-84.
17. Benowitz NL, Gourlay SG. Cardiovascular toxicity of nicotine: implications for nicotine replacement therapy. *J Am Coll Cardiol.* 1997;29(7):1422-31.
18. Jamal A, Gentzke A, Hu SS, Cullen KA, Apelberg BJ, Homa DM, et al. Tobacco use among middle and high school students-United States, 2011-2016. *Centers for Disease Control and Prevention*; 2017 June 16, 2017.
19. Bers DM. Calcium cycling and signaling in cardiac myocytes. *Annu Rev Physiol.* 2008;70:23-49.
20. Dewenter M, von der Lieth A, Katus HA, Backs J. Calcium signaling and transcriptional regulation in cardiomyocytes. *Circ Res.* 2017;121(8):1000-20.
21. Cartwright EJ, Mohamed T, Oceandy D, Neyses L. Calcium signaling dysfunction in heart disease. *Biofactors.* 2011;37(3):175-81.
22. Hoshijima M, Knoll R, Pashmforoush M, Chien KR. Reversal of calcium cycling defects in advanced heart failure toward molecular therapy. *J Am Coll Cardiol.* 2006;48(9 Suppl 1):A15-23.
23. Hanna ST. Nicotine effect on cardiovascular system and ion channels. *J Cardiovasc Pharmacol.* 2006;47(3):348-58.
24. Zhou X, Sheng Y, Yang R, Kong X. Nicotine promotes cardiomyocyte apoptosis via oxidative stress and altered apoptosis-related gene expression. *Cardiology.* 2010;115(4):243-50.
25. Li N, Si B, Ju JF, Zhu M, You F, Wang D, et al. Nicotine induces cardiomyocyte hypertrophy through TRPC3-mediated Ca(2+)/NFAT signalling pathway. *Can J Cardiol.* 2016;32(10):1260 e1- e10.
26. Albuquerque EX, Pereira EF, Alkondon M, Rogers SW. Mammalian nicotinic acetylcholine receptors: from structure to function. *Physiol Rev.* 2009;89(1):73-120.
27. Mazloom R, Eftekhari G, Rahimi-Balaei M, Khori V, Hajizadeh S, Dehpour AR, et al. The role of alpha7 nicotinic acetylcholine receptor in modulation of heart rate dynamics in endotoxemic rats. *PLoS One.* 2013;8(12):e82251.

28. Ishizuka T, Goshima H, Ozawa A, Watanabe Y. Effect of nicotine on the proliferation and differentiation of mouse induced pluripotent stem cells. *Curr Med Chem*. 2012;19(30):5164-9.
29. Chuai M, Weijer CJ. The mechanisms underlying primitive streak formation in the chick embryo. *Curr Top Dev Biol*. 2008;81:135-56.
30. Brade T, Pane LS, Moretti A, Chien KR, Laugwitz KL. Embryonic heart progenitors and cardiogenesis. *Cold Spring Harb Perspect Med*. 2013;3(10):a013847.
31. Maillet M, van Berlo JH, Molkentin JD. Molecular basis of physiological heart growth: fundamental concepts and new players. *Nat Rev Mol Cell Biol*. 2013;14(1):38-48.
32. Laflamme MA, Murry CE. Heart regeneration. *Nature*. 2011;473(7347):326-35.
33. Andersen ND, Ramachandran KV, Bao MM, Kirby ML, Pitt GS, Hutson MR. Calcium signaling regulates ventricular hypertrophy during development independent of contraction or blood flow. *J Mol Cell Cardiol*. 2015;80:1-9.
34. Lin YF, Swinburne I, Yelon D. Multiple influences of blood flow on cardiomyocyte hypertrophy in the embryonic zebrafish heart. *Dev Biol*. 2012;362(2):242-53.
35. Rottbauer W, Baker K, Wo ZG, Mohideen MA, Cantiello HF, Fishman MC. Growth and function of the embryonic heart depend upon the cardiac-specific L-type calcium channel alpha1 subunit. *Dev Cell*. 2001;1(2):265-75.
36. Tyser RC, Miranda AM, Chen CM, Davidson SM, Srinivas S, Riley PR. Calcium handling precedes cardiac differentiation to initiate the first heartbeat. *Elife*. 2016;5.
37. Marks AR. Calcium cycling proteins and heart failure: mechanisms and therapeutics. *J Clin Invest*. 2013;123(1):46-52.
38. Zhang T, Brown JH. Role of Ca²⁺/calmodulin-dependent protein kinase II in cardiac hypertrophy and heart failure. *Cardiovasc Res*. 2004;63(3):476-86.
39. Erickson JR. Mechanisms of CaMKII activation in the heart. *Front Pharmacol*. 2014;5:59.
40. Anderson ME, Brown JH, Bers DM. CaMKII in myocardial hypertrophy and heart failure. *J Mol Cell Cardiol*. 2011;51(4):468-73.
41. MacLennan DH, Kranias EG. Phospholamban: a crucial regulator of cardiac contractility. *Nat Rev Mol Cell Biol*. 2003;4(7):566-77.
42. Rodriguez P, Kranias EG. Phospholamban: a key determinant of cardiac function and dysfunction. *Arch Mal Coeur Vaiss*. 2005;98(12):1239-43.

43. Schulman H, Anderson ME. Ca/Calmodulin-dependent protein kinase II in heart failure. *Drug Discov Today Dis Mech.* 2010;7(2):e117-e22.
44. Frey N, Katus HA, Olson EN, Hill JA. Hypertrophy of the heart: a new therapeutic target? *Circulation.* 2004;109(13):1580-9.
45. Pearce PC, Hawkey C, Symons C, Olsen EG. Role of calcium in the induction of cardiac hypertrophy and myofibrillar disarray. Experimental studies of a possible cause of hypertrophic cardiomyopathy. *Br Heart J.* 1985;54(4):420-7.
46. Sei CA, Irons CE, Sprenkle AB, McDonough PM, Brown JH, Glembotski CC. The alpha-adrenergic stimulation of atrial natriuretic factor expression in cardiac myocytes requires calcium influx, protein kinase C, and calmodulin-regulated pathways. *J Biol Chem.* 1991;266(24):15910-6.
47. Dirx E, da Costa Martins PA, De Windt LJ. Regulation of fetal gene expression in heart failure. *Biochim Biophys Acta.* 2013;1832(12):2414-24.
48. Du XJ. Divergence of hypertrophic growth and fetal gene profile: the influence of beta-blockers. *Br J Pharmacol.* 2007;152(2):169-71.
49. Nagueh SF, Shah G, Wu Y, Torre-Amione G, King NM, Lahmers S, et al. Altered titin expression, myocardial stiffness, and left ventricular function in patients with dilated cardiomyopathy. *Circulation.* 2004;110(2):155-62.
50. Ehler E, Moore-Morris T, Lange S. Isolation and culture of neonatal mouse cardiomyocytes. *J Vis Exp.* 2013(79).
51. Peter AK, Bjerke MA, Leinwand LA. Biology of the cardiac myocyte in heart disease. *Mol Biol Cell.* 2016;27(14):2149-60.
52. Kimes BW, Brandt BL. Properties of a clonal muscle cell line from rat heart. *Exp Cell Res.* 1976;98(2):367-81.
53. Tan X, Wang DB, Lu X, Wei H, Zhu R, Zhu SS, et al. Doxorubicin induces apoptosis in H9c2 cardiomyocytes: role of overexpressed eukaryotic translation initiation factor 5A. *Biol Pharm Bull.* 2010;33(10):1666-72.
54. Zordoky BN, El-Kadi AO. H9c2 cell line is a valuable in vitro model to study the drug metabolizing enzymes in the heart. *J Pharmacol Toxicol Methods.* 2007;56(3):317-22.
55. Watkins SJ, Borthwick GM, Arthur HM. The H9C2 cell line and primary neonatal cardiomyocyte cells show similar hypertrophic responses in vitro. *In Vitro Cell Dev Biol Anim.* 2011;47(2):125-31.

56. Branco AF, Pereira SP, Gonzalez S, Gusev O, Rizvanov AA, Oliveira PJ. Gene expression profiling of H9c2 myoblast differentiation towards a cardiac-like phenotype. *PLoS One*. 2015;10(6):e0129303.
57. Witek P, Korga A, Burdan F, Ostrowska M, Nosowska B, Iwan M, et al. The effect of a number of H9C2 rat cardiomyocytes passage on repeatability of cytotoxicity study results. *Cytotechnology*. 2016;68(6):2407-15.
58. Claycomb WC, Lanson NA, Jr., Stallworth BS, Egeland DB, Delcarpio JB, Bahinski A, et al. HL-1 cells: a cardiac muscle cell line that contracts and retains phenotypic characteristics of the adult cardiomyocyte. *Proc Natl Acad Sci U S A*. 1998;95(6):2979-84.
59. White SM, Constantin PE, Claycomb WC. Cardiac physiology at the cellular level: use of cultured HL-1 cardiomyocytes for studies of cardiac muscle cell structure and function. *Am J Physiol Heart Circ Physiol*. 2004;286(3):H823-9.
60. NIH stem cell information home page Bethesda, MD: National Institutes of Health; 2016 [Available from: stemcells.nih.gov/info/basics/1.htm].
61. Zeddou M, Briquet A, Relic B, Josse C, Malaise MG, Gothot A, et al. The umbilical cord matrix is a better source of mesenchymal stem cells (MSC) than the umbilical cord blood. *Cell Biol Int*. 2010;34(7):693-701.
62. Pozzobon M, Piccoli M, De Coppi P. Stem cells from fetal membranes and amniotic fluid: markers for cell isolation and therapy. *Cell Tissue Bank*. 2014;15(2):199-211.
63. Pelaez D, Huang CY, Cheung HS. Isolation of pluripotent neural crest-derived stem cells from adult human tissues by connexin-43 enrichment. *Stem Cells Dev*. 2013;22(21):2906-14.
64. Charbord P. Bone marrow mesenchymal stem cells: historical overview and concepts. *Hum Gene Ther*. 2010;21(9):1045-56.
65. Gimble JM, Guilak F, Nuttall ME, Sathishkumar S, Vidal M, Bunnell BA. In vitro differentiation potential of mesenchymal stem cells. *Transfus Med Hemother*. 2008;35(3):228-38.
66. Kornblum HI. Introduction to neural stem cells. *Stroke*. 2007;38(2 Suppl):810-6.
67. Bearzi C, Rota M, Hosoda T, Tillmanns J, Nascimbene A, De Angelis A, et al. Human cardiac stem cells. *Proc Natl Acad Sci U S A*. 2007;104(35):14068-73.
68. Okita K, Ichisaka T, Yamanaka S. Generation of germline-competent induced pluripotent stem cells. *Nature*. 2007;448(7151):313-7.

69. Gneccchi M, Zhang Z, Ni A, Dzau VJ. Paracrine mechanisms in adult stem cell signaling and therapy. *Circ Res*. 2008;103(11):1204-19.
70. Genovese JA, Spadaccio C, Chachques E, Schussler O, Carpentier A, Chachques JC, et al. Cardiac pre-differentiation of human mesenchymal stem cells by electrostimulation. *Front Biosci (Landmark Ed)*. 2009;14:2996-3002.
71. Menasche P. Stem cells for clinical use in cardiovascular medicine: current limitations and future perspectives. *Thromb Haemost*. 2005;94(4):697-701.
72. Siegel G, Krause P, Wohrle S, Nowak P, Ayturan M, Kluba T, et al. Bone marrow-derived human mesenchymal stem cells express cardiomyogenic proteins but do not exhibit functional cardiomyogenic differentiation potential. *Stem Cells Dev*. 2012;21(13):2457-70.
73. Beltrami AP, Barlucchi L, Torella D, Baker M, Limana F, Chimenti S, et al. Adult cardiac stem cells are multipotent and support myocardial regeneration. *Cell*. 2003;114(6):763-76.
74. Santini MP, Forte E, Harvey RP, Kovacic JC. Developmental origin and lineage plasticity of endogenous cardiac stem cells. *Development*. 2016;143(8):1242-58.
75. Sultana N, Zhang L, Yan J, Chen J, Cai W, Razzaque S, et al. Resident c-kit(+) cells in the heart are not cardiac stem cells. *Nat Commun*. 2015;6:8701.
76. Yang X, Pabon L, Murry CE. Engineering adolescence: maturation of human pluripotent stem cell-derived cardiomyocytes. *Circ Res*. 2014;114(3):511-23.
77. Dolnikov K, Shilkrut M, Zeevi-Levin N, Gerecht-Nir S, Amit M, Danon A, et al. Functional properties of human embryonic stem cell-derived cardiomyocytes: intracellular Ca²⁺ handling and the role of sarcoplasmic reticulum in the contraction. *Stem Cells*. 2006;24(2):236-45.
78. Hwang HS, Kryshtal DO, Feaster TK, Sanchez-Freire V, Zhang J, Kamp TJ, et al. Comparable calcium handling of human iPSC-derived cardiomyocytes generated by multiple laboratories. *J Mol Cell Cardiol*. 2015;85:79-88.
79. Messner B, Bernhard D. Smoking and cardiovascular disease: mechanisms of endothelial dysfunction and early atherogenesis. *Arterioscler Thromb Vasc Biol*. 2014;34(3):509-15.
80. Buchanan DM, Arnold SV, Gosch KL, Jones PG, Longmore LS, Spertus JA, et al. Association of smoking status with angina and health-related quality of life after acute myocardial infarction. *Circ Cardiovasc Qual Outcomes*. 2015;8(5):493-500.
81. Watkins SJ, Borthwick GM, Oakenfull R, Robson A, Arthur HM. Angiotensin II-induced cardiomyocyte hypertrophy in vitro is TAK1-dependent and Smad2/3-independent. *Hypertens Res*. 2012;35(4):393-8.

82. Wahl EA, Schenck TL, Machens HG, Egana JT. Acute stimulation of mesenchymal stem cells with cigarette smoke extract affects their migration, differentiation, and paracrine potential. *Sci Rep*. 2016;6:22957.
83. Benowitz NL. Pharmacology of nicotine: addiction, smoking-induced disease, and therapeutics. *Annu Rev Pharmacol Toxicol*. 2009;49:57-71.
84. Stepanov I, Fujioka N. Bringing attention to e-cigarette pH as an important element for research and regulation. *Tob Control*. 2015;24(4):413-4.
85. Lindell G, Lunell E, Graffner H. Transdermally administered nicotine accumulates in gastric juice. *Eur J Clin Pharmacol*. 1996;51(3-4):315-8.
86. Nemezc A, Prevost MS, Menny A, Corringer PJ. Emerging molecular mechanisms of signal transduction in pentameric ligand-gated ion channels. *Neuron*. 2016;90(3):452-70.
87. Lax P, Fucile S, Eusebi F. Ca(2+) permeability of human heteromeric nAChRs expressed by transfection in human cells. *Cell Calcium*. 2002;32(2):53-8.
88. Wang XJ, Liu YF, Wang QY, Tsuruoka M, Ohta K, Wu SX, et al. Functional expression of alpha 7 nicotinic acetylcholine receptors in human periodontal ligament fibroblasts and rat periodontal tissues. *Cell Tissue Res*. 2010;340(2):347-55.
89. Kim SY, Kang KL, Lee JC, Heo JS. Nicotinic acetylcholine receptor alpha7 and beta4 subunits contribute nicotine-induced apoptosis in periodontal ligament stem cells. *Mol Cells*. 2012;33(4):343-50.
90. Kalamida D, Poulas K, Avramopoulou V, Fostieri E, Lagoumintzis G, Lazaridis K, et al. Muscle and neuronal nicotinic acetylcholine receptors. Structure, function and pathogenicity. *FEBS J*. 2007;274(15):3799-845.
91. Lin W, Hirata N, Sekino Y, Kanda Y. Role of alpha7-nicotinic acetylcholine receptor in normal and cancer stem cells. *Curr Drug Targets*. 2012;13(5):656-65.
92. Seroby N, Jagannathan S, Orlovskaya I, Schraufstatter I, Skok M, Loring J, et al. The cholinergic system is involved in regulation of the development of the hematopoietic system. *Life Sci*. 2007;80(24-25):2352-60.
93. Ben-Yehudah A, Campanaro BM, Wakefield LM, Kinney TN, Brekosky J, Eisinger VM, et al. Nicotine exposure during differentiation causes inhibition of N-myc expression. *Respir Res*. 2013;14:119.
94. Ishizuka T, Ozawa A, Goshima H, Watanabe Y. Involvement of nicotinic acetylcholine receptor in the proliferation of mouse induced pluripotent stem cells. *Life Sci*. 2012;90(17-18):637-48.

95. Moser N, Mechawar N, Jones I, Gochberg-Sarver A, Orr-Urtreger A, Plomann M, et al. Evaluating the suitability of nicotinic acetylcholine receptor antibodies for standard immunodetection procedures. *J Neurochem*. 2007;102(2):479-92.
96. Landgraf D, Barth M, Layer PG, Sperling LE. Acetylcholine as a possible signaling molecule in embryonic stem cells: studies on survival, proliferation and death. *Chem Biol Interact*. 2010;187(1-3):115-9.
97. Hoogduijn MJ, Cheng A, Genever PG. Functional nicotinic and muscarinic receptors on mesenchymal stem cells. *Stem Cells Dev*. 2009;18(1):103-12.
98. Schraufstatter IU, DiScipio RG, Khaldoyanidi SK. Alpha 7 subunit of nAChR regulates migration of human mesenchymal stem cells. *J Stem Cells*. 2009;4(4):203-15.
99. Zablotni A, Dakischew O, Trinkaus K, Hartmann S, Szalay G, Heiss C, et al. Regulation of acetylcholine receptors during differentiation of bone mesenchymal stem cells harvested from human reaming debris. *Int Immunopharmacol*. 2015;29(1):119-26.
100. Palpant NJ, Hofsteen P, Pabon L, Reinecke H, Murry CE. Cardiac development in zebrafish and human embryonic stem cells is inhibited by exposure to tobacco cigarettes and e-cigarettes. *PLoS One*. 2015;10(5):e0126259.
101. Jackson KJ, Muldoon PP, Walters C, Damaj MI. Neuronal calcium/calmodulin-dependent protein kinase II mediates nicotine reward in the conditioned place preference test in mice. *Behav Pharmacol*. 2016;27(1):50-6.
102. The top 10 causes of death: World Health Organization; 2014 [Available from: <http://www.who.int/mediacentre/factsheets/fs310/en/>].
103. van den Borne SW, Diez J, Blankesteyn WM, Verjans J, Hofstra L, Narula J. Myocardial remodeling after infarction: the role of myofibroblasts. *Nature reviews Cardiology*. 2010;7(1):30-7.
104. Matar AA, Chong JJ. Stem cell therapy for cardiac dysfunction. *SpringerPlus*. 2014;3:440.
105. Elnakish MT, Hassan F, Dakhllallah D, Marsh CB, Alhaider IA, Khan M. Mesenchymal stem cells for cardiac regeneration: translation to bedside reality. *Stem cells international*. 2012;2012:646038.
106. Martin-Rendon E, Brunskill SJ, Hyde CJ, Stanworth SJ, Mathur A, Watt SM. Autologous bone marrow stem cells to treat acute myocardial infarction: a systematic review. *European heart journal*. 2008;29(15):1807-18.
107. Mohsin S, Siddiqi S, Collins B, Sussman MA. Empowering adult stem cells for myocardial regeneration. *Circulation research*. 2011;109(12):1415-28.

108. Gao Q, Guo M, Jiang X, Hu X, Wang Y, Fan Y. A cocktail method for promoting cardiomyocyte differentiation from bone marrow-derived mesenchymal stem cells. *Stem cells international*. 2014;2014:162024.
109. Qian Q, Qian H, Zhang X, Zhu W, Yan Y, Ye S, et al. 5-Azacytidine induces cardiac differentiation of human umbilical cord-derived mesenchymal stem cells by activating extracellular regulated kinase. *Stem Cells Dev*. 2012;21(1):67-75.
110. Rose RA, Jiang H, Wang X, Helke S, Tsoporis JN, Gong N, et al. Bone marrow-derived mesenchymal stromal cells express cardiac-specific markers, retain the stromal phenotype, and do not become functional cardiomyocytes in vitro. *Stem cells (Dayton, Ohio)*. 2008;26(11):2884-92.
111. Menasche P. Cardiac cell therapy: lessons from clinical trials. *Journal of molecular and cellular cardiology*. 2011;50(2):258-65.
112. Bartunek J, Behfar A, Dolatabadi D, Vanderheyden M, Ostojic M, Dens J, et al. Cardiopoietic stem cell therapy in heart failure: the C-CURE (Cardiopoietic stem Cell therapy in heart failURE) multicenter randomized trial with lineage-specified biologics. *J Am Coll Cardiol*. 2013;61(23):2329-38.
113. Xin LZ, Govindasamy V, Musa S, Abu Kasim NH. Dental stem cells as an alternative source for cardiac regeneration. *Med Hypotheses*. 2013;81(4):704-6.
114. Mayo V, Sawatari Y, Huang CY, Garcia-Godoy F. Neural crest-derived dental stem cells--where we are and where we are going. *J Dent*. 2014;42(9):1043-51.
115. Arminan A, Gandia C, Bartual M, Garcia-Verdugo JM, Lledo E, Mirabet V, et al. Cardiac differentiation is driven by NKX2.5 and GATA4 nuclear translocation in tissue-specific mesenchymal stem cells. *Stem Cells Dev*. 2009;18(6):907-18.
116. Gandia C, Arminan A, Garcia-Verdugo JM, Lledo E, Ruiz A, Minana MD, et al. Human dental pulp stem cells improve left ventricular function, induce angiogenesis, and reduce infarct size in rats with acute myocardial infarction. *Stem cells (Dayton, Ohio)*. 2008;26(3):638-45.
117. Huang CY, Pelaez D, Dominguez-Bendala J, Garcia-Godoy F, Cheung HS. Plasticity of stem cells derived from adult periodontal ligament. *Regenerative medicine*. 2009;4(6):809-21.
118. Bronner ME. Formation and migration of neural crest cells in the vertebrate embryo. *Histochem Cell Biol*. 2012;138(2):179-86.
119. Lo CW, Waldo KL, Kirby ML. Gap junction communication and the modulation of cardiac neural crest cells. *Trends Cardiovasc Med*. 1999;9(3-4):63-9.

120. Xu X, Li WE, Huang GY, Meyer R, Chen T, Luo Y, et al. Modulation of mouse neural crest cell motility by N-cadherin and connexin 43 gap junctions. *J Cell Biol.* 2001;154(1):217-30.
121. Stoller JZ, Epstein JA. Cardiac neural crest. *Semin Cell Dev Biol.* 2005;16(6):704-15.
122. Keith MC, Bolli R. "String theory" of c-kit(pos) cardiac cells: a new paradigm regarding the nature of these cells that may reconcile apparently discrepant results. *Circ Res.* 2015;116(7):1216-30.
123. Tamura Y, Matsumura K, Sano M, Tabata H, Kimura K, Ieda M, et al. Neural crest-derived stem cells migrate and differentiate into cardiomyocytes after myocardial infarction. *Arterioscler Thromb Vasc Biol.* 2011;31(3):582-9.
124. Hatzistergos KE, Takeuchi LM, Saur D, Seidler B, Dymecki SM, Mai JJ, et al. cKit+ cardiac progenitors of neural crest origin. *Proc Natl Acad Sci U S A.* 2015;112(42):13051-6.
125. Calderone A. Nestin+ cells and healing the infarcted heart. *Am J Physiol Heart Circ Physiol.* 2012;302(1):H1-9.
126. Rohr S. Role of gap junctions in the propagation of the cardiac action potential. *Cardiovasc Res.* 2004;62(2):309-22.
127. Lumbreras V, Bas E, Gupta C, Rajguru SM. Pulsed infrared radiation excites cultured neonatal spiral and vestibular ganglion neurons by modulating mitochondrial calcium cycling. *Journal of neurophysiology.* 2014;112(6):1246-55.
128. Dittami GM, Rajguru SM, Lasher RA, Hitchcock RW, Rabbitt RD. Intracellular calcium transients evoked by pulsed infrared radiation in neonatal cardiomyocytes. *The Journal of physiology.* 2011;589(Pt 6):1295-306.
129. Jenkins MW, Wang YT, Doughman YQ, Watanabe M, Cheng Y, Rollins AM. Optical pacing of the adult rabbit heart. *Biomedical optics express.* 2013;4(9):1626-35.
130. Bas E, Van De Water TR, Lumbreras V, Rajguru S, Goss G, Hare JM, et al. Adult human nasal mesenchymal-like stem cells restore cochlear spiral ganglion neurons after experimental lesion. *Stem cells and development.* 2014;23(5):502-14.
131. Jenkins MW, Duke AR, Gu S, Chiel HJ, Fujioka H, Watanabe M, et al. Optical pacing of the embryonic heart. *Nature photonics.* 2010;4:623-6.
132. Smith NI, Kumamoto Y, Iwanaga S, Ando J, Fujita K, Kawata S. A femtosecond laser pacemaker for heart muscle cells. *Optics express.* 2008;16(12):8604-16.
133. Livak KJ, Schmittgen TD. Analysis of relative gene expression data using real-time quantitative PCR and the 2(-Delta Delta C(T)) Method. *Methods.* 2001;25(4):402-8.

134. Dorn GW, 2nd. Apoptotic and non-apoptotic programmed cardiomyocyte death in ventricular remodelling. *Cardiovascular research*. 2009;81(3):465-73.
135. Lien CL, Wu C, Mercer B, Webb R, Richardson JA, Olson EN. Control of early cardiac-specific transcription of Nkx2-5 by a GATA-dependent enhancer. *Development*. 1999;126(1):75-84.
136. Pilon N, Raiwet D, Viger RS, Silversides DW. Novel pre- and post-gastrulation expression of Gata4 within cells of the inner cell mass and migratory neural crest cells. *Dev Dyn*. 2008;237(4):1133-43.
137. Verzi MP, Agarwal P, Brown C, McCulley DJ, Schwarz JJ, Black BL. The transcription factor MEF2C is required for craniofacial development. *Dev Cell*. 2007;12(4):645-52.
138. Abraham MR, Henrikson CA, Tung L, Chang MG, Aon M, Xue T, et al. Antiarrhythmic engineering of skeletal myoblasts for cardiac transplantation. *Circulation research*. 2005;97(2):159-67.
139. Fernandes S, van Rijen HV, Forest V, Evain S, Leblond AL, Merot J, et al. Cardiac cell therapy: overexpression of connexin43 in skeletal myoblasts and prevention of ventricular arrhythmias. *J Cell Mol Med*. 2009;13(9B):3703-12.
140. Roell W, Lewalter T, Sasse P, Tallini YN, Choi BR, Breitbach M, et al. Engraftment of connexin 43-expressing cells prevents post-infarct arrhythmia. *Nature*. 2007;450(7171):819-24.
141. Arrenberg AB, Stainier DY, Baier H, Huisken J. Optogenetic control of cardiac function. *Science (New York, NY)*. 2010;330(6006):971-4.
142. Boyle PM, Williams JC, Ambrosi CM, Entcheva E, Trayanova NA. A comprehensive multiscale framework for simulating optogenetics in the heart. *Nature communications*. 2013;4:2370.
143. Sobie EA. Getting heart cells on the same wavelength: infrared triggering of Ca²⁺ transients in cardiac myocytes. *The Journal of physiology*. 2011;589(Pt 6):1243-4.
144. Liu Q, Frerck MJ, Holman HA, Jorgensen EM, Rabbitt RD. Exciting cell membranes with a blustering heat shock. *Biophysical journal*. 2014;106(8):1570-7.
145. Okunade O, Santos-Sacchi J. IR laser-induced perturbations of the voltage-dependent solute carrier protein SLC26a5. *Biophysical journal*. 2013;105(8):1822-8.
146. Shapiro MG, Homma K, Villarreal S, Richter CP, Bezanilla F. Infrared light excites cells by changing their electrical capacitance. *Nature communications*. 2012;3:736.

147. Iwanaga S, Kaneko T, Fujita K, Smith N, Nakamura O, Takamatsu T, et al. Location-dependent photogeneration of calcium waves in HeLa cells. *Cell biochemistry and biophysics*. 2006;45(2):167-76.
148. David G, Barrett JN, Barrett EF. Evidence that mitochondria buffer physiological Ca²⁺ loads in lizard motor nerve terminals. *The Journal of physiology*. 1998;509 (Pt 1):59-65.
149. Szabadkai G, Duchen MR. Mitochondria: the hub of cellular Ca²⁺ signaling. *Physiology (Bethesda, Md)*. 2008;23:84-94.
150. Oyama K, Mizuno A, Shintani SA, Itoh H, Serizawa T, Fukuda N, et al. Microscopic heat pulses induce contraction of cardiomyocytes without calcium transients. *Biochemical and biophysical research communications*. 2012;417(1):607-12.
151. Takeuchi T. Regulation of cardiomyocyte proliferation during development and regeneration. *Dev Growth Differ*. 2014;56(5):402-9.
152. Lian X, Zhang J, Azarin SM, Zhu K, Hazeltine LB, Bao X, et al. Directed cardiomyocyte differentiation from human pluripotent stem cells by modulating Wnt/beta-catenin signaling under fully defined conditions. *Nat Protoc*. 2013;8(1):162-75.
153. Ruiz JP, Pelaez D, Dias J, Ziebarth NM, Cheung HS. The effect of nicotine on the mechanical properties of mesenchymal stem cells. *Cell Health Cytoskeleton*. 2012;4:29-35.
154. Ng TK, Carballosa CM, Pelaez D, Wong HK, Choy KW, Pang CP, et al. Nicotine alters MicroRNA expression and hinders human adult stem cell regenerative potential. *Stem Cells Dev*. 2013;22(5):781-90.
155. Shannon TR, Ginsburg KS, Bers DM. Quantitative assessment of the SR Ca²⁺ leak-load relationship. *Circ Res*. 2002;91(7):594-600.
156. Dulce RA, Yiginer O, Gonzalez DR, Goss G, Feng N, Zheng M, et al. Hydralazine and organic nitrates restore impaired excitation-contraction coupling by reducing calcium leak associated with nitroso-redox imbalance. *J Biol Chem*. 2013;288(9):6522-33.
157. Grynkiewicz G, Poenie M, Tsien RY. A new generation of Ca²⁺ indicators with greatly improved fluorescence properties. *J Biol Chem*. 1985;260(6):3440-50.
158. Akazawa H, Komuro I. Roles of cardiac transcription factors in cardiac hypertrophy. *Circ Res*. 2003;92(10):1079-88.
159. Toko H, Zhu W, Takimoto E, Shiojima I, Hiroi Y, Zou Y, et al. Csx/Nkx2-5 is required for homeostasis and survival of cardiac myocytes in the adult heart. *J Biol Chem*. 2002;277(27):24735-43.
160. Morkin E. Control of cardiac myosin heavy chain gene expression. *Microsc Res Tech*. 2000;50(6):522-31.

161. Pasquale F, Syrris P, Kaski JP, Mogensen J, McKenna WJ, Elliott P. Long-term outcomes in hypertrophic cardiomyopathy caused by mutations in the cardiac troponin T gene. *Circ Cardiovasc Genet*. 2012;5(1):10-7.
162. Sergeeva IA, Christoffels VM. Regulation of expression of atrial and brain natriuretic peptide, biomarkers for heart development and disease. *Biochim Biophys Acta*. 2013;1832(12):2403-13.
163. Ziviani E, Lippi G, Bano D, Munarriz E, Guiducci S, Zoli M, et al. Ryanodine receptor-2 upregulation and nicotine-mediated plasticity. *EMBO J*. 2011;30(1):194-204.
164. Man J, Barnett P, Christoffels VM. Structure and function of the Nppa-Nppb cluster locus during heart development and disease. *Cell Mol Life Sci*. 2018;75(8):1435-44.
165. Roy A, Fields WC, Rocha-Resende C, Resende RR, Guatimosim S, Prado VF, et al. Cardiomyocyte-secreted acetylcholine is required for maintenance of homeostasis in the heart. *FASEB J*. 2013;27(12):5072-82.
166. Govind AP, Vezina P, Green WN. Nicotine-induced upregulation of nicotinic receptors: underlying mechanisms and relevance to nicotine addiction. *Biochem Pharmacol*. 2009;78(7):756-65.
167. Roof SR, Shannon TR, Janssen PM, Ziolo MT. Effects of increased systolic Ca(2)(+) and phospholamban phosphorylation during beta-adrenergic stimulation on Ca(2)(+) transient kinetics in cardiac myocytes. *Am J Physiol Heart Circ Physiol*. 2011;301(4):H1570-8.
168. Han JW, Lee YH, Yoen SI, Abramowitz J, Birnbaumer L, Lee MG, et al. Resistance to pathologic cardiac hypertrophy and reduced expression of CaV1.2 in Trpc3-depleted mice. *Mol Cell Biochem*. 2016;421(1-2):55-65.
169. Eder P, Molkentin JD. TRPC channels as effectors of cardiac hypertrophy. *Circ Res*. 2011;108(2):265-72.
170. Feng Z, Li W, Ward A, Piggott BJ, Larkspur ER, Sternberg PW, et al. A *C. elegans* model of nicotine-dependent behavior: regulation by TRP-family channels. *Cell*. 2006;127(3):621-33.
171. Dvorakova M, Lips KS, Bruggmann D, Slavikova J, Kuncova J, Kummer W. Developmental changes in the expression of nicotinic acetylcholine receptor alpha-subunits in the rat heart. *Cell Tissue Res*. 2005;319(2):201-9.
172. Al Hariri M, Zibara K, Farhat W, Hashem Y, Soudani N, Al Ibrahim F, et al. Cigarette smoking-induced cardiac hypertrophy, vascular inflammation and injury are attenuated by antioxidant supplementation in an animal model. *Front Pharmacol*. 2016;7:397.

173. Pohanka M. Alpha7 nicotinic acetylcholine receptor is a target in pharmacology and toxicology. *Int J Mol Sci.* 2012;13(2):2219-38.
174. Wu CH, Lee CH, Ho YS. Nicotinic acetylcholine receptor-based blockade: applications of molecular targets for cancer therapy. *Clin Cancer Res.* 2011;17(11):3533-41.
175. Sossalla S, Fluschnik N, Schotola H, Ort KR, Neef S, Schulte T, et al. Inhibition of elevated Ca²⁺/calmodulin-dependent protein kinase II improves contractility in human failing myocardium. *Circ Res.* 2010;107(9):1150-61.
176. Deng G, Orfila JE, Dietz RM, Moreno-Garcia M, Rodgers KM, Coultrap SJ, et al. Autonomous CaMKII activity as a drug target for histological and functional neuroprotection after resuscitation from cardiac arrest. *Cell Rep.* 2017;18(5):1109-17.
177. Reid JL, Millar JA, Struthers AD. Nifedipine--studies on its mechanism of action and interaction with other circulatory control mechanisms in man. *Postgrad Med J.* 1983;59 Suppl 2:98-103.
178. Jung Y, Hsieh LS, Lee AM, Zhou Z, Coman D, Heath CJ, et al. An epigenetic mechanism mediates developmental nicotine effects on neuronal structure and behavior. *Nat Neurosci.* 2016;19(7):905-14.
179. Potthoff MJ, Olson EN. MEF2: a central regulator of diverse developmental programs. *Development.* 2007;134(23):4131-40.
180. Munoz JP, Collao A, Chiong M, Maldonado C, Adasme T, Carrasco L, et al. The transcription factor MEF2C mediates cardiomyocyte hypertrophy induced by IGF-1 signaling. *Biochem Biophys Res Commun.* 2009;388(1):155-60.
181. Kaneda R, Takada S, Yamashita Y, Choi YL, Nonaka-Sarukawa M, Soda M, et al. Genome-wide histone methylation profile for heart failure. *Genes Cells.* 2009;14(1):69-77.
182. Robison AJ. Emerging role of CaMKII in neuropsychiatric disease. *Trends Neurosci.* 2014;37(11):653-62.
183. Hashimoto K. Targeting of alpha7 nicotinic acetylcholine receptors in the treatment of schizophrenia and the use of auditory sensory gating as a translational biomarker. *Curr Pharm Des.* 2015;21(26):3797-806.